

INVESTIGATION OF THE TUNABILITY AND MODIFICATION OF S-NITROSO
GLUTATHIONE-INCORPORATED NITRIC OXIDE-RELEASING HYDROGELS FOR
ANTIMICROBIAL BIOMEDICAL APPLICATIONS

by

LORI M. ESTES BRIGHT

(Under the Direction of HITESH HANDA)

ABSTRACT

The use of hydrogels in biomedical applications is widespread and constantly progressing, as the high water uptake affords tissue-like mechanical properties and facile functionality. Moreover, the gaseous molecule, nitric oxide (NO), has been shown to be responsible for various endogenous physiological functions including acting as a potent antimicrobial, released from macrophages during infection and wound healing processes. Consequently, the fabrication of hydrogel materials comprising synthetic NO donor molecules, such as S-nitrosothiols (RSNOs), reveals hydrogels with active functionalities such as enhanced antibacterial activity. However, hydrogel manipulation and fabrication techniques have consequences on NO release and donor stability. This dissertation aims to investigate the broad-spectrum antimicrobial efficacy of NO through a series of three projects, each with increasing complexity in aqueous and hydrogel systems. First, NO released from GSNO in aqueous solutions was tested against commercially available bacterial strains and clinically isolated drug-resistant bacteria strains of the same species. Similar killing capabilities demonstrate the clinical potential of such NO-releasing

treatments. Second, the water-soluble NO donor, GSNO, was embedded into an alginate hydrogel, crosslinked into spherical beads and characterized for NO release, antibacterial capacity, and biocompatibility with mammalian cells. Lastly, GSNO in combination with a fluoride salt was incorporated into a co-system of alginate and Pluronic F-127 hydrogels. The composite system displayed potential for dual functional treatment of dental caries through bacterial killing and biofilm dispersion, and prevention of demineralization of a tooth enamel model. Taken together, the addition of GSNO to alginate hydrogels provides tunable NO release with the opportunity for further modifications specific to the biomedical application in question.

INDEX WORDS: Nitric oxide, S-nitrosoglutathione, GSNO, Antimicrobial, Hydrogel,
Alginate, Antibacterial

INVESTIGATION OF THE TUNABILITY AND MODIFICATION OF S-
NITROSOGLUTATHIONE-INCORPORATED NITRIC OXIDE-RELEASING
HYDROGELS FOR ANTIMICROBIAL BIOMEDICAL APPLICATIONS

by

LORI M. ESTES BRIGHT

B.S., The University of Georgia, 2018

A Dissertation Submitted to the Graduate Faculty of The University of Georgia in Partial
Fulfillment of the Requirements for the Degree

DOCTOR OF PHILOSOPHY

ATHENS, GEORGIA

2023

© 2023

Lori M. Estes Bright

All Rights Reserved

INVESTIGATION OF THE TUNABILITY AND MODIFICATION OF S-
NITROSOGLUTATHIONE-INCORPORATED NITRIC OXIDE-RELEASING
HYDROGELS FOR ANTIMICROBIAL BIOMEDICAL APPLICATIONS

by

LORI M. ESTES BRIGHT

Major Professor: Hitesh Handa

Committee: James Warnock
Larry Hornak
Cheryl Gomillion
Vincent Starai

Electronic Version Approved:

Ron Walcott

Vice Provost for Graduate Education and Dean of the Graduate School

The University of Georgia

May 2023

DEDICATION

I would like to dedicate this dissertation to my dad. I apologize for not studying the migration of the caribou. Maybe that will be my next dissertation topic. I hope I made you proud. I love you and I miss you every day.

ACKNOWLEDGEMENTS

The past five years have been some of the best and worst years of my life, and I would not be here without the people in my life. Oftentimes, the days were long and the years were short, but the support and encouragement were constant through it all.

First, I would like to thank the members of my committee, Dr. James Warnock, Dr. Cheryl Gomillion, Dr. Larry Hornak, and Dr. Vinny Starai. Thank you all for your guidance in my projects and your support these last five years. I hope to make you all proud in the next phase of my biomedical engineering career.

I owe a huge debt of gratitude to Dr. Hitesh Handa. You have been a mentor and a friend all these years, and have always had an open door, no matter what you had going on. Thank you for seeing my potential and helping me grow to become a better researcher and scientist. Thank you for the opportunities you presented me with, and for pushing me to do more work than I wanted to sometimes. Thank you for listening to all of my successes and my failures, and for trusting my leadership and opinions. I do not think I would have made it through a Ph.D. if you were not my mentor. Thank you for helping me prepare for my future and helping me succeed in my present.

Thank you to Dr. Brisbois for your guidance and knowledge these last few years. Thank you also to my fellow lab mates. Dr. Priyadarshini Singha, Dr. Jitendra Pant, Dr. Megan Douglass Brooks, and Dr. Arnab Mondal, thank you for your mentorship and leadership. Thank you to Mark Garren, thank you for sharing your breadth of knowledge and providing the most precise edits possible. We started this together and I look forward to seeing what all you will accomplish. Thank you to Dr. James Manuel, Jianwen Li, Dr.

Sama Ghalei, and Dr. Ryan Devine for your helpful hints and creative solutions. Dr. Ekrem Ozkan and Dr. Anil Kumar, it was a pleasure to work with you both and learn more about the possibilities of surface functionalization and nanomedicine, as well as see the love you both have for your beautiful families. Dr. Manjot Kaur Chug, although the CDC bioreactors brought us together, I hope to never touch a clinical bacteria isolate ever again and hope you never have to either. Rashmi Pandey, I am forever grateful for your knowledge of various assays. Lauren Griffin, thank you for keeping the lab running and organized. Divine Francis, keep those surfaces terrified of water and oil, and never change your joyful laugh. Dr. Morgan Ashcraft, thank you for your help with bacteria troubleshooting. Sarah Wilson and Elaine Wu, I will always remember the fun of NOA troubleshooting days, no matter how much I try to forget. Patrick Maffe, best of luck finding a more fun bioreactor setup partner, and don't forget to round those ODs precisely. Stephen Thompson and Vince Pinon, thank you both for your kindness and willingness to talk through all the problems that do arise in my projects. Tia Shorter, Grace Nguyen, and Aasma Sapkota, in the short time I worked with y'all I am hopeful for the future of the lab and am excited for your successes. Adam Goodman, Annalise Tucker, Emme Collett, Natalie Ashcraft, Sankeerth Kanumari, Sierra Milligan, and Shruti Kumthekar, take pride in our lab. Working here and with these people is a gift. Make the most of it and challenge yourself every day. Dr. Arpita Shome, thank you for your assistance and perspective, and for helping me with my scientific writing. Izzy Martinez, Dagney Crowley, Anastasia Marx, and Myddie Parker, I have high hopes for your grad school experience. Never be afraid to ask questions and welcome to the team!

A rather strong thank you goes out to Mrs. Margaret Sapp for helping with just about any behind-the-scenes issue regarding grad school that you could imagine. You always went out of your way and above and beyond what was required of your job title to

make sure that I, and every other engineering grad student, had all questions answered at all times. If I could award you an honorary Ph.D. for all of your assistance, I would, because you put in more work than anyone gives you credit for.

Additionally, I would like to thank my family. My husband, Ethan, my Momma, Stacey, my sister, Jessica, and my Dad, Rick; as well as Rita, Uncle Rick, and Aunt Marjorie. You all are my biggest supporters and love me so well. Thank you for believing in me, making me laugh, telling me how proud you are of me, and reminding me why I was working so hard all this time. I would also like to thank my in-laws, Bobby and Roxanne, as well as Adam, Shannon, Landon, Jennifer, Josh, Jake, and Rhyan. Y'all are the best second family I could've ever hoped for, and I am so grateful to be a part of it all.

Thank you to my friends, Olivia, KB, Caroline, Cliff, Emily, Kyle, Sydney, Hannah, Amber, and Parker. Our weekly get-togethers brought joy to a sometimes-monotonous lab life. Y'all make the late-night inoculations and early-morning re-inoculations worth it all. And those no longer in Athens; Athena, Emily, and Lane, I am grateful for your friendship and the good times we shared.

Lastly, I would like to thank Athens, GA. What a wonderful place to be stuck for 5 years doing a Ph.D. Thank you for the delicious food, breweries, movie nights, concerts, farmer's markets, UGA events. Thank you for the brilliant fall leaves and soothing cherry blossoms. This town will forever hold a place in my heart, and you can bet I'll be back to see it, even though Donna Changs was replaced.

TABLE OF CONTENTS

	Page
ACKNOWLEDGEMENTS.....	v
LIST OF TABLES	x
LIST OF FIGURES	xi
CHAPTER 1: INTRODUCTION AND LITERATURE REVIEW	1
1.1. Introduction	1
1.2. Considerations when fabricating NO-releasing hydrogels.....	5
1.3. Antimicrobial applications of NO-releasing hydrogels.....	11
1.4. Conclusions.....	17
1.5. Dissertation overview	18
1.6. References.....	20
CHAPTER 2: COMPARATIVE STUDY OF THE BROAD-SPECTRUM ANTIBACTERIAL ACTIVITY OF NITRIC OXIDE AGAINST CLINICALLY ISOLATED DRUG- RESISTANT BACTERIA	29
2.1 Introduction	31
2.2 Materials and Methods	33
2.3 Results and Discussion	37
2.4 Conclusions.....	51
2.5 References.....	53

CHAPTER 3: BIOMIMETIC GASOTRANSMITTER-RELEASING ALGINATE BEADS FOR BIOCOMPATIBLE ANTIMICROBIAL THERAPY	57
3.1 Introduction	59
3.2 Materials and Methods	62
3.3 Results and Discussion	69
3.4 Conclusions	82
3.5 References	85
CHAPTER 4: DUAL ACTION NITRIC OXIDE AND FLUORIDE ION-RELEASING HYDROGELS FOR COMBATTING DENTAL CARIES	94
4.1 Introduction	96
4.2 Materials and Methods	99
4.3 Results and Discussion	111
4.4 Conclusions	134
4.5 References	137
CHAPTER 5: CONCLUSIONS AND FUTURE DIRECTIONS	146
5.1. Conclusions	146
5.2. Future Directions	148
5.3. References	152
APPENDICES	153
APPENDIX A	154
APPENDIX B	165
APPENDIX C	173

LIST OF TABLES

	Page
Table 1.1 Previously studied antibacterial NO-releasing hydrogels.....	16

LIST OF FIGURES

	Page
Figure 1.1 Physiological roles of nitric oxide	3
Figure 1.2 Nitric oxide synthase (NOS) pathway for endogenous NO production	4
Figure 1.3 Design constraints and fabrication considerations	7
Figure 1.4 Properties of NO hydrogels affected by degree of crosslinking	9
Figure 2.1 NO release from GSNO	38
Figure 2.2 <i>E. coli</i> growth curves.....	41
Figure 2.3 <i>P. aeruginosa</i> growth curves	43
Figure 2.4 MRSA growth curves	44
Figure 2.5 <i>S. epidermidis</i> growth curves.....	46
Figure 2.6 Metabolic assay of GSNO-treated bacteria.....	48
Figure 2.7 Membrane permeability of GSNO-treated bacteria	51
Figure 3.1 Alginate bead fabrication scheme	70
Figure 3.2 Morphological characterizations of alginate beads.....	71
Figure 3.3 Physical characterization of alginate beads	75
Figure 3.4 Nitric oxide release characteristics of alginate beads.....	78
Figure 3.5 Antibacterial activity of alginate beads	80
Figure 3.6 Biocompatibility assessment of alginate beads	82

Figure 4.1 Effective treatment of dental caries with the NO and fluoride ion-releasing hydrogels.....	99
Figure 4.2 Overview of the NO-releasing hydrogel system	112
Figure 4.3 Physical and mechanical characterization of PA gels	114
Figure 4.4 Overview of NO release from fabricated hydrogels.....	119
Figure 4.5 Analysis of fluoride in hydrogels	124
Figure 4.6 Analysis of antibacterial efficacy of gels against <i>S. mutans</i>	127
Figure 4.7 Demineralization prevention potential of PA gels in a hydroxyapatite disc model	131
Figure 4.8 Cytocompatibility evaluation of fabricated gels.....	134
Figure 5.1 Covalent attachment of NO donor to PVA hydrogel.....	151

CHAPTER 1

INTRODUCTION AND LITERATURE REVIEW

1.1. Introduction

Hydrogels are characterized by their highly hydrophilic nature, consisting of three-dimensional polymer networks that can be modified through methods such as crosslinking, freeze-drying, swelling, and degradation. Hydrogels can be classified in many ways, the most general distinction being natural versus synthetic hydrogels. Natural hydrogels such as hyaluronic acid (HA), collagen, fibrin, alginate, and chitosan are derived from naturally occurring components, making them exceptionally biocompatible. On the other hand, synthetic hydrogels are constructed from synthetic monomer or polymer chains and are considered more flexible for tuning since the exact structure, and molecular weight are known and can be easily reproduced if fabrication conditions are maintained^{1,2}. Examples of synthetic polymers include poly(vinyl alcohol) (PVA), poly (ethylene glycol) (PEG), poly(acryl amide) (PAA), poly(lactic acid) (PLA), poly(ϵ -caprolactone) (PCL), and many more^{1,2}. Both natural and synthetic hydrogels can be crosslinked to enhance mechanical properties, which can be categorized in two ways: physical and chemical. Physical crosslinking is considered reversible as polymers are held together by secondary forces such as H-bonding, ionic bonding, or hydrophobic forces and are more susceptible to degradation³. Conversely, chemical crosslinking involves the formation of covalent bonds between polymer chains within the matrix². Further characterization of hydrogels can include polymer charge, crystallinity, sensitivity to stimuli, hydrogel form, porosity, mechanical properties, and bioactivity, which are explored extensively in previous review papers¹⁻⁶.

The large water content of hydrogels is accredited to the functional groups of constituent networks, which accords them with a structure that is similar to extracellular matrix (ECM) in tissues, making them useful in biomedical applications like tissue engineering, cell encapsulation, drug delivery, and wound healing ⁶. Furthermore, although hydrogels show great promise in multiple biomedical applications, the addition of active agents such as nitric oxide to the formulation endows a biologically active component, further enhancing the scope of use.

The discovery of the plethora of physiological functions of nitric oxide (NO) opened up vast new research fields and led to its crowned achievement as Molecule of the Year by *Science* in 1992 ⁷. The endogenously produced gaseous signaling molecule, or gasotransmitter, is responsible for several regulatory roles and host responses throughout the body, including vasodilation, infection control, and neurotransmission (**Figure 1.1**). Nitric oxide is produced by three isoforms of NO synthase (NOS): neuronal NOS (nNOS), endothelial NOS (eNOS), and inducible NOS (iNOS), all through the L-arginine – Nitric oxide pathway (**Figure 1.2**) ⁸⁻¹⁰.

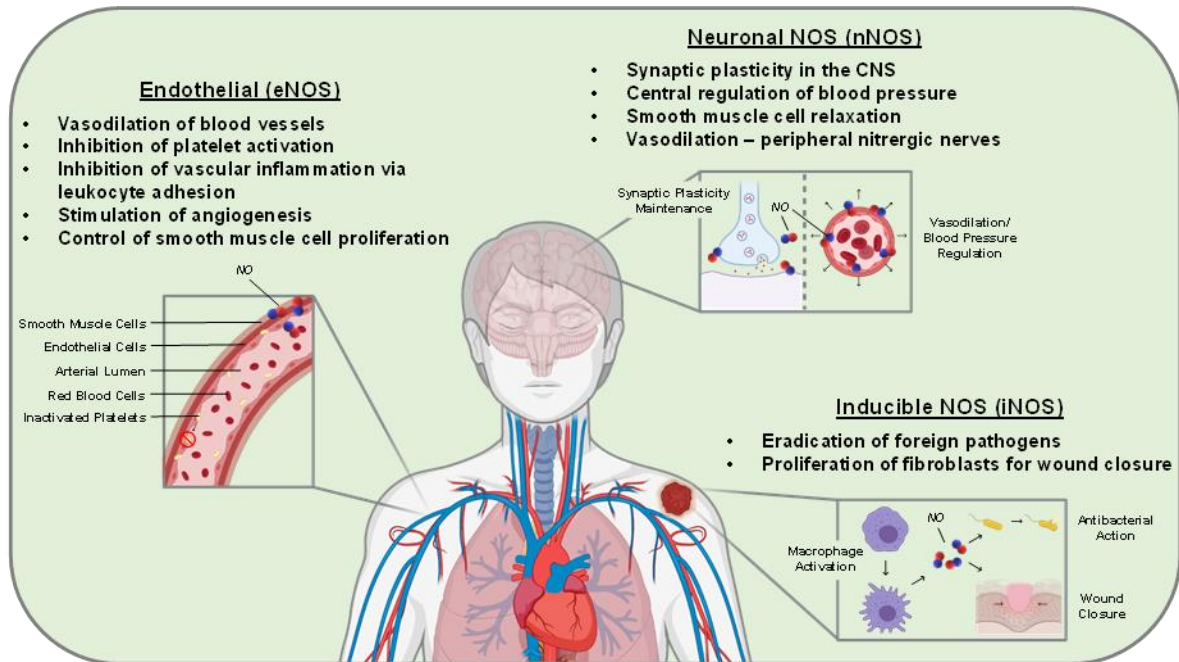


Figure 1.1 Physiological roles of nitric oxide. NO plays a crucial role in multiple parts of the body as it is released by three different nitric oxide synthase (NOS) enzymes, each correlating to various physiological responses in vivo.

Neuronal NOS is found within specific neurons in the brain, the spinal cord, and several other peripheral nerves and is responsible for maintaining synaptic plasticity, regulating central blood pressure, and causing vasodilation via peripheral nitrenergic nerves⁸. Also appropriately named, eNOS is primarily expressed in endothelial cells and plays a role in vasodilation, inhibition of platelet aggregation and adhesion, inhibition of leucocyte adhesion and vascular inflammation, control of vascular smooth muscle proliferation, activation of endothelial progenitor cells, and stimulation of angiogenesis^{8, 11}. Both nNOS and eNOS are Ca²⁺-dependent, whereas iNOS is Ca²⁺-independent and is upregulated by cytokines, microbial lipopolysaccharides, immune complexes, cell-to-cell contact, and various antibiotics^{8, 12}. Although primarily found in macrophages as part of the immune response, iNOS can be stimulated in a wide range of cells as long as inducing agents are

present⁸. The release of NO as an immune response is utilized mainly as an antimicrobial agent, as the NO radical is highly effective at inducing nitrosative stress to microbial membranes, proteins, and DNA¹³. Due to NO's potency, research into antimicrobial NO-releasing therapies is extensive. However, the use of NO in research and clinical applications requires the use of a delivery vehicle due to the instability of NO donor molecules in physiological conditions. Various platforms such as nanoparticles and polymeric delivery platforms provide a more stabilized release of NO and a more favorable material interaction with living cells and tissues. One such vehicle for NO release that has been used extensively in research is hydrogels.

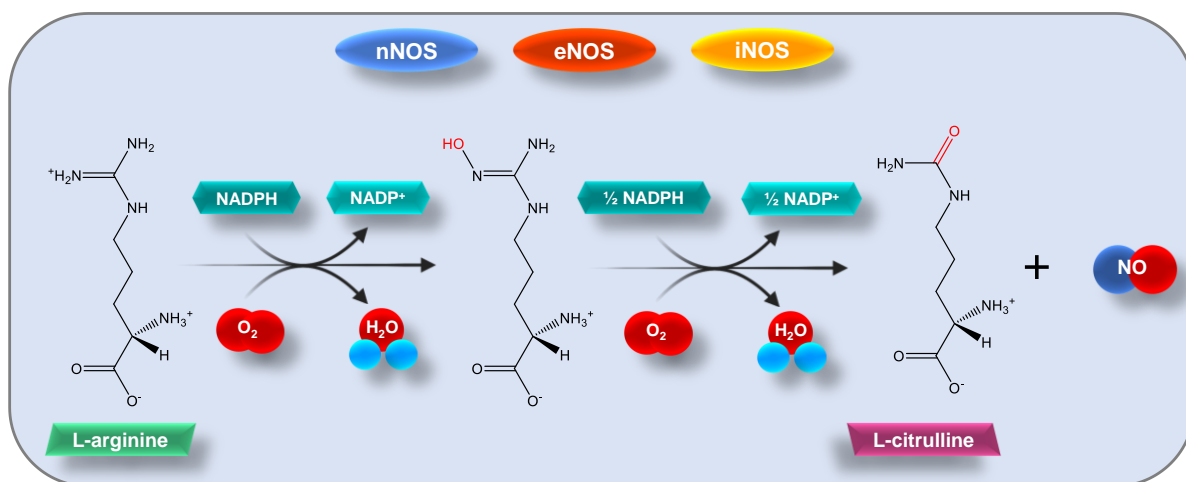


Figure 1.2 Nitric oxide synthase (NOS) pathway for endogenous NO production

Comprehensive research about the antimicrobial effects of NO-releasing hydrogels and applications will be discussed below. The tailoring of NO-releasing hydrogels for such applications shines a light on the novel advancements possible in the biomedical field when complex chemical solutions are substituted with scientists taking cues from human physiology on maintaining health and homeostasis. This literature

review focuses on the release of NO from various hydrogel systems for biomedical applications and the design considerations that lead to such effective treatments.

1.2. Considerations when fabricating NO-releasing hydrogels

1.2.1 Hydrogel fabrication and modification techniques

The hydrophilic nature of hydrogels that imbues applicability in biomedical scenarios also requires careful consideration during fabrication due to the reduced mechanical integrity associated with high water swelling. In most cases, chemical or physical crosslinking methods are utilized to prevent the complete dissolution of the hydrophilic groups of the material in water and bodily fluids ¹⁴. However, the degree of crosslinking greatly determines other hydrogel properties that affect the material's efficacy, such as porosity, water uptake, biodegradability, NO release, biocompatibility, and viscosity (**Figure 1.3**). For instance, a greater degree of crosslinking can lead to higher viscosity gel with less biodegradability and biocompatibility. The choice of material and crosslinking method allows for specialized hydrogel designs fit for virtually any biomedical application.

The highly tunable nature of hydrogels allows for countless design strategies and material properties. When creating a NO-releasing hydrogel, knowing which properties are ideal for the chosen application and which will lead to complications is essential. Some modifications are as simple as adding a plasticizer to a hydrogel formulation to increase flexibility or decrease the viscosity ^{15, 16} or embedding the NO-releasing mixture into an already formed ointment or gel ^{17, 18}. Other methods of enhancing the mechanical properties of a hydrogel system include casting the gel into an electrospun polymer mat ^{19, 20} or combining multiple hydrogel types into a single formulation ²¹⁻³⁰. For example, Pluronic hydrogels are often combined with natural polymers such as alginate ^{21, 31} or chitosan ²⁷ to improve mechanical strength and biocompatibility.

Modifications must be thoroughly considered in some scenarios, as strict design constraints exist for a particular application. For instance, when designing a NO-releasing hydrogel for ocular applications to decrease ocular pressure and fight bacterial infections, parameters such as light penetration and transparency, appropriate gas diffusion, and swelling properties, as well as corneal cell biocompatibility cannot be overlooked ^{29, 32}. Similarly, this application might permit the use of a NO photo donor, allowing for NO release triggered by visible light traveling to the eye (**Figure 1.3A**). Other applications suitable for the implementation of an NO photo donor are those in which the hydrogel will be placed external to a patient *in vivo*, such as dermal vasodilation enhancement ³³, utilization of a wound adhesive ²², and exterior infection treatment ³⁴. On the other hand, hydrogel treatment of blood vessel injury caused by stenting is more likely to use a NO donor that is thermally or hydrolytically degraded while being applied perivascularly ³⁵⁻³⁷ or as a stent coating ²⁵ for localized NO therapy (**Figure 1.3B**). Although hydrogel wound dressings possess many ideal properties such as high swelling capacity, gas exchange permeability, and biocompatibility, they can be improved further with the addition of fibrin microparticles to endow adhesive properties (**Figure 1.3 C-F**) ²² or application as a powder that forms a gel upon exposure to wound exudates, allowing for an exact fit to irregular wound sites ²⁴.

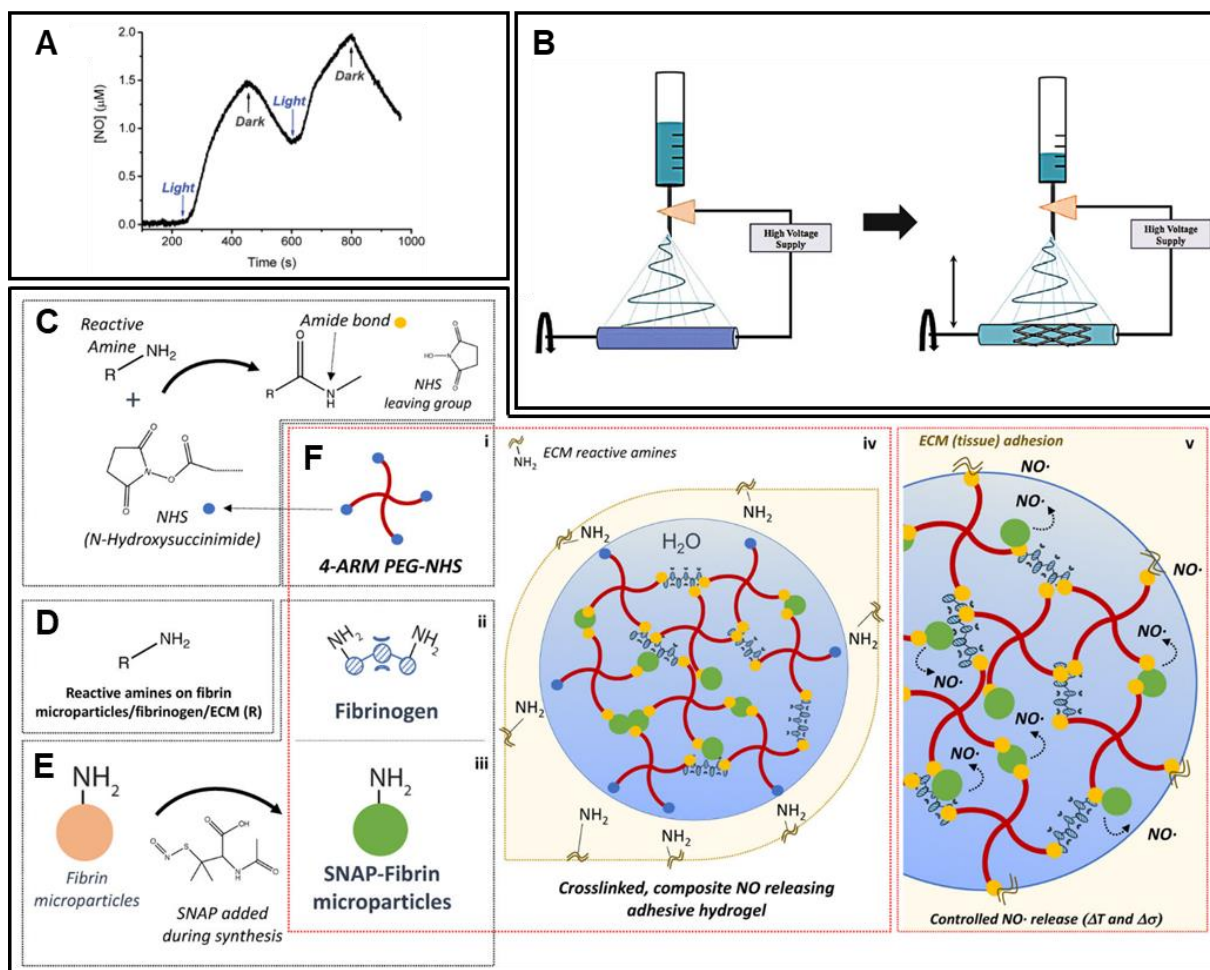


Figure 1.3 Design constraints and fabrication considerations must be taken into account when creating a material for a specific application. (A) When designing for ocular applications, the use of a NO photo donor allows for enhanced NO release upon irradiation with visible light. (B) NO therapy designed for co-transplantation of a vascular stent is facilitated by coating the metal stent with the NO-releasing nanofiber gel using an electrospinning technique. When tailoring a gel for wound healing applications, tissue adhesivity was one of the goals for a poly(ethylene) glycol-N-hydroxy succinimide (PEG-NHS) fibrinogen adhesive hydrogel that contained SNAP-embedded fibrin microparticles. (C) Crosslinking of the gel occurred as the NHS formed a stable amide bond with (D) reactive amines present in fibrinogen. Following (E) synthesis of the SNAP-fibrin microparticles, (F i-iii) each element of the adhesive hydrogel went through (F iv) in-situ curing that led to (F v) adhesion between the tissue and hydrogel and consequent NO release. A was reproduced/adapted from Seggio, M., et al. (2020). "A thermoresponsive gel photoreleasing nitric oxide for potential ocular applications." *Journal of Materials*

Chemistry B **8**(39): 9121-9128, with permission from the Royal Society of Chemistry, Great Britain. B was reproduced/adapted from Oh, B. and C. H. Lee (2014). "Nanofiber-coated drug-eluting stent for the stabilization of mast cells." *Pharm Res* **31**(9): 2463-2478, with permission from Springer Nature. C-F was reprinted/adapted with permission from {Joseph, C. A., et al. (2019). "Development of an Injectable Nitric Oxide Releasing Poly(ethylene) Glycol-Fibrin Adhesive Hydrogel." *ACS Biomater Sci Eng* **5**(2): 959-969.} Copyright {2019} American Chemical Society.

While some properties and characteristics of hydrogels, such as polymer type and NO donor, can be specifically chosen and modified to fit an application, many fabrication processes along the way can have lasting effects on hydrogel quality. The consequences of hydrogel fabrication and modification methods should be well understood when designing a hydrogel for specific applications. For instance, crosslinking of hydrogels can drastically affect almost all other hydrogel properties (**Figure 1.4**). A simple example of this is the relationship between cross-linking and the swelling capacity of hydrogels: increased crosslinking that is often performed to enhance mechanical properties or prevent donor leaching decreases the swelling potential of hydrogels due to the increased density of polymer chains within the matrix and limited space for water molecules to invade³⁸. The pore size of hydrogels affects the swelling potential, which can be modulated depending on fabrication techniques and procedures. Decreasing pore size corresponds to an increased total surface area of the gel leading to a greater swelling capacity³⁹. For hydrogels with NO donor embedded into the bulk hydrogel, greater swelling capacity directly correlates to higher NO release from the hydrogel as water-polymer contact increases. Therefore, NO release is altered and can be modified by transforming the pore size of the bulk hydrogel. Furthermore, porosity can often be affected by freeze-thaw cycles sometimes used to induce physical crosslinking of hydrogels⁴⁰. The slight manipulations and alterations performed to achieve ideal crosslinking and mechanical

properties can have lasting effects on the biological efficacy of NO-releasing hydrogels and should always be considered from all angles before final formulation.

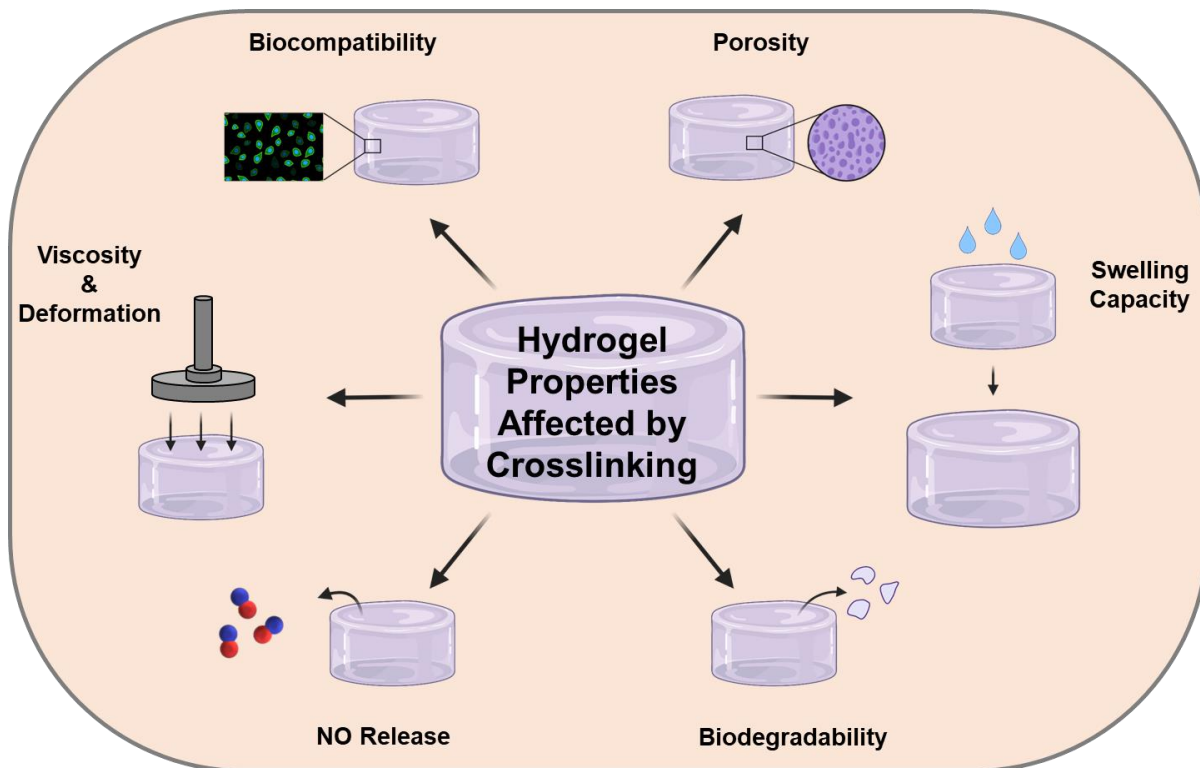


Figure 1.4 Properties of NO hydrogels affected by degree of crosslinking. The crosslinking of hydrogels allows for enhanced mechanical properties, though the effects can be seen in other essential hydrogel properties such as porosity, swelling capacity, biodegradability, NO release, biocompatibility, and resistance to deformation.

1.2.2 Nitric oxide incorporation strategies

Incorporating NO donors into a hydrogel system presents several challenges researchers have creatively overcome in recent years. One strategy is the direct physical inclusion of a NO donor molecule^{16, 18, 27, 31, 41-44}, such as *S*-nitrosoglutathione (GSNO), a water-soluble *S*-nitrosothiol (RSNO) molecule that releases NO in the presence of heat, light, and metal ions⁴⁵. Interestingly, GSNO is simply the *S*-nitrosated derivative of glutathione, the most abundant cellular thiol that is also readily taken in and processed by

several microbes, enhancing the antibacterial effects of NO therapy ^{13, 45}. Although the solubility of GSNO seems promising, the high water uptake of hydrogels leads to excessive GSNO leaching, which can induce cellular toxicity if present in sufficient quantities ^{27, 41}. Several other small molecules NO donors that have been utilized in hydrogels include S-Nitroso-N-acetylpenicillamine (SNAP) ²², S-nitrosocysteine (Cys-NO) ^{36, 37, 46}, and nitroglycerin ¹⁸. Rather than physical incorporation, several hydrogels have been induced with NO-releasing capabilities through 'nitrosation' of amines, a term that refers to the specific chemical reactions where a nitrosonium ion (NO⁺) is added to a nucleophilic group. The analogous term, 'nitrosylation,' is more specific and refers to the direct addition of NO to a reactant, though it is more appropriately used in biological/physiological contexts ⁴⁷. Nevertheless, the nitrosation of amines through high-pressure NO gas leads to the formation of diazeniumdiolates (NONOates) ^{17, 23, 26, 32, 35, 37, 46, 48-55} that spontaneously hydrolyze to NO in aqueous media ⁵⁶. Nitrosation of thiol moieties is another technique for imparting NO donating capability to the hydrophilic polymer systems and generally provides a more stable and prolonged NO release compared to NONOates ^{15, 28, 38, 46, 57-59}. A unique technique utilizes nitrosyl ruthenium species for NO release as they have increased thermal stability and release NO in a controlled manner via light irradiation ^{33, 60}. The final method of endowing hydrogels with NO-releasing capabilities draws directly from endogenous environments, where a donor produces molecules that are utilized by cells found in the treatment site. In one study, L-arginine is cleaved from the donor molecule by peptidase enzymes that is then utilized by activated macrophages to produce NO ⁶¹. Similarly, ammonia deposited as a result of gelatin crosslinking by microbial transglutaminase is partially oxidated through biosynthetic coupling with the urea cycle to continuously release NO ⁶².

1.3. Antimicrobial applications of NO-releasing hydrogels

The antimicrobial potency of NO lies in the highly reactive nature of the nonpolar, uncharged, free radical molecule. Once produced, NO readily diffuses through microbial membranes, reacting rapidly with oxygen (O₂), thiols, and metals, producing an array of reactive nitrogen (RNS) and oxygen species (ROS), each uniquely capable of inducing nitrosative and oxidative stress to foreign pathogens. Peroxynitrite (OONO⁻) is a highly reactive and toxic molecule produced by the reaction of NO with O₂⁻ known to cause oxidative damage to multiple cellular targets^{12, 13, 63}. Other ROS and RNS such as nitrogen dioxide (NO₂[•]), dinitrogen trioxide (N₂O₃), dinitrogen tetroxide (N₂O₄), hydrogen peroxide (H₂O₂), and hydroxide ([•]OH) species can modify proteins and lipids as well as deaminate DNA^{13, 63}. NO's reaction with thiols can lead to S-nitrosation of proteins, resulting in the creation of temporary NO reservoirs and altering protein function through disulfide bond formation⁶³. In terms of metal reactions, NO can deplete cellular iron stores and inactivate essential enzymes through the reaction with cellular iron or iron-sulfur complexes⁶³. Although these antimicrobial strategies of NO have been previously identified, the exact critical targets responsible for microbial death have yet to be discovered¹³.

NO-releasing hydrogels for antimicrobial applications should have a stable and prolonged release of NO, a facile synthesis process, and bactericidal efficacy. Through various modifications, hydrogel systems can utilize these characteristics to eradicate microbes *in vitro* and *in vivo*^{16, 50}. Often, the NO-releasing hydrogel can be functionalized to carry either synthetic or natural antimicrobial agents in addition to its inherent antimicrobial properties. For example, when combined with a NO donor, S-nitroso-mercaptosuccinic acid, silver metal nanoparticle-loaded hydrogels can achieve potent anticancer and local antimicrobial effects without systemic toxicity¹⁵. Natural antimicrobial agents extracted from plants and animals, such as chitosan, have gained increasing

attention for their inherent biocompatibility and bioavailability. Chitosan is a polycationic polysaccharide biopolymer that gained popularity for its known activity to promote wound healing and encourage surface endothelialization. One recent study highlighted a synergistic enhancement in chitosan's anti-biofilm ability against methicillin-resistant *Staphylococcus aureus* (MRSA) when prepared as a NO-releasing hydrogel with GSNO¹⁶. The hydrogel's *in vivo* performance was evaluated on diabetic mouse models and demonstrated excellent dispersal of MRSA biofilm and wound healing efficacy within 15 days⁶⁴. Comparatively, an injectable and self-healing chitosan hydrogel was imbued with NO-releasing capabilities through covalent attachment of *N*-acetyl-cysteine, followed by nitrosation and crosslinking with HA using aldehyde-modified polyethylene glycol (PEG)⁶⁵. When tested for antimicrobial efficacy, the chitosan-NO gel showed a 2-log reduction in *E. coli* after only 1.5 h and a 1-log reduction in *Staphylococcus epidermidis* (*S. epidermidis*) after 4 h exposure. Hence, chitosan is a common polymer of choice for NO-releasing hydrogels as it enhances antimicrobial effects. Natural-derived carboxymethyl cellulose (CMC) is a water-soluble polymer attractive for its biocompatibility, ability to increase solution viscosity, and adhesiveness to tissue surface⁴⁹. CMC derivatives modified with NONOates previously developed by Feura et al. can adhere to periodontal pocket tissue proteins and concomitantly reduce common periodontopathogens such as *Porphyromonas gingivalis* (*P. gingivalis*) and *Aggregatibacter actinomycetemcomitans* (*A. actinomycetemcomitans*)⁴⁹. Besides naturally derived antibiotic agents, bio-inspired bactericidal substances have also been utilized in NO-releasing hydrogels. Silver nanoparticles synthesized from green tea extract were incorporated into an alginate hydrogel with NO donor, *S*-nitroso-mercaptosuccinic acid (*S*-nitroso-MSA), for topical antibacterial applications. The combination had a synergistic effect against common infectious pathogens *E. coli*, *S. aureus*, and *S. mutans*¹⁵.

During the synthesis process of NO-releasing hydrogels, Pluronic or Poloxamer are copolymers of poly(ethylene oxide) (PEO) and poly(propylene oxide) (PPO) that are often used as the polymer matrix due to their tunable and thermoresponsive characteristics. PEO segments are more hydrophilic, whereas PPO segments are more hydrophobic ⁶⁶. The PPO segments provide a desirable microenvironment for the incorporation of lipophilic molecules such as NO. Therefore, the NO release stability, duration, and photochemical delivery in hydrogels can be tuned by adjusting the number of the PEO/PPO segments in the polymer ⁴². Pluronic F127 (PEO-PPO-PEO) hydrogel has been used as a NO delivery vehicle for various antimicrobial studies. In some cases, GSNO was blended into a Pluronic F127 – chitosan hydrogel matrix where a 3-log reduction in CFUs against MRSA and multidrug-resistant *P. aeruginosa* (MDRPA) was achieved ²⁷. A similarly designed hydrogel utilized Pluronic F-127 combined with GSNO and alginate ²¹. Since the PEO segment of the Pluronic has weak mechanical strength and rapid erosion toxicity, alginate was added for its bio-adhesive property and increased cell viability. The resulting hydrogel exhibited potent bactericidal activity against Gram-positive MRSA and Gram-negative MDRPA with sustained NO release for up to 7 days. Other studies also linked tri-block polymer Pluronic F-68 with branched polyethyleneimine (BPEI) for conjugation of NONOates for a sufficient release profile that induces bactericidal action against *S. aureus*, MRSA, and *E. coli* ²⁶. NO-releasing low molecular weight alginate oligosaccharides have reported the unique ability to alter biofilm morphology and mucin assembly and, therefore can be used as an adjuvant therapy to conventional antibiotics. Moreover, low-molecular-weight HA has shown promising results in wound healing *in vivo* murine models due to its intrinsic tissue remodeling properties. The combination of HA and NO-releasing biopolymer reduced the bacteria viability of *E. coli*, *P. aeruginosa*, *S. aureus*, and *E. faecalis* by 3-logs over 4 h ⁶⁴.

In addition to the aforementioned processes to synthesize NO-releasing hydrogels, the self-assembling peptide-functionalized hydrogel can also provide similar antibacterial characteristics and properties. Antimicrobial peptide MSI-78, or pexiganan, has a broad spectrum of antimicrobial activity against microbes and a high likelihood for self-assembly due to its hydrophobic and aromatic-rich peptide sequence⁶⁷⁻⁶⁹. The self-assembled hydrogel can be triggered by the addition of sodium hydroxide, which induces an immediate phase transition to translucent gel. The combined system of self-assembled hydrogel and NO donor NONOate can induce the slow kinetic release of NO for up to 15 days^{48, 70}. In addition to pH shift triggers, light-induced self-assembly supramolecular hydrogel with bactericidal action has also been developed. Spontaneous self-assembly of the hydrogel can be achieved by interaction between poly- β -cyclodextrin polymer, hydrophobically modified dextran, and NO photo-donor bearing an adamantyl appendage. The resulting gel network prevented the leaching of the NO photo-donor compound upon visible light excitation while maintaining bactericidal actions³⁴. A hyaluronic acid nanogel was contrived to be NO-releasing following a crosslinking process with divinyl sulfone followed by the physical incorporation of SNAP and a specifically designed antimicrobial peptide. The combination of antimicrobials led to the successful killing of *E. coli*, *S. aureus*, and *P. aeruginosa* in planktonic and biofilm form, though NO release, measured by UV-Vis Spectroscopy only lasted ~24 h⁷¹.

Another appealing class of NO-releasing hydrogel is injectable S-nitrosothiolated gelatin (GeISNO) with gelatin-based hydrogels formed by horseradish peroxidase/H₂O₂ reaction. Upon thermal, light, and oxidizing agent-driven stimulus, this hydrogel generates OONO⁻ *in situ* from released NO and H₂O₂ residues for up to 14 days³⁸. Prolonged storage of NO-releasing hydrogels can be achieved by *in situ* hydrogel-forming/NO-releasing powder dressings (NO/GP) developed by Yoo et al. The powder was fabricated by

blending and micronizing GSNO, pectin, alginate, and polyethylene glycol (PEG) ²⁴. The NO/GP powder remained stable for more than four months when stored at 4 or 37 °C and displayed sustained NO release for 18 hours upon gel formation. Moreover, incubation with NO/GP resulted in a 6-log reduction in colony-forming units (CFUs) of MRSA and *P. aeruginosa*. NO-releasing hydrogels possess impressive antimicrobial potential and can be fabricated through a variety of techniques depending on the application conditions and environment (**Table 1.1**).

In addition, NO-releasing hydrogels with antimicrobial capabilities are promising in the treatment of *in vivo* infections. In the human setting, one NO-releasing hydrogel has progressed to a phase 2 clinical trial for the treatment of molluscum contagiosum, a common viral skin infection among children. The gel under investigation is composed of berdazimer sodium that has been synthesized to carry a NONOates NO donor on its polysiloxane backbone and was developed by Novan Inc. (NC, USA). The isopropyl alcohol-based topical gel was co-administered with a phosphate-buffered CMC-based hydrogel at the time of use. During the phase 2, randomized clinical trial with 256 participants, berdazimer sodium-based NO-releasing hydrogel demonstrated minimal adverse effects and increased molluscum contagiosum lesion clearance compared to the control ⁵⁰. Although a larger study is needed to provide additional safety assessments for the hydrogel system, this study highlights the potential clinical translation of NO-releasing hydrogels against bacterial infections *in vivo*.

Table 1.1 Previously studied antibacterial NO-releasing hydrogels

Material	NO Donor	Antibacterial Capability	Ref.
Silver nanoparticle-loaded alginate hydrogel	S-nitroso-MSA	Complete bacterial killing after 2 h for <i>S. mutans</i> UA159, <i>S. aureus</i> (ATCC 25920), and <i>E. coli</i> (ATCC 25922)	15
Chitosan	S-nitrosoglutathione (GSNO)	> 3 log reduction in colony forming units (CFUs) against MRSA (USA300)	16
Chitosan and PEG-modified Hyaluronic acid	S-nitroso- <i>N</i> -acetylcysteine (SNAC)	> 2 log reduction in <i>E. coli</i> (ATCC 25922) after 1.5 h and > 1 log reduction in <i>S. epidermidis</i> (ATCC 12228) after 4 h	65
Carboxymethylcellulose (CMC) derivatives	Diazeniumdiolates (NONOates)	3 log reduction in CFUs against planktonic <i>P. gingivalis</i> (ATCC A7436) and <i>A. actinomycetemcomitans</i> (ATCC 43717)	49
Pluronic F-127 - chitosan hydrogel	GSNO	Minimal inhibitory concentration of 0.5 $\mu\text{g}\cdot\text{mL}^{-1}$ against <i>P. aeruginosa</i> (ATCC 27853)	27
Pluronic F-127-alginate hydrogel	GSNO	> 3 log reduction in CFUs against MRSA (KNRRB 3089) and MDRPA (KNRRB 2200)	21
Pluronic F-68 with branched polyethyleneimine (BPEI)	NONOates	3 log reduction against <i>E. coli</i> (KCCM 25922), <i>S. aureus</i> (KCCM 29213), and MRSA (KCCM 33591)	26
Self-assemble peptide N-Fmoc-Pexiganan (MSI-78)	NONOates	Complete bacterial killing after 2 h for <i>E. coli</i>	48
Poky-β-cyclodextrin polymer with hydrophobically modified dextran	Tailored NO photo-donor bearing an adamantyl appendage	> 3 log reduction in CFUs against antibiotic-resistant <i>E. coli</i> DH5 α	34

Hyaluronic acid nanogel with antimicrobial peptide	SNAP	Minimum inhibitory concentrations of 1.6 mg/mL (<i>E. coli</i>), 0.4 mg/mL (<i>P. aeruginosa</i>), and 0.8 mg/mL (MRSA ATCC BAA 1683)	71
Gelatin-based hydrogel	S-nitrosothiolated gelatin	Almost 50% inhibition of <i>E. coli</i> (ATCC 11775) and <i>S. aureus</i> (ATCC 14458) with 0.28 µmol/mL of NO-hydrogels. Eradication of <i>S. aureus</i> at 0.58 µmol/mL of NO-hydrogels	38
Alginate-pectin-PEG powder dressing	GSNO	6-log reduction in CFUs of MRSA (USA300) and <i>P. aeruginosa</i> (PA01)	24
Poly-ε-lysine (pεK) gel	NONOates	5-, 4-log reduction in CFUs against <i>P. aeruginosa</i> (PA01) and <i>S. aureus</i> (ATCC 25922), respectively	32
Hyaluronic acid hydrogel	NONOates	3 log reduction in CFUs against <i>E. coli</i> , <i>P. aeruginosa</i> , <i>S. aureus</i> , and <i>Enterococcus faecalis</i>	64
Berdazimer sodium in CMC gel	NONOates	37.5% of patients receiving the gel achieved complete clearance of molluscum contagiosum in the clinical study	50

1.4. Conclusions

The utilization of NO-releasing hydrogels spans various research areas within the biomedical field, for a good reason. Relatively simple and highly innovative designs alike have shown successful implementation of NO hydrogels for preventing and treating microbial infections in applications from wound healing to the dental sector. The capacity of NO-releasing hydrogels to further advance treatment options for patients in all sectors of medical care lies in the fine-tuning possibilities of hydrogel systems, along with the numerous and potent biological functions of NO.

1.5. Dissertation overview

The goal of this dissertation is to build on the knowledge of the research before me, while filling in the gap of knowledge that exists around fine-tuning and modifying NO-releasing hydrogels for antimicrobial treatment. Throughout the following projects, I hope to answer this **Essential Research Question: How can GSNO be utilized in alginate-based hydrogels for clinical infection treatment?**

To begin, I am going to take a step back from hydrogels specifically and investigate the broad-spectrum antibacterial activity of S-nitrosoglutathione (GSNO) and its clinical capabilities in Chapter 2. As a water-soluble NO donor, GSNO has been widely used in hydrogel systems to combat dangerous pathogens. However, there has yet to be a direct comparison of GSNO-treatment of commercially available bacterial species and clinically isolated antibiotic-resistant bacteria. Therefore, GSNO treatment of commercially available and clinically isolated bacterial strains will be compared in this study. Bacterial viability will be determined by absorbance values through growth curves, metabolic activity, and membrane permeability following NO treatment. The success of GSNO antibacterial treatment will be investigated for applicability in clinical settings.

Chapter 3 dives into the integration of GSNO into an alginate-based hydrogel. A unique crosslinking strategy is utilized to create alginate beads with two different GSNO concentrations. The porosity, size distribution, water uptake, and storage stability of the beads will be examined. Further, the NO release from both bead types will display the potential to fine-tune physiological activity of the material through variations in NO-donor impregnation. The antibacterial potential of the NO release from the alginate beads will then be tested against one Gram-negative and one Gram-positive bacterium. Lastly, the beads will be examined for biocompatibility with mammalian cells.

Increasing the complexity of the hydrogel design, Chapter 4 encompasses an application-specific design of a co-polymer gel for the treatment of dental caries. Rather than using alginate alone, here it is combined with a synthetic polymer, Pluronic-F127 to enhance the mechanical properties of the gel. Further, GSNO in addition to NaF is added to the hydrogel to allow for simultaneous NO and F⁻ release in physiological conditions. The release of both components is measured and tested for success in biofilm dispersion and killing, as well as prevention of demineralization of a hydroxyapatite tooth enamel model. Finally, the gel is analyzed for compatibility with two types of mammalian cells present in the dental environment. Overall, the hydrogel properties and functionalities are discussed with the addition of each new component to the alginate-Pluronic gel.

In conclusion, I hope to adequately answer the essential research question through these three projects and provide clarity for how NO release and material properties of alginate hydrogels can be modified to fit specific biomedical applications. Further, the clinical capabilities of NO as an antimicrobial will be demonstrated through direct clinical isolate testing and material design for application of biocompatible hydrogels.

1.6 References

1. Chirani, N.; Gritsch, L.; Motta, F. L.; Fare, S., History and applications of hydrogels. *Journal of biomedical sciences* **2015**, 4 (2).
2. Vasile, C.; Pamfil, D.; Stoleru, E.; Baican, M., New Developments in Medical Applications of Hybrid Hydrogels Containing Natural Polymers. *Molecules* **2020**, 25 (7), 1539.
3. Hoffman, A. S., Hydrogels for biomedical applications. *Advanced drug delivery reviews* **2012**, 64, 18-23.
4. Catoira, M. C.; Fusaro, L.; Di Francesco, D.; Ramella, M.; Boccafoschi, F., Overview of natural hydrogels for regenerative medicine applications. *Journal of Materials Science: Materials in Medicine* **2019**, 30 (10), 115.
5. González-Henríquez, C. M.; Sarabia-Vallejos, M. A.; Rodríguez-Hernandez, J., Advances in the fabrication of antimicrobial hydrogels for biomedical applications. *Materials* **2017**, 10 (3), 232.
6. Thakur, S.; Thakur, V. K.; Arotiba, O. A., History, Classification, Properties and Application of Hydrogels: An Overview. In *Hydrogels*, Springer: 2018; pp 29-50.
7. Koshland Jr, D. E., The molecule of the year. *Science* **1992**, 258 (5090), 1861-1862.
8. Förstermann, U.; Sessa, W. C., Nitric oxide synthases: regulation and function. *European heart journal* **2012**, 33 (7), 829-837.
9. Knowles, R. G.; Moncada, S., Nitric oxide synthases in mammals. *Biochem J* **1994**, 298 (Pt 2), 249-58.
10. Moncada, S.; Higgs, A., The L-arginine-nitric oxide pathway. *The New England journal of medicine* **1993**, 329 (27), 2002-12.
11. Anggard, E., Nitric oxide: mediator, murderer, and medicine. *The Lancet* **1994**, 343 (8907), 1199-1206.

12. Bogdan, C., Nitric oxide and the immune response. *Nature immunology* **2001**, 2 (10), 907.
13. Fang, F. C., Perspectives series: host/pathogen interactions. Mechanisms of nitric oxide-related antimicrobial activity. *The Journal of clinical investigation* **1997**, 99 (12), 2818-2825.
14. Augustine, R.; Alhussain, H.; Zahid, A. A.; Raza Ur Rehman, S.; Ahmed, R.; Hasan, A., Crosslinking Strategies to Develop Hydrogels for Biomedical Applications. Springer Singapore: 2021; pp 21-57.
15. Urzedo, A. L.; Gonçalves, M. C.; Nascimento, M. H.; Lombello, C. B.; Nakazato, G.; Seabra, A. B., Cytotoxicity and Antibacterial Activity of Alginate Hydrogel Containing Nitric Oxide Donor and Silver Nanoparticles for Topical Applications. *ACS Biomaterials Science & Engineering* **2020**, 6 (4), 2117-2134.
16. Choi, M.; Hasan, N.; Cao, J.; Lee, J.; Hlaing, S. P.; Yoo, J.-W., Chitosan-based nitric oxide-releasing dressing for anti-biofilm and in vivo healing activities in MRSA biofilm-infected wounds. *International journal of biological macromolecules* **2020**, 142, 680-692.
17. Kang, Y.; Kim, J.; Lee, Y. M.; Im, S.; Park, H.; Kim, W. J., Nitric oxide-releasing polymer incorporated ointment for cutaneous wound healing. *Journal of Controlled Release* **2015**, 220, 624-630.
18. Hotkar, M. S.; Avachat, A. M.; Bhosale, S. S.; Oswal, Y. M., Preliminary investigation of topical nitroglycerin formulations containing natural wound healing agent in diabetes-induced foot ulcer. *Int Wound J* **2015**, 12 (2), 210-7.
19. Zhou, X.; Wang, H.; Zhang, J.; Li, X.; Wu, Y.; Wei, Y.; Ji, S.; Kong, D.; Zhao, Q., Functional poly(ϵ -caprolactone)/chitosan dressings with nitric oxide-releasing property improve wound healing. *Acta biomaterialia* **2017**, 54, 128-137.

20. Silva, S. Y.; Rueda, L. C.; Marquez, G. A.; Lopez, M.; Smith, D. J.; Calderon, C. A.; Castillo, J. C.; Matute, J.; Rueda-Clausen, C. F.; Orduz, A.; Silva, F. A.; Kampeerapappun, P.; Bhide, M.; Lopez-Jaramillo, P., Double blind, randomized, placebo controlled clinical trial for the treatment of diabetic foot ulcers, using a nitric oxide releasing patch: PATHON. *Trials* **2007**, *8*, 26.
21. Cao, J.; Su, M.; Hasan, N.; Lee, J.; Kwak, D.; Kim, D. Y.; Kim, K.; Lee, E. H.; Jung, J. H.; Yoo, J.-W., Nitric Oxide-Releasing Thermoresponsive Pluronic F127/Alginate Hydrogel for Enhanced Antibacterial Activity and Accelerated Healing of Infected Wounds. *Pharmaceutics* **2020**, *12* (10), 926.
22. Joseph, C. A.; McCarthy, C. W.; Tyo, A. G.; Hubbard, K. R.; Fisher, H. C.; Altscheffel, J. A.; He, W.; Pinnaratip, R.; Liu, Y.; Lee, B. P.; Rajachar, R. M., Development of an Injectable Nitric Oxide Releasing Poly(ethylene) Glycol-Fibrin Adhesive Hydrogel. *ACS Biomater Sci Eng* **2019**, *5* (2), 959-969.
23. Kim, J.; Lee, Y.; Singha, K.; Kim, H. W.; Shin, J. H.; Jo, S.; Han, D.-K.; Kim, W. J., NONOates–polyethylenimine hydrogel for controlled nitric oxide release and cell proliferation modulation. *Bioconjugate chemistry* **2011**, *22* (6), 1031-1038.
24. Lee, J.; Hlaing, S. P.; Cao, J.; Hasan, N.; Ahn, H. J.; Song, K. W.; Yoo, J. W., In Situ Hydrogel-Forming/Nitric Oxide-Releasing Wound Dressing for Enhanced Antibacterial Activity and Healing in Mice with Infected Wounds. *Pharmaceutics* **2019**, *11* (10).
25. Oh, B.; Lee, C. H., Nanofiber-coated drug eluting stent for the stabilization of mast cells. *Pharmaceutical research* **2014**, *31* (9), 2463-78.
26. Park, J.; Kim, J.; Singha, K.; Han, D.-K.; Park, H.; Kim, W. J., Nitric oxide integrated polyethylenimine-based tri-block copolymer for efficient antibacterial activity. *Biomaterials* **2013**, *34* (34), 8766-8775.

27. Pelegriño, M.; de Araujo Lima, B.; do Nascimento, M.; Lombello, C.; Brocchi, M.; Seabra, A., Biocompatible and Antibacterial Nitric Oxide-Releasing Pluronic F-127/Chitosan Hydrogel for Topical Applications. *Polymers* **2018**, *10* (4).
28. Schanuel, F. S.; Santos, K. S. R.; Monte-Alto-Costa, A.; de Oliveira, M. G., Combined nitric oxide-releasing poly (vinyl alcohol) film/F127 hydrogel for accelerating wound healing. *Colloids and Surfaces B: Biointerfaces* **2015**, *130*, 182-191.
29. Seggio, M.; Tessaro, A. L.; Nostro, A.; Ginestra, G.; Graziano, A. C.; Cardile, V.; Acierno, S.; Russo, P.; Catanzano, O.; Quaglia, F., A thermoresponsive gel photoreleasing nitric oxide for potential ocular applications. *Journal of Materials Chemistry B* **2020**, *8* (39), 9121-9128.
30. Zahid, A. A.; Ahmed, R.; Raza Ur Rehman, S.; Augustine, R.; Tariq, M.; Hasan, A., Nitric oxide releasing chitosan-poly (vinyl alcohol) hydrogel promotes angiogenesis in chick embryo model. *Int J Biol Macromol* **2019**, *136*, 901-910.
31. Estes Bright, L. M.; Garren, M. R. S.; Ashcraft, M.; Kumar, A.; Husain, H.; Brisbois, E. J.; Handa, H., Dual Action Nitric Oxide and Fluoride Ion-Releasing Hydrogels for Combating Dental Caries. *ACS Applied Materials & Interfaces* **2022**, *14* (19), 21916-21930.
32. Aveyard, J.; Deller, R. C.; Lace, R.; Williams, R. L.; Kaye, S. B.; Kolegraff, K. N.; Curran, J. M.; D'Sa, R. A., Antimicrobial nitric oxide releasing contact lens gels for the treatment of microbial keratitis. *ACS applied materials & interfaces* **2019**, *11* (41), 37491-37501.
33. de Santana, D. C. A. S.; Pupo, T. T.; Sauaia, M. G.; da Silva, R. S.; Lopez, R. F. V., Nitric oxide photorelease from hydrogels and from skin containing a nitro-ruthenium complex. *International journal of pharmaceutics* **2010**, *391* (1-2), 21-28.

34. Kandoth, N.; Mosinger, J.; Gref, R.; Sortino, S., A NO photoreleasing supramolecular hydrogel with bactericidal action. *Journal of materials chemistry. B* **2013**, *1* (28), 3458-3463.
35. Taite, L. J.; West, J. L., Sustained delivery of nitric oxide from poly (ethylene glycol) hydrogels enhances endothelialization in a rat carotid balloon injury model. *Cardiovascular Engineering and Technology* **2011**, *2* (2), 113-123.
36. Lipke, E. A.; West, J. L., Localized delivery of nitric oxide from hydrogels inhibits neointima formation in a rat carotid balloon injury model. *Acta biomaterialia* **2005**, *1* (6), 597-606.
37. Bohl Masters, K. S.; Lipke, E. A.; Rice, E. E.; Liel, M. S.; Myler, H. A.; Zygourakis, C.; Tulis, D. A.; West, J. L., Nitric oxide-generating hydrogels inhibit neointima formation. *Journal of Biomaterials Science, Polymer Edition* **2005**, *16* (5), 659-672.
38. Thi, T. T. H.; Lee, Y.; Le Thi, P.; Park, K. D., Nitric oxide-releasing injectable hydrogels with high antibacterial activity through in situ formation of peroxyxynitrite. *Acta biomaterialia* **2018**, *67*, 66-78.
39. Cabrini, F. M.; Champeau, M.; de Oliveira, M. G., Effect of Pluronic F127 on the 3D pore morphology of poly (N-isopropylacrylamide-co-acrylic acid) hydrogels and their nitric oxide release from S-nitrosoglutathione. *Journal of Applied Polymer Science* **2020**, 49056.
40. Simões, M. M.; de Oliveira, M. G., Poly(vinyl alcohol) films for topical delivery of S-nitrosoglutathione: effect of freezing-thawing on the diffusion properties. *Journal of biomedical materials research. Part B, Applied biomaterials* **2010**, *93* (2), 416-24.
41. Shishido, S. I. M.; Seabra, A. B.; Loh, W.; de Oliveira, M. G., Thermal and photochemical nitric oxide release from S-nitrosothiols incorporated in Pluronic F127 gel: potential uses for local and controlled nitric oxide release. *Biomaterials* **2003**, *24* (20), 3543-3553.

42. Picheth, G. F.; Marini, T. C.; Taladriz-Blanco, P.; Shimamoto, G. G.; Dos Santos, G.; Meneau, F.; de Oliveira, M. G., Influence of Pluronic F127 microenvironments on the photochemical nitric oxide release from S-nitrosoglutathione. *J Colloid Interface Sci* **2019**, *544*, 217-229.
43. Skeff, M. A.; Brito, G. A.; de Oliveira, M. G.; Braga, C. M.; Cavalcante, M. M.; Baldim, V.; Holanda-Afonso, R. C.; Silva-Boghossian, C. M.; Colombo, A. P.; Ribeiro, R. A.; Moura-Neto, V.; Leitão, R. F., S-nitrosoglutathione accelerates recovery from 5-fluorouracil-induced oral mucositis. *PLoS One* **2014**, *9* (12), e113378.
44. Bright, L. M. E.; Griffin, L.; Mondal, A.; Hopkins, S.; Ozkan, E.; Handa, H., Biomimetic gasotransmitter-releasing alginate beads for biocompatible antimicrobial therapy. *Journal of Colloid and Interface Science* **2022**, 911-921.
45. Broniowska, K. A.; Diers, A. R.; Hogg, N., S-nitrosoglutathione. *Biochimica et Biophysica Acta (BBA)-General Subjects* **2013**, *1830* (5), 3173-3181.
46. Bohl, K. S.; West, J. L., Nitric oxide-generating polymers reduce platelet adhesion and smooth muscle cell proliferation. *Biomaterials* **2000**, *21* (22), 2273-2278.
47. Heinrich, T. A.; Da Silva, R. S.; Miranda, K. M.; Switzer, C. H.; Wink, D. A.; Fukuto, J. M., Biological nitric oxide signalling: chemistry and terminology. *British Journal of Pharmacology* **2013**, *169* (7), 1417-1429.
48. Durão, J.; Vale, N.; Gomes, S.; Gomes, P.; Barrias, C. C.; Gales, L., Nitric Oxide Release from Antimicrobial Peptide Hydrogels for Wound Healing. *Biomolecules* **2018**, *9* (1).
49. Feura, E. S.; Yang, L.; Schoenfisch, M. H., Antibacterial activity of nitric oxide-releasing carboxymethylcellulose against periodontal pathogens. *Journal of Biomedical Materials Research Part A* **2020**.
50. Hebert, A. A.; Siegfried, E. C.; Durham, T.; de León, E. N.; Reams, T.; Messersmith, E.; Maeda-Chubachi, T., Efficacy and tolerability of an investigational nitric

- oxide-releasing topical gel in patients with molluscum contagiosum: A randomized clinical trial. *Journal of the American Academy of Dermatology* **2020**, 82 (4), 887-894.
51. Kapadia, M. R.; Chow, L. W.; Tsihlis, N. D.; Ahanchi, S. S.; Eng, J. W.; Murar, J.; Martinez, J.; Popowich, D. A.; Jiang, Q.; Hrabie, J. A., Nitric oxide and nanotechnology: a novel approach to inhibit neointimal hyperplasia. *Journal of vascular surgery* **2008**, 47 (1), 173-182.
52. Nie, Y.; Zhang, K.; Zhang, S.; Wang, D.; Han, Z.; Che, Y.; Kong, D.; Zhao, Q.; Han, Z.; He, Z.-X., Nitric oxide releasing hydrogel promotes endothelial differentiation of mouse embryonic stem cells. *Acta biomaterialia* **2017**, 63, 190-199.
53. Park, K.; Dawson, J. I.; Oreffo, R. O. C.; Kim, Y. H.; Hong, J., Nanoclay-Polyamine Composite Hydrogel for Topical Delivery of Nitric Oxide Gas via Innate Gelation Characteristics of Laponite. *Biomacromolecules* **2020**.
54. Yao, X.; Liu, Y.; Gao, J.; Yang, L.; Mao, D.; Stefanitsch, C.; Li, Y.; Zhang, J.; Ou, L.; Kong, D., Nitric oxide releasing hydrogel enhances the therapeutic efficacy of mesenchymal stem cells for myocardial infarction. *Biomaterials* **2015**, 60, 130-140.
55. Zhang, K.; Chen, X.; Li, H.; Feng, G.; Nie, Y.; Wei, Y.; Li, N.; Han, Z.; Han, Z.; Kong, D., A Nitric Oxide-Releasing Hydrogel for Enhancing the Therapeutic Effects of Mesenchymal Stem Cell Therapy for Hindlimb Ischemia. *Acta biomaterialia* **2020**.
56. Davies, K. M.; Wink, D. A.; Saavedra, J. E.; Keefer, L. K., Chemistry of the diazeniumdiolates. 2. Kinetics and mechanism of dissociation to nitric oxide in aqueous solution. *Journal of the American Chemical Society* **2001**, 123 (23), 5473-5481.
57. Lourenço, S. D. M.; de Oliveira, M. G., Topical photochemical nitric oxide release from porous poly (vinyl alcohol) membrane for visible light modulation of dermal vasodilation. *Journal of Photochemistry and Photobiology A: Chemistry* **2017**, 346, 548-558.

58. Marcelli, R. H.; de Oliveira, M. G., Nitric oxide-releasing poly(vinyl alcohol) film for increasing dermal vasodilation. *Colloids Surf B Biointerfaces* **2014**, *116*, 643-51.
59. Miller, M.; Megson, I., Recent developments in nitric oxide donor drugs. *British journal of pharmacology* **2007**, *151* (3), 305-321.
60. Yu, Y. T.; Shi, S. W.; Wang, Y.; Zhang, Q. L.; Gao, S. H.; Yang, S. P.; Liu, J. G., A Ruthenium Nitrosyl-Functionalized Magnetic Nanoplatform with Near-Infrared Light-Controlled Nitric Oxide Delivery and Photothermal Effect for Enhanced Antitumor and Antibacterial Therapy. *ACS Appl Mater Interfaces* **2020**, *12* (1), 312-321.
61. Vong, L. B.; Bui, T. Q.; Tomita, T.; Sakamoto, H.; Hiramatsu, Y.; Nagasaki, Y., Novel angiogenesis therapeutics by redox injectable hydrogel-Regulation of local nitric oxide generation for effective cardiovascular therapy. *Biomaterials* **2018**, *167*, 143-152.
62. Kang, M. L.; Kim, H. S.; You, J.; Choi, Y. S.; Kwon, B. J.; Park, C. H.; Baek, W.; Kim, M. S.; Lee, Y. J.; Im, G. I.; Yoon, J. K.; Lee, J. B.; Sung, H. J., Hydrogel cross-linking-programmed release of nitric oxide regulates source-dependent angiogenic behaviors of human mesenchymal stem cell. *Science advances* **2020**, *6* (9), eaay5413.
63. De Groote, M. A.; Fang, F. C., NO inhibitions: antimicrobial properties of nitric oxide. *Clinical Infectious Diseases* **1995**, *21* (Supplement_2), S162-S165.
64. Maloney, S. E.; McGrath, K. V.; Ahonen, M. J. R.; Soliman, D. S.; Feura, E. S.; Hall, H. R.; Wallet, S. M.; Maile, R.; Schoenfisch, M. H., Nitric Oxide-Releasing Hyaluronic Acid as an Antibacterial Agent for Wound Therapy. *Biomacromolecules* **2020**.
65. Yang, Y.; Zhou, Y.; Li, Y.; Guo, L.; Zhou, J.; Chen, J., Injectable and self-healing hydrogel containing nitric oxide donor for enhanced antibacterial activity. *Reactive and Functional Polymers* **2021**, 105003.
66. Akash, M. S.; Rehman, K., Recent progress in biomedical applications of Pluronic (PF127): Pharmaceutical perspectives. *J Control Release* **2015**, *209*, 120-38.

67. Orbach, R.; Adler-Abramovich, L.; Zigerson, S.; Mironi-Harpaz, I.; Seliktar, D.; Gazit, E., Self-assembled Fmoc-peptides as a platform for the formation of nanostructures and hydrogels. *Biomacromolecules* **2009**, *10* (9), 2646-51.
68. Bowerman, C. J.; Ryan, D. M.; Nissan, D. A.; Nilsson, B. L., The effect of increasing hydrophobicity on the self-assembly of amphipathic beta-sheet peptides. *Mol Biosyst* **2009**, *5* (9), 1058-69.
69. Ma, M.; Kuang, Y.; Gao, Y.; Zhang, Y.; Gao, P.; Xu, B., Aromatic-aromatic interactions induce the self-assembly of pentapeptidic derivatives in water to form nanofibers and supramolecular hydrogels. *J Am Chem Soc* **2010**, *132* (8), 2719-28.
70. Moon, C.-Y.; Nam, O. H.; Kim, M.; Lee, H.-S.; Kaushik, S. N.; Cruz Walma, D. A.; Jun, H.-W.; Cheon, K.; Choi, S. C., Effects of the nitric oxide releasing biomimetic nanomatrix gel on pulp-dentin regeneration: Pilot study. *PloS one* **2018**, *13* (10), e0205534.
71. Fasiku, V. O.; Omolo, C. A.; Kiruri, L. W.; Devnarain, N.; Faya, M.; Mocktar, C.; Govender, T., A hyaluronic acid-based nanogel for the co-delivery of nitric oxide (NO) and a novel antimicrobial peptide (AMP) against bacterial biofilms. *International Journal of Biological Macromolecules* **2022**.

CHAPTER 2

COMPARATIVE STUDY OF THE BROAD-SPECTRUM ANTIBACTERIAL ACTIVITY OF NITRIC OXIDE AGAINST CLINICALLY ISOLATED DRUG-RESISTANT BACTERIA¹

¹ L. M. Estes Bright, M. K. Chug, S. Thompson, M. Brooks, E. J. Brisbois, and H. Handa.
2023. To be submitted to *Journal of Colloid and Interface Science*.

ABSTRACT

The development of drug-resistant microorganisms is taking a heavy toll on the biomedical world. Not only are clinical infections costly, but they are becoming increasingly dangerous as bacteria that once responded to standard antibiotic treatment are developing resistance mechanisms that require innovative treatment strategies. Nitric oxide (NO) is a gaseous molecule produced endogenously that has shown potent antibacterial capabilities in numerous research studies. Its multimechanistic antibacterial methods prevent the development of resistance and have shown potential as an alternative to antibiotics. However, there has yet to be a direct comparison study evaluating the antibacterial properties of NO against laboratory and clinically isolated bacterial strains. Herein, commercially available and clinically isolated drug-resistant bacterial strains are compared side-by-side for growth and viability following treatment with NO from *S*-nitrosoglutathione (GSNO), an NO donor molecule. Evaluation of growth kinetics, metabolic activity, and membrane stability will reveal the translational success of NO as an antibacterial therapy and potential alternative to standard antibiotic treatment.

KEYWORDS: *S*-nitrosoglutathione, antibacterial, nitric oxide, clinical, infection

2.1 Introduction

Hospitalization for a minor injury or surgical procedure can lead to disastrous financial and medical outcomes due to the prevalence of hospital-acquired infections (HAIs). Such infections can develop from lack of complete sterility at a surgical site, as well as the implantation or insertion of various medical devices.^{1,2} HAIs are so prevalent in modern medicine that the U.S. Centers for Disease Control and Prevention estimate that 1 in 31 healthcare patients are currently suffering from an HAI on any chosen day.³ Moreover, many of these infections are caused by antimicrobial-resistant microorganisms that have adapted through horizontal gene transfer or persister cell survival to no longer respond to standard antibiotic treatment.⁴⁻⁶ The timeline between antibiotic development and documented resistance is diminishing, as the medical world struggles to keep up with infection-treatment demand. One class of antibiotics, lipoglycopeptides, were first marketed in 2009 and showed promise initially, as it had dual action of inhibiting peptidoglycan synthesis and destabilizing the bacterial cell membrane.⁷ Unfortunately, recent cases have been found already documenting resistance development.⁸ Although infections have diversified and advanced, development and commercialization of new treatments has fallen behind the surge. Antibiotics or antibiotic cocktails are still the standard-of-care for most infections, further promoting resistance development and overlooking the issue at hand. In short, multi-mechanistic antimicrobial treatments must be developed that can kill drug-resistant bacteria and do not further promote resistance development.

One potential therapy that has been utilized in biomedical research for infection treatment is nitric oxide (NO), an endogenously produced gasotransmitter. Within the body, NO is used as a vasodilator, promoter of cell growth, neurotransmitter, and as an antimicrobial molecule released by the immune system to fight foreign pathogens.⁹⁻¹¹ As

a highly reactive free radical molecule, NO quickly reacts with environmental species to produce reactive oxygen species (ROS) and reactive nitrogen species (RNS) that induce oxidative and nitrosative stress to microbes.¹² Through this process, NO does not have a single mode of bacterial killing like most antibiotics. Rather, it attacks all aspects of the microbe, from deactivation of essential enzymes, to lipid peroxidation and breakdown of the bacterial membrane, to direct assault on DNA and DNA repair systems.^{12, 13} This multi-mechanistic strategy ensures that bacteria are unable to successfully mutate or adapt to survive all realms of onslaught. In fact, a previous study showed that when *Staphylococcus aureus* (*S. aureus*), methicillin-resistant *S. aureus* (MRSA), *Staphylococcus epidermidis* (*S. epidermidis*), *Escherichia coli* (*E. coli*), and *Pseudomonas aeruginosa* (*P. aeruginosa*) were exposed to NO-releasing particles, no increase in minimum inhibitory concentration (MIC) was seen for bacteria capable of surviving lethal doses of NO. Further, a serial mutagenesis assay was performed that showed no increase in MIC following repeated exposure to sub-inhibitory concentrations of NO.¹⁴ Though more in-depth studies are needed to confirm the long-term lack of resistance development, NO as an antibacterial treatment shows impressive promise for infection control. However, there has yet to be a direct investigation of the clinical capabilities of NO as an antimicrobial solution. Success in research studies has not yet been shown for potential translation to a clinical setting with more infectious and resistance pathogens.

Here we have, for the first time, characterized the growth and metabolic activity of 'standard' commercially available bacterial strains alongside clinically isolated strains of the same species with varying levels of drug-resistance. S-nitrosoglutathione (GSNO), an endogenous NO donor molecule, was chosen for the study due to its high solubility in aqueous solutions. GSNO concentrations ranging from 1 mM to 17.5 mM were characterized for NO release and used in all subsequent studies. The antibacterial nature

of NO released from GSNO was investigated against two Gram-positive and two Gram-negative commercial and drug-resistant bacterial strains. Through growth curve analysis, metabolic quantification, and membrane permeability studies, the broad-spectrum capabilities of NO were directly compared amongst lab strains and drug-resistant clinical isolates.

2.2 Materials and Methods

2.2.1 Materials

Antifoam concentrate, dimethyl sulfoxide (DMSO), and MHB broth and agar were purchased from Sigma Aldrich. The Griess assay reagent kit was purchased from Thermo Fisher Scientific (Waltham, MA, USA). The MTT assay was obtained from Roche (Basel, Switzerland). Nitrocefin was acquired from Cayman Chemical Company (Ann Arbor, MI, USA). All lab strains of bacteria; *Escherichia coli* (ATCC 25922), *Pseudomonas aeruginosa* (ATCC 9027), methicillin-resistant *Staphylococcus aureus* (ATCC BAA 41), and *Staphylococcus epidermidis* (ATCC 35984); were purchased from the American Type Tissue Collection (ATCC). All clinical strains of bacteria; *Escherichia coli* (AR-0077), *Pseudomonas aeruginosa* (AR-0230), methicillin-resistant *Staphylococcus aureus* (AR-1003), and *Staphylococcus epidermidis* (AR-0726); were clinical isolates obtained from the Centers for Disease Control.

2.2.2 S-nitrosoglutathione synthesis

The synthesis of S-nitrosoglutathione was based on a previously described protocol. In short, 2.7 g of reduced glutathione was added to 20 mL of DI water. 6.25 mL of 2 M HCl was added to this mixture. Upon addition of the acid and subsequent vortexing, the glutathione dissolved. The solution was chilled in an ice bath for ten minutes, and then 645 mg of sodium nitrite was added. The solution turned a dark red color and was kept at 0°C in the dark for 40 minutes. Fifteen milliliters of chilled acetone was then added with

stirring. After ten minutes, a light pink precipitate formed. The precipitate was isolated by vacuum filtration and dried overnight under vacuum. After drying, the nitrosated glutathione was stored at -20°C. UV-Vis spectroscopy of the final product showed the characteristic RSNO peak at 340 nm (**Figure 2.S1**). Further, Fourier Transform Infrared Spectroscopy (FTIR) revealed the disappearance of the thiol peak and successful conjugation of the NO bond in the synthesized GSNO molecule (**Figure 2.S2**).

2.2.3 GSNO solution

The antimicrobial GSNO treatment solutions were made by first making a stock solution of 35 mM GSNO in MHB. The stock was then sterile filtered and treatment solutions were diluted to make final treatments at 2x concentrations. Identical solutions were made of 2x concentrations of GSNO, but in PBS instead of MHB for nitrocefin studies.

2.2.4 Nitric oxide release from GSNO

The nitric oxide (NO) release from the GSNO solutions was measured using the gold standard Zysense chemiluminescence Nitric Oxide Analyzer (NOA) 280i (Frederick, CO). For this study, GSNO powder (> 90% purity) was weighed out and dissolved in 9 mL of MHB media. Samples were tested for NO release at 7 different concentrations (1, 5, 7.5, 10, 12.5, 15, and 17.5 mM) to analyze the NO release profile under physiological conditions. In order to evaluate the NO release, first the baseline reading was obtained by adding 1 mL of MHB media with 35 μ L of antifoam agent into an amber NOA cell and allowed to run for 3-5 min. Later, 1 mL of the testing concentration was added to the NOA cell such that the final testing concentration of the solution was 1, 5, 7.5, 10, 12.5, 15, and 17.5 mM. Nitric oxide released from the solutions at physiological temperature (37 °C) was detected by the photomultiplier tube and resultant ppm/ppb of NO released was collected at 1 sec intervals. Samples were incubated at 37 °C in between experiments and NO

release was quantified at 0, 6 and 24 h timepoints (n = 3). Data from the study was normalized to the volume of the solution and presented as mean \pm standard deviation.

2.2.5 Bacterial preparation

The preparation of the bacterial solutions began with the inoculation of a single colony of the specified microbe into MHB media. The inoculum was placed in a shaking incubator (150 rpm, 37 °C) until log-phase growth was reached. At this point, the bacterial suspension was collected by centrifugation, rinsed once with PBS, and resuspended into MHB media. The absorbance of the suspension was measured using UV-Vis Spectroscopy and diluted to give a final bacterial concentration of $\sim 10^7$ CFU mL⁻¹, which was confirmed for each bacterial strain using serial dilutions, agar plating, and colony counting (**Figure 2.S3**). The prepared bacterial solution was then used for growth curve, MTT, and propidium iodide assays.

2.2.6 Growth curve studies

Growth curves of Gram-positive and Gram-negative bacterial species were studied to investigate the antimicrobial potential of NO-releasing GSNO against standardized strains and clinical bacterial isolates. GSNO and bacterial solutions were prepared as described above, then equal volumes of each were added to the wells of a 96-well plate. The well plate was sealed with parafilm and placed in a multi-plate reader (BioTek, Winooski, VT, USA) at a maintained temperature of 37 °C with constant agitation. The absorbance of the wells was read at 600 nm every 30 minutes for 24 h, yielding a growth curve. A blank prepared with media (controls) and GSNO in media (treatments) was used to calculate final absorbance values. Growth curves (n = 3 wells per treatment) were confirmed with biological triplicates and the average absorbances from each experiment were used to calculate growth relative to control growth. Absorbance changes < 0.1 OD over the 24 h period for individual wells were deemed as no growth and these values were

not further analyzed. Growth curves were plotted in GraphPad and fitted to the Gompertz growth model, a model commonly used to plot bacterial growth kinetics.^{15, 16} The Gompertz model has been regarded as the best model to describe bacterial growth data as it is easy to use, with all three equation parameters relating to a biological meaning.¹⁷

2.2.7 MTT metabolic activity assay

The metabolic activity of bacteria with varying GSNO treatments was quantified using an MTT assay, with modifications from a previous protocol.¹⁸ In short, GSNO in MHB media at 2x concentrations and bacterial solutions containing 10^8 CFU mL⁻¹ in MHB media were combined with equal volumes into microcentrifuge tubes. The tubes were then covered and placed in a shaking incubator (37 °C and 150 rpm) for 24 h. At that time, microcentrifuge tubes were centrifuged for 15 min, the supernatant was discarded, and the bacterial pellet was resuspended in PBS. Following vortexing, 90 µL of each tube was added to a 96-well plate along with 10 µL of the MTT reagent at a treatment concentration of 0.5 mg mL⁻¹. The well plate was then placed in a shaking incubator (37 °C and 150 rpm) for 30 minutes. During this time, bacteria with functioning metabolisms enzymatically reduced the tetrazolium dye to yield an insoluble formazan salt. After 30 minutes, 100 µL of DMSO was added to the wells to dissolve the formazan salt, which was then measured using OD₅₇₀ on a plate reader.

2.2.8 Propidium iodide membrane permeability assay

The antibacterial efficacy of GSNO via membrane degradation or permeation was investigated using a microplate propidium iodide (PI) assay, with modifications from a prior protocol.¹⁹ In short, bacterial suspensions were prepared as previously described and added in equal volumes with PBS (negative control) or GSNO treatments to Eppendorf tubes and incubated at 37 °C and 150 rpm for 4 h. Following incubation, tubes were centrifuged at 13,000 g for 10 min, rinsed with PBS, and centrifuged again. The

supernatant was discarded, and $10 \mu\text{g mL}^{-1}$ PI was added to each tube. Bacterial cells were incubated with PI for 30 min at $37 \text{ }^\circ\text{C}$ and 150 rpm, followed by centrifugation and two PBS rinsing steps. Finally, the bacteria were resuspended in $200 \mu\text{L}$ PBS and $150 \mu\text{L}$ from each tube was added to the well of a black-walled 96-well plate. Fluorescence was measured on a plate reader at an excitation of 542 nm and emission of 600 nm for 15 minutes and averages were plotted for analysis.

2.2.9 Statistical analysis

Data obtained for all studies are expressed as mean \pm standard deviation. Statistical analysis was performed using two-way ANOVA and p values < 0.05 were considered statistically significant for all experiments. $N \geq 3$ were used for each treatment in all studies.

2.3 Results and Discussion

2.3.1 Nitric oxide release from GSNO

Nitric oxide release from GSNO, and other RSNO molecules, is catalyzed by heat, light, hydrolysis, and metal ions (**Figure 2.1A**). GSNO is a naturally synthesized endogenous mediator of NO with elevated stability, innate biocompatibility and potential to release NO in physiological conditions.^{20, 21} Therefore, inclusion of GSNO as an NO donating compound for the development of biocompatible materials with antibacterial potential is of considerable interest. The NO release from the GSNO solutions was measured using a chemiluminescence NO analyzer at three different timepoints (0, 6 and 24 h) at $37 \text{ }^\circ\text{C}$ (**Figure 2.1B**). Results from the study show a positive correlation between GSNO concentration and NO release levels (**Table 2.S1**). It was observed that the lower concentrations of GSNO (1, 5, and 7.5 mM) showed a sharp decline in the NO release levels from 0 to 24 h of testing timepoint. Notably, the levels of NO release increased with increasing concentration of GSNO up to 10 mM in MHB at 0 h time point. However,

concentrations above 10 mM showed no significant increase in NO release at 0 h timepoint suggesting saturation of release at higher concentrations at the initial timepoint. Nonetheless, the NO release from these higher concentration samples (10, 12.5, and 15 mM) were seen to increase at 6 and 24 h. This can be attributed to the greater rate of cleavage of NO from GSNO at physiological conditions (pH 7.4 and 37 °C) over longer durations of time.²⁰ This data aligns with the previously reported studies where the NO release from GSNO solution can be modulated via changing the concentration of the solution at physiological conditions for at least 24 h.²²

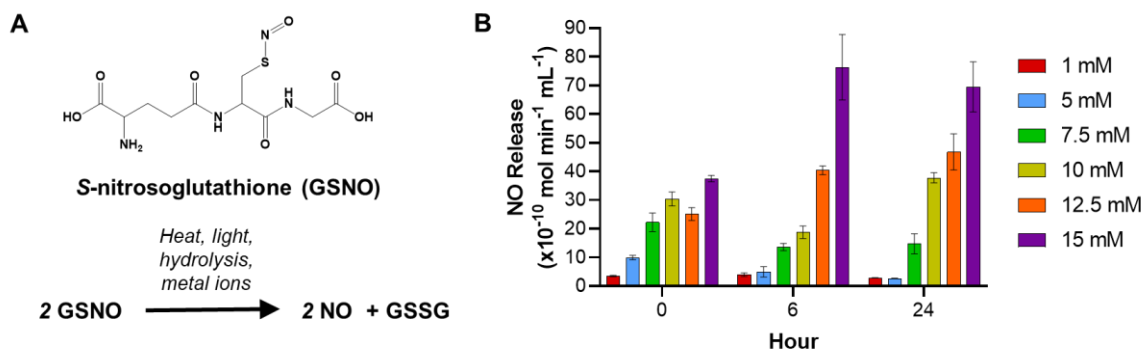


Figure 2.1 NO release from GSNO **A)** is catalyzed by heat, light, hydrolysis, and metal ions. **B)** Release of NO from the GSNO concentrations utilized in the following studies was quantified at 0 h, 6 h, and 24 h.

2.3.2 Growth curve studies

The exponential growth of bacteria can be partitioned into four phases: lag, exponential, stationary, and death.²³ The lag phase describes the time when the specific growth rate is essentially zero, shortly after the inoculum has been placed into fresh medium.²⁴ The exponential phase follows, after the initial population size has doubled and the growth rate is approaching its maximum value, found at the inflection point and described as the lag time.¹⁶ Following the maximum growth, the population enters into the

stationary phase, characterized by no net growth of bacteria, as growth is balanced equally by cell death. Lastly, bacteria enter the death phase, where more viable cells are dying than are metabolizing and dividing. However, the death phase is not deeply analyzed in this paper, as we are more interested in the initial growth of bacteria following GSNO treatment. Observation of the growth profiles of control and GSNO treated bacterial strains gives us premier insight to the time-dependent inhibition and complete killing of NO. As most infections can be more easily controlled in the first few hours, delay of initial growth is crucial to proper infection control.

2.3.2.1 *Escherichia coli*

The first tested pathogen was *Escherichia coli* (*E. coli*), a Gram-negative bacterium associated with multiple types of HAIs, from SSI to medical-device associated pneumonia, especially in pediatric populations.^{1, 25} The commercial strain (lab) and clinical strain were treated with the same concentrations of GSNO over a 24 h period with promising results. Growth of the lab strain was consistent until the 15 mM treatment, where total killing occurred (**Figure 2.2A**). However, the clinical strain began showing inhibition at 10 mM, with greater delay for 12.5 mM and bacteriostatic behavior at 15 mM (**Figure 2.2B**). Fitting the representative growth curves to a Gompertz growth equation allows us to quantify the relative growth and inhibition following treatment (**Tables 2.S2-3**).²⁶ Various models have been used to characterize bacterial growth and the Gompertz model has been distinguished as a model with high accuracy and ease of use, consolidating growth factors into 3 parameters.¹⁷

$$Y = Y_M * \left(\frac{Y_0}{Y_M} \right)^{e(-K*x)}$$

In the Gompertz equation and using the notation provided in GraphPad, Y_0 is the starting population and Y_M is the maximum population asymptote. K determines the lag time, as

$1/K$ is the x -value of the inflection point of the curve, the x -axis intercept of the tangent of the maximum growth rate (**Figure 2.S4**). Plotting the x -values of the inflection point can visually demonstrate changes in lag time for bacterial growth with GSNO treatment. As shown in **Figure 2.2C**, there is enhanced lag time for the clinical *E. coli* bacterial strain at GSNO concentrations of 10 mM, 12.5 mM, and 15 mM, whereas lab *E. coli* only showed delay at 12.5 mM. Lag time for lab *E. coli* at 15 mM was not plotted as that treatment did not show growth > 0.1 OD over the 24 h period and thus was not further analyzed. This enhanced lag time means that when the same concentration of GSNO was used to treat the lab and clinical *E. coli* strains, there was a delay in growth for the clinical strain that was seen at lower treatment values compared to the lab strain. However, when experiments in biological triplicates were analyzed for growth relative to control wells after 24 h of treatment, there was no statistically significant difference among GSNO treatment concentrations in lab vs. clinical *E. coli* (**Figure 2.2D**) and the same number of wells showed growth for both strains (**Figure 2.2E**). In summary, although some wells of clinical *E. coli* showed delayed growth following GSNO treatment at higher concentrations, overall antibacterial efficacy of GSNO against both *E. coli* strains does not appear to differ. This demonstrates the potential for favorable clinical treatment against *E. coli* for NO-releasing materials tested only against laboratory strains.

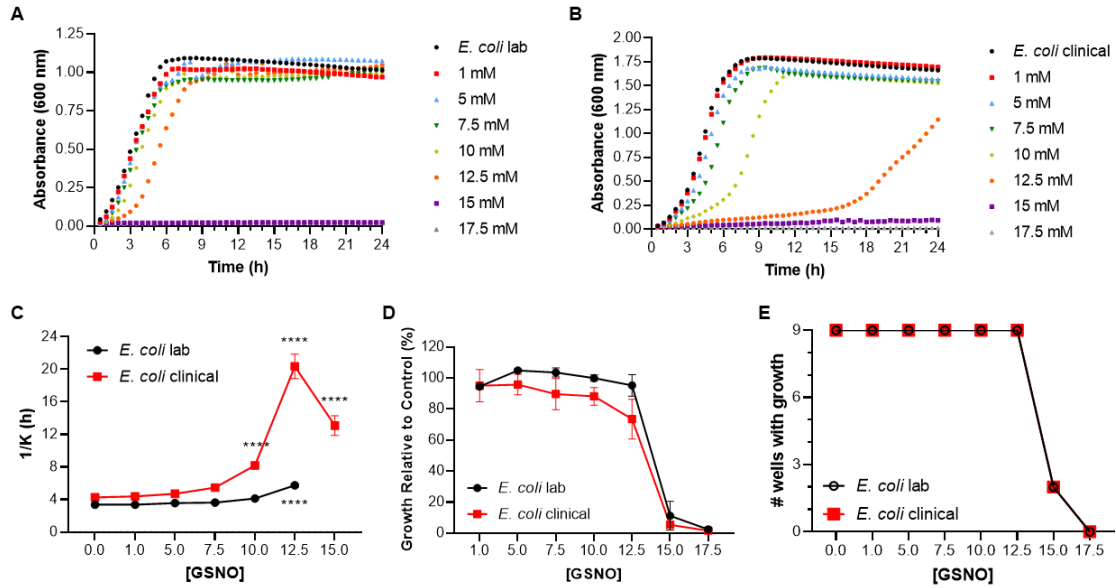


Figure 2.2 *E. coli* growth curves of **A)** lab and **B)** clinical strains. **C)** calculated lag time of each GSNO treatment following Gompertz growth curve fitting. **D)** Relative growth of each GSNO treatment compared to treatment with just MHB (control). **E)** Report of the number of wells (out of 9 total) with growth in 3 independent studies combined for both lab and clinical strains. Statistical significance is denoted by **** $p < 0.0001$.

2.3.2.2 *Pseudomonas aeruginosa*

The second Gram-negative bacteria tested in this study was *Pseudomonas aeruginosa* (*P. aeruginosa*). *P. aeruginosa* is often responsible for CAUTIs, SSIs, and VAP, a highly opportunistic pathogen.^{1, 27} There is also increasing concern for *P. aeruginosa* infections, as its relatively large genome has shown factors associated with antibiotic resistance of almost all classes of antibiotics. Thus, the need for alternative infection treatments is vital, and NO could provide the respite that the biomedical world is looking for. The commercial strain of *P. aeruginosa* (ATCC 9027) was purchased from ATCC with no known drug resistance, while the clinical strain (AR-0230) was isolated by the CDC and characterized for antibiotic resistance against 11 of the 14 tested antibiotics including amikacin, cefepime, ceftazidime, ciprofloxacin, doripenem, gentamicin,

imipenem, levofloxacin, meropenem, piperacillin-tazobactam, and tobramycin. From these studies, the known resistance mechanisms were classified as: (aac(3)-IId, aadA2, cmlA1, dfrB5, OXA-4, OXA-50, PAO, tet(G), VIM-2. This vast array of defensive tactics provides a slew of issues for antibiotics, but NO killing mechanisms are not target-specific and could therefore overcome these protections.

Looking at the representative 24 h growth curves for the lab and clinical strains, it does not appear that the antibacterial capabilities of NO against *P. aeruginosa* are inhibited by the multitude of antibiotic resistance mechanisms found in the clinical strain (**Figure 2.3A-B**). As growth of lab *P. aeruginosa* at the 12.5 mM GSNO treatment is inhibited for several hours, it displays complete lack of growth for the clinical strain at the same concentration. Even at the 10 mM treatment concentration, both lab and clinical *P. aeruginosa* strains exhibit significantly enhanced lag times (**Figure 2.3C, Tables 2.S4-5**), with fewer overall clinical wells displaying growth in 3 separate experiments (**Figure 2.3E**). However, when relative growth compared to control wells over 3 independent experiments was analyzed, there was no significant difference between the lab and clinical strains (**Figure 2.3D**). All in all, both Gram-negative bacteria strains tested revealed no lack of antibacterial efficacy of NO regardless of the antibiotic mechanisms present in the clinical strains.

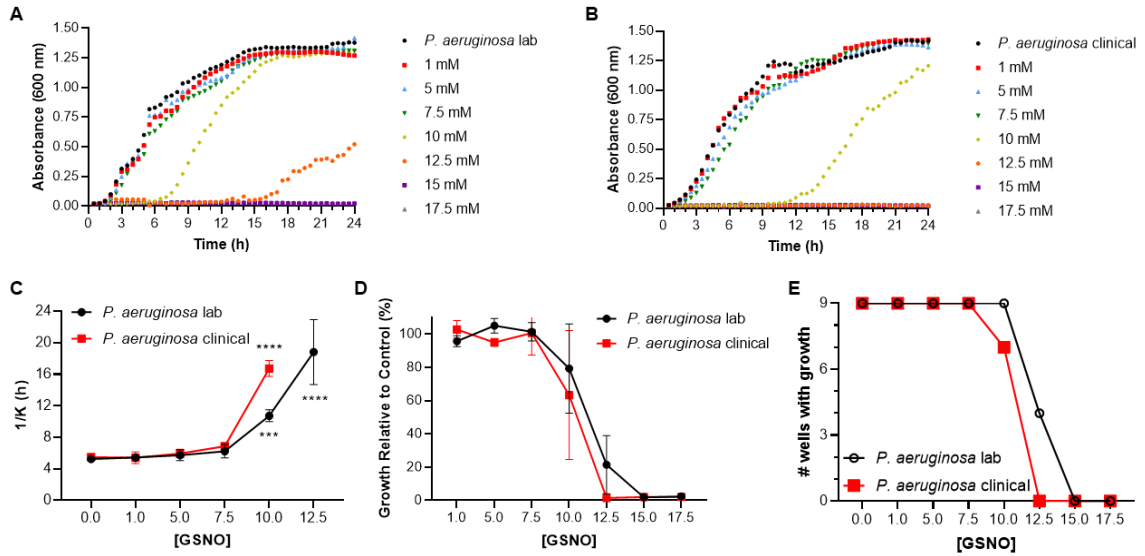


Figure 2.3 *P. aeruginosa* growth curves of **A)** lab and **B)** clinical strains. **C)** calculated lag time of each GSNO treatment following Gompertz growth curve fitting. **D)** Relative growth of each GSNO treatment compared to treatment with just MHB (control). **E)** Report of the number of wells (out of 9 total) with growth in 3 independent studies combined for both lab and clinical strains. Statistical significance is denoted by *** $p < 0.001$ and **** $p < 0.0001$.

2.3.2.3 Methicillin-resistant *Staphylococcus aureus*

Staphylococcus aureus (*S. aureus*) is abundantly present on the human skin, and therefore a large contributor to biomedical infections such as bloodstream infections, surgical site infections, and pneumonia.^{28, 29} The widespread use of antibiotics in *S. aureus* treatment has led to the development of methicillin-resistant *S. aureus* (MRSA), which is now one of the most common pathogens associated with HAIs.²⁸ The commercially available lab strain of MRSA that was tested is ATCC BAA 41, while the clinically isolated strain is AR-1003, with a known resistance to penicillin via the *mecA* resistance mechanism. The *mecA* gene is responsible for encoding a penicillin binding protein (PBP2a) that has a significantly lower affinity for β -lactam antibiotics.³⁰ *S. aureus* strains with this resistance are able to actively continue carrying out cell wall biosynthesis even

during treatment with antibiotic levels that have shown to cause inhibition, making infection treatment more difficult.

Plots of the 24 h growth curves of both strains revealed similar trends, with growth up to the 15 mM GSNO treatment (**Figure 2.4A-B**). Though 17.5 mM showed complete killing for both strains, significantly increased lag time before growth was seen at concentrations of 10 mM and higher for both lab and clinical (**Figure 2.4C, Tables 2.S6-7**). Further, when growth relative to controls and number of wells with growth was analyzed, both strains displayed decreased growth at the same GSNO treatment concentrations and comparable measures of growth (**Figure 2.4D-E**). Once again, NO antibacterial efficacy was not inhibited in the clinical isolate of MRSA compared to the commercially purchased strain.

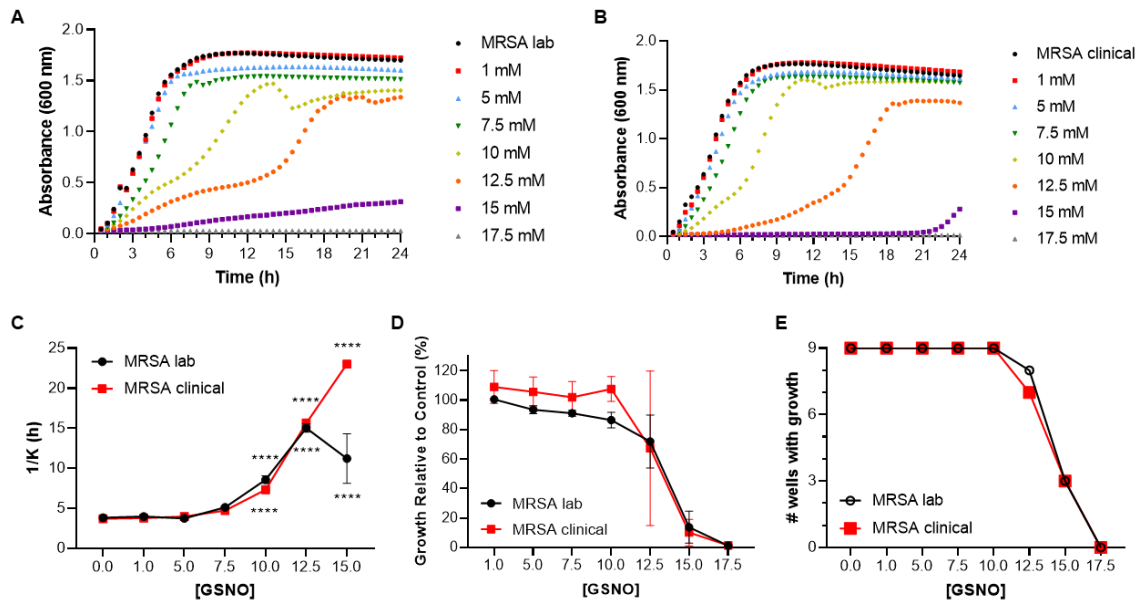


Figure 2.4 MRSA growth curves of A) lab and B) clinical strains. C) Relative growth of each GSNO treatment compared to treatment with just MHB (control). D) Report of the number of wells (out of 9 total) with growth in 3 independent studies combined for both lab and clinical strains. Statistical significance is denoted by ** $p < 0.0001$.**

2.3.2.4 *Staphylococcus epidermidis*

Staphylococcus epidermidis (*S. epidermidis*) is another bacterium, along with *S. aureus*, that is a component of healthy skin microflora. However, it has now become one of the most frequently involved pathogens in HAIs, especially those involving indwelling medical devices.^{31,32} Common infections caused by *S. epidermidis* include cardiac device, vascular graft, surgical site, prosthetic joint, and central venous system shunt infections.³³ As a dangerous and highly pathogenic bacteria, *S. epidermidis* treatment with NO is of high interest and importance. The commercially purchased strain of *S. epidermidis* used for studies is ATCC 35984, while the clinical isolate is AR-0726. Following resistance analysis, *S. epidermidis* AR-0726 displayed resistance to erythromycin, gentamicin, levofloxacin, linezolid, oxacillin, and penicillin, with *mecA* as the diagnosed resistance mechanism.

Growth curves of both *S. epidermidis* strains demonstrated similar levels of growth inhibition by GSNO (**Figure 2.5A-B**). While 15 mM and 17.5 mM completely prevented microbial growth, 10 mM and 12.5 mM both showed enhanced inhibition. In fact, the lag times for 10 mM and 12.5 mM GSNO treatment were significantly increased compared to the control wells (**Figure 2.5C, Tables 2.S8-9**). When comparing three biological replicate studies, clinical *S. epidermidis* showed greater growth inhibition at the 10 mM and 12.5 mM treatment levels compared to the lab strain, and also exhibited fewer wells with growth overall (**Figure 2.5D-E**).

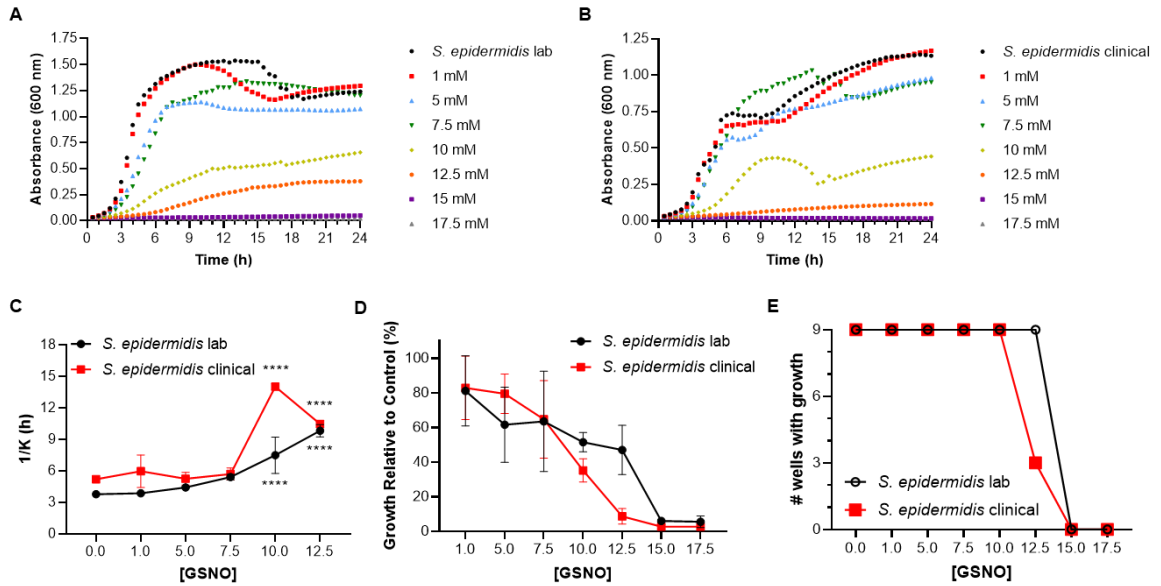


Figure 2.5 *S. epidermidis* growth curves of **A)** lab and **B)** clinical strains. **C)** Relative growth of each GSNO treatment compared to treatment with just MHB (control). **D)** Report of the number of wells (out of 9 total) with growth in 3 independent studies combined for both lab and clinical strains. Statistical significance is denoted by **** $p < 0.0001$.

2.3.3 Metabolic activity and membrane permeability of NO-treated bacteria

For all four tested bacterial species, treatment with varying concentrations of GSNO revealed comparable killing efficiency against lab and clinical isolate strains. Measuring bacterial growth with absorbance is widely used and accepted, as the optical density of a solution at 600 nm is directly correlated with the number of bacteria present in the solution. However, absorbance is a better indicator of bacterial quantity rather than a measure of the viability of the cells. Therefore, an MTT assay and propidium iodide membrane permeability assay were performed to investigate the relative viability of the bacteria following GSNO treatment at the concentrations utilized in the above studies.

To investigate the effect of NO on the metabolic activity of the varying strains of bacteria, a colorimetric MTT assay was performed. In metabolically active cells, the

tetrazolium dye is reduced to an insoluble formazan salt by NADPH-dependent oxidoreductase enzymes. The purple formazan salt is then dissolved and the absorbance of the solution is measured, which is correlated to the number of metabolically-active bacteria present.³⁴ Treatment of bacteria with NO is expected to show a reduction in metabolic activity, as NO has been found to oxidize proteins and nitrosate thiols, which can modify protein functions. NO can also directly attack bacterial DNA and DNA repair systems, altering the overall function of the cell. Further, NO and its many reactive side-products are capable of inactivating numerous enzymes involved in metabolic activity and physiological signal transduction.^{12, 35, 36}

Metabolic activity of a bacterial solution treated for 24 h with GSNO was measured on all 4 bacterial species, including both lab and clinical strains. Treatment of lab *E. coli* revealed an rise in metabolic activity for 1 mM GSNO, followed by a decline with increasing GSNO concentrations, with the exception of 12.5 mM (**Figure 2.6A**). Clinical *E. coli* displayed less of a concentration-dependent response, with no significant change in metabolic activity until 15 mM treatment. NO demonstrated similar antibacterial effects against lab and clinical strains of *P. aeruginosa*, with complete knockout of metabolic activity at 12.5 mM GSNO and only slight decrease after 10 mM GSNO treatment of the clinical strain (**Figure 2.6B**). Gram-positive bacterial treatment showed similar results. The MRSA lab strain exhibited dose-dependent reduction in metabolic activity, whereas no significant changes were seen in the clinical strain until 12.5 mM treatment (**Figure 2.6C**). Clinical *S. epidermidis* showed metabolic reduction at 7.5 mM treatment, while both lab and clinical displayed decreased to no metabolic activity at 10 mM treatments and beyond (**Figure 2.6D**). The MTT assay revealed that reduction in metabolic activity appeared to be strain-specific, with variations in susceptibility to metabolic reduction.

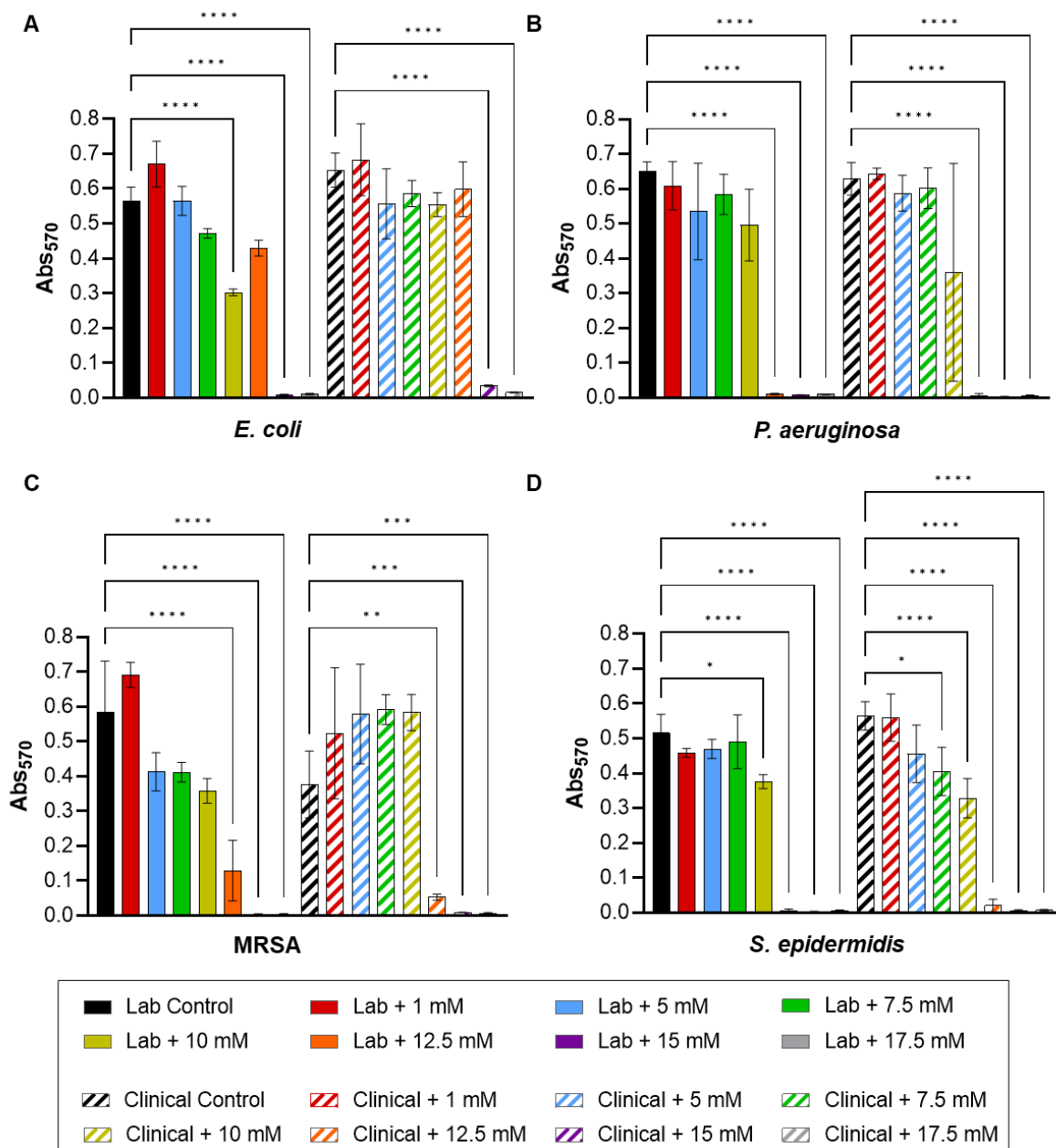


Figure 2.6 Metabolic activity of **A)** *E. coli*, **B)** *P. aeruginosa*, **C)** MRSA, and **D)** *S. epidermidis* following 24 h treatment of GSNO. Statistical analysis is denoted by * $p < 0.05$, ** $p < 0.01$, *** $p < 0.001$, and **** $p < 0.0001$ compared to untreated bacteria.

Aside from quantifying metabolic activity of the bacteria, another method for determining viability is through measurement of the membrane permeability, as disrupted

bacterial membranes allow leakage of internal cell components or complete lysis of the cell, leading to bacterial cell death. As NO is a free radical gas, it can penetrate into bacterial membranes, causing damage to the lipid structures that protect the internal cell components. Further, it has been shown to disrupt membrane transports, creating gaps in the membrane that lead to cell death.^{12, 35, 36} Membrane permeability of NO-treated bacteria was determined using a propidium iodide assay. Propidium iodide (PI) is a fluorescent dye that binds to the DNA of cells. However, it is unable to penetrate the cell membranes of actively living cells, so it is often used to signal cell death for quantification or microscopy.³⁷

Membrane permeability studies were initially conducted after 24 h to mimic all prior studies, but by that time point, higher GSNO concentrations had completely ruptured bacterial membranes, allowing PI-stained internal cell components to get washed away during the rinsing steps of the procedure. Therefore, higher GSNO treatments displayed limited fluorescence due to the lack of somewhat-intact cells present. Therefore, quantification of the PI stain in bacteria was obtained after 4 h treatment of the various GSNO concentrations. Analysis after only 4 h gives greater insight to the mechanism of NO's antibacterial capacity at varying GSNO concentrations. The first pathogen tested, *E. coli*, revealed that the lab strain showed significant membrane degradation at 10, 12.5, 15, and 17.5 mM GSNO (**Figure 2.7A**). In comparison, a statistically significant increase in relative fluorescence units (RFU) compared to control was only seen at the highest GSNO concentration tested against the clinical strain. As shown in the earlier studies conducted, similar killing was achieved by 24 h, suggesting that the clinical isolate of *E. coli* is not as susceptible to membrane permeation by NO in the first few hours of treatment. The second Gram-negative pathogen tested was *P. aeruginosa*, which showed comparable increases in membrane permeability by PI at each increasing GSNO treatment (**Figure 2.7B**). MRSA

4 h treatment with GSNO demonstrated a stepwise increase in RFU as GSNO concentration increased, with similar permeability seen for both lab and clinical strains (**Figure 2.7C**). *S. epidermidis* revealed a similar trend, displaying significant membrane degradation beginning at 12.5 mM GSNO for lab and 10 mM GSNO for clinical strains (**Figure 2.7D**). For all four bacterial species examined, *E. coli* was the only one that showed significant differences between the lab and clinical pathogens in terms of membrane penetration by PI in the 4 h study. Further studies should be conducted to explore the time-dependence of these variations within the *E. coli* species.

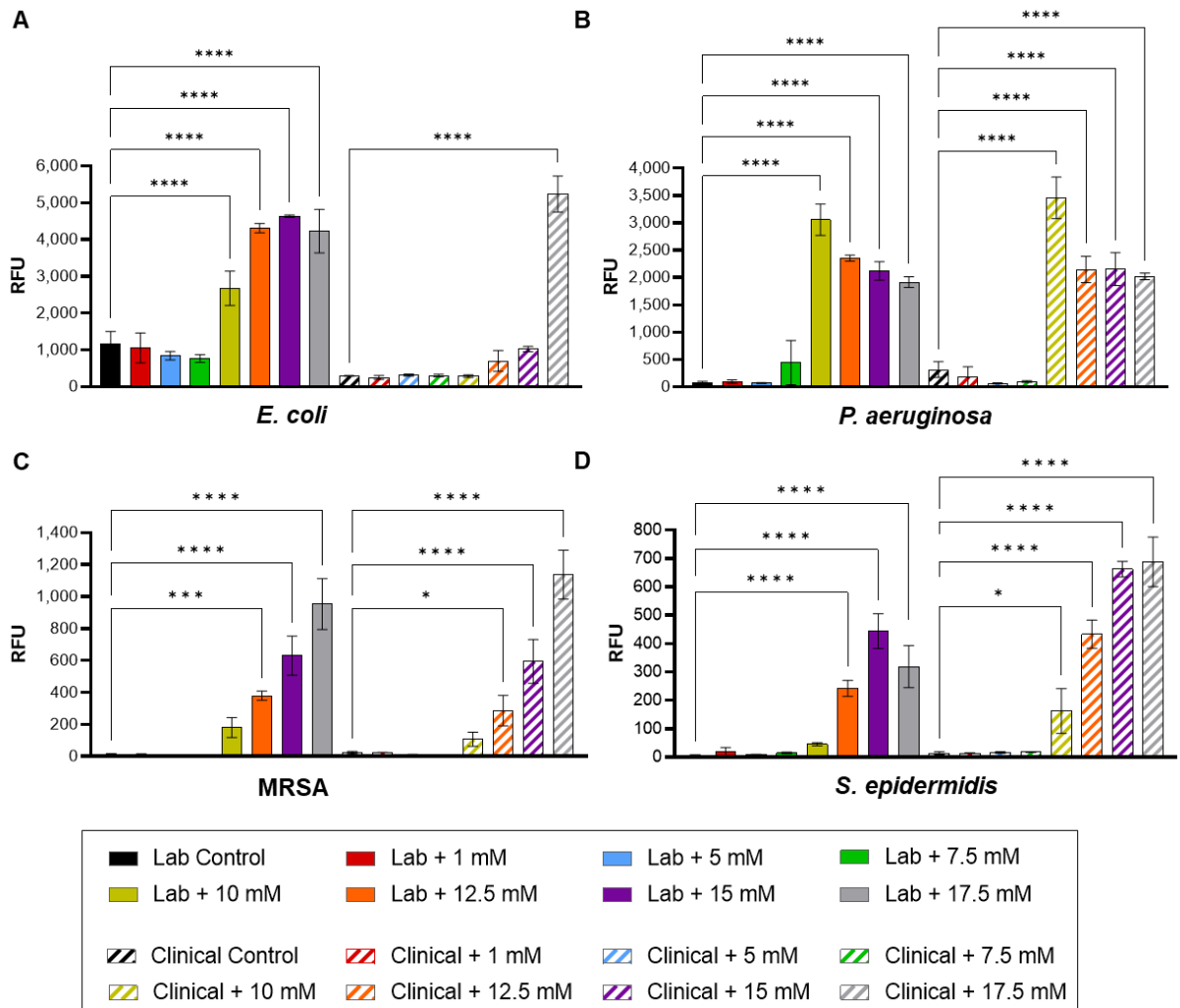


Figure 2.7 Membrane permeability of **A)** *E. coli*, **B)** *P. aeruginosa*, **C)** MRSA, and **D)** *S. epidermidis* following treatment with GSNO, as determined by propidium iodide penetration.

2.4 Conclusions

In summary, commercially available and clinically isolated bacteria samples of *E. coli*, *P. aeruginosa*, MRSA, and *S. epidermidis* were treated with GSNO concentrations ranging from 1 mM to 17.5 mM. The antibacterial activity of NO released from GSNO was compared to determine if NO could successfully inhibit and kill bacteria with known drug-resistance mechanisms as well as those without. Growth curve analysis of all pathogens

revealed comparable levels of killing by NO, and oftentimes clinical strains showed greater susceptibility within a 24 h period. Fitting of growth curves to a Gompertz growth model revealed enhanced lag times for clinical isolates in all four bacteria strains. Analysis of the metabolic activity of all GSNO-treated bacteria revealed analogous diminishing of bacterial metabolism due to the multi-mechanistic antibacterial approach of NO gas. Lastly, a membrane permeability assay was performed using propidium iodide that revealed equivalent membrane degradation or permeation by NO in three of the four pathogens tested. The Gram-negative pathogen, *E. coli*, revealed a more dose-dependent response to NO treatment for the lab strain, whereas the clinical strain did not show penetration until 17.5 mM GSNO. Further studies should be conducted to investigate the intricacies of any variations seen in treatment of bacteria with NO, as its nonspecific antibacterial mechanisms highlight its potential as an alternative to antibiotics in clinical infection treatment.

Author Contributions

Lori M. Estes Bright: Conceptualization, Development of Methodology, Validation, Formal Analysis, Investigation, Writing – Original Draft, Visualization. **Manjot Kaur Chug:** Investigation, Formal Analysis, Writing – Review and Editing, Visualization. **Stephen Thompson:** Validation, Investigation, Formal Analysis, Writing – Review and Editing. **Megan Brooks:** Conceptualization, Methodology, Supervision. **Elizabeth J. Brisbois:** Supervisions, Resources, Funding Acquisition. **Hitesh Handa:** Supervision, Resources, Funding Acquisition.

2.5 References

1. Babcock, H. M.; Zack, J. E.; Garrison, T.; Trovillion, E.; Kollef, M. H.; Fraser, V. J., Ventilator-associated pneumonia in a multi-hospital system differences in microbiology by location. *Infection Control & Hospital Epidemiology* **2003**, *24* (11), 853-858.
2. Lobdell, K. W.; Stamou, S.; Sanchez, J. A., Hospital-Acquired Infections. *Surgical Clinics of North America* **2012**, *92* (1), 65-77.
3. HAI Data. <https://www.cdc.gov/hai/data/index.html>.
4. Chokshi, A.; Sifri, Z.; Cennimo, D.; Horng, H., Global contributors to antibiotic resistance. *Journal of global infectious diseases* **2019**, *11* (1), 36.
5. De Oliveira, D. M.; Forde, B. M.; Kidd, T. J.; Harris, P. N.; Schembri, M. A.; Beatson, S. A.; Paterson, D. L.; Walker, M. J., Antimicrobial resistance in ESKAPE pathogens. *Clinical microbiology reviews* **2020**, *33* (3), e00181-19.
6. Reygaert, W. C., An overview of the antimicrobial resistance mechanisms of bacteria. *AIMS microbiology* **2018**, *4* (3), 482.
7. Wenzler, E.; Rodvold, K. A., Telavancin: the long and winding road from discovery to food and drug administration approvals and future directions. *Clinical Infectious Diseases* **2015**, *61* (suppl_2), S38-S47.
8. Kussmann, M.; Karer, M.; Obermueller, M.; Schmidt, K.; Barousch, W.; Moser, D.; Nehr, M.; Ramharter, M.; Poepl, W.; Makristathis, A.; Winkler, S.; Thalhammer, F.; Burgmann, H.; Lagler, H., Emergence of a dalbavancin induced glycopeptide/lipoglycopeptide non-susceptible *Staphylococcus aureus* during treatment of a cardiac device-related endocarditis. *Emerging Microbes & Infections* **2018**, *7* (1), 1-10.
9. Anggard, E., Nitric oxide: mediator, murderer, and medicine. *The Lancet* **1994**, *343* (8907), 1199-1206.
10. Cals-Grierson, M. M.; Ormerod, A. D., Nitric oxide function in the skin. *Nitric Oxide* **2004**, *10* (4), 179-193.

11. Fang, F. C.; Vazquez-Torres, A., Nitric oxide production by human macrophages: there's NO doubt about it. *American Journal of Physiology-Lung Cellular and Molecular Physiology* **2002**, *282* (5), L941-L943.
12. De Groote, M. A.; Fang, F. C., NO inhibitions: antimicrobial properties of nitric oxide. *Clinical Infectious Diseases* **1995**, *21* (Supplement_2), S162-S165.
13. DeGroote, M. A.; Fang, F. C., Antimicrobial properties of nitric oxide. In *Nitric oxide and infection*, Springer: 2002; pp 231-261.
14. Privett, B. J.; Broadnax, A. D.; Bauman, S. J.; Riccio, D. A.; Schoenfisch, M. H., Examination of bacterial resistance to exogenous nitric oxide. *Nitric Oxide* **2012**, *26* (3), 169-173.
15. Tjørve, K. M. C.; Tjørve, E., The use of Gompertz models in growth analyses, and new Gompertz-model approach: An addition to the Unified-Richards family. *PLOS ONE* **2017**, *12* (6), e0178691.
16. Annadurai, G.; Rajesh Babu, S.; Srinivasamoorthy, V. R., Development of mathematical models (Logistic, Gompertz and Richards models) describing the growth pattern of *Pseudomonas putida* (NICM 2174). *Bioprocess Engineering* **2000**, *23* (6), 607-612.
17. Zwietering, M. H.; Jongenburger, I.; Rombouts, F. M.; Van 'T Riet, K., Modeling of the Bacterial Growth Curve. *Applied and Environmental Microbiology* **1990**, *56* (6), 1875-1881.
18. Oh, Y. J.; Hong, J., Application of the MTT-based colorimetric method for evaluating bacterial growth using different solvent systems. *Lwt* **2022**, *153*, 112565.
19. Gao, L.; Cheng, J.; Shen, Z.; Zhang, G.; Liu, S.; Hu, J., Orchestrating Nitric Oxide and Carbon Monoxide Signaling Molecules for Synergistic Treatment of MRSA Infections. *Angewandte Chemie International Edition* **2022**, *61* (3).

20. Broniowska, K. A.; Diers, A. R.; Hogg, N., S-nitrosoglutathione. *Biochimica et Biophysica Acta (BBA)-General Subjects* **2013**, *1830* (5), 3173-3181.
21. Broniowska, K. A.; Hogg, N., The Chemical Biology of S-Nitrosothiols. *Antioxidants & Redox Signaling* **2012**, *17* (7), 969-980.
22. Ashcraft, M.; Douglass, M.; Garren, M.; Mondal, A.; Bright, L. E.; Wu, Y.; Handa, H., Nitric Oxide-Releasing Lock Solution for the Prevention of Catheter-Related Infection and Thrombosis. *ACS Appl Bio Mater* **2022**, 1519-1527.
23. Maier, R. M.; Pepper, I. L., Bacterial growth. In *Environmental microbiology*, Elsevier: 2015; pp 37-56.
24. Yates, G. T.; Smotzer, T., On the lag phase and initial decline of microbial growth curves. *Journal of Theoretical Biology* **2007**, *244* (3), 511-517.
25. Monegro, A. F.; Muppidi, V.; Regunath, H., Hospital acquired infections. In *StatPearls [Internet]*, StatPearls Publishing: 2020.
26. Martin, J. D.; Werner, B. G.; Hotchkiss, J. H., Effects of Carbon Dioxide on Bacterial Growth Parameters in Milk as Measured by Conductivity. *Journal of Dairy Science* **2003**, *86* (6), 1932-1940.
27. Bassetti, M.; Vena, A.; Croxatto, A.; Righi, E.; Guery, B., How to manage *Pseudomonas aeruginosa* infections. *Drugs in context* **2018**, *7*.
28. Pantosti, A.; Venditti, M., What is MRSA? *European Respiratory Journal* **2009**, *34* (5), 1190-1196.
29. Hoban, D. J.; Biedenbach, D. J.; Mutnick, A. H.; Jones, R. N., Pathogen of occurrence and susceptibility patterns associated with pneumonia in hospitalized patients in North America: results of the SENTRY Antimicrobial Surveillance Study (2000). *Diagnostic microbiology and infectious disease* **2003**, *45* (4), 279-285.
30. Peacock, S. J.; Paterson, G. K., Mechanisms of Methicillin Resistance in *Staphylococcus aureus*. *Annual Review of Biochemistry* **2015**, *84* (1), 577-601.

31. Gomes, F.; Teixeira, P.; Oliveira, R., Mini-review: *Staphylococcus epidermidis* as the most frequent cause of nosocomial infections: old and new fighting strategies. *Biofouling* **2014**, *30* (2), 131-141.
32. Cerca, N.; Martins, S.; Cerca, F.; Jefferson, K. K.; Pier, G. B.; Oliveira, R.; Azeredo, J., Comparative assessment of antibiotic susceptibility of coagulase-negative staphylococci in biofilm versus planktonic culture as assessed by bacterial enumeration or rapid XTT colorimetry. *Journal of Antimicrobial Chemotherapy* **2005**, *56* (2), 331-336.
33. Rogers, K. L.; Fey, P. D.; Rupp, M. E., Coagulase-negative staphylococcal infections. *Infectious disease clinics of North America* **2009**, *23* (1), 73-98.
34. Braissant, O.; Astasov-Frauenhoffer, M.; Waltimo, T.; Bonkat, G., A review of methods to determine viability, vitality, and metabolic rates in microbiology. *Frontiers in Microbiology* **2020**, *11*, 547458.
35. Fang, F. C., Perspectives series: host/pathogen interactions. Mechanisms of nitric oxide-related antimicrobial activity. *The Journal of clinical investigation* **1997**, *99* (12), 2818-2825.
36. Fang, F. C., Antimicrobial reactive oxygen and nitrogen species: concepts and controversies. *Nature Reviews Microbiology* **2004**, *2* (10), 820-832.
37. Williams, S.; Hong, Y.; Danavall, D.; Howard-Jones, M.; Gibson, D.; Frischer, M.; Verity, P., Distinguishing between living and nonliving bacteria: evaluation of the vital stain propidium iodide and its combined use with molecular probes in aquatic samples. *Journal of Microbiological Methods* **1998**, *32* (3), 225-236.

CHAPTER 3
BIOMIMETIC GASOTRANSMITTER-RELEASING ALGINATE BEADS FOR
BIOCOMPATIBLE ANTIMICROBIAL THERAPY²

² L. M. Estes Bright, L. Griffin, A. Mondal, S. Hopkins, E. Ozkan, and H. Handa. 2022.
Journal of Colloid and Interface Science. 628:911-921.

Reprinted here with permission of the publisher.

ABSTRACT

Alginate is widely used in biomedical applications due to its structural and mechanical similarities to human tissue and high biocompatibility. Further, simple ionic crosslinking of alginate allows for the formation of alginate beads capable of drug delivery. S-nitrosoglutathione is a water-soluble molecule that releases nitric oxide in physiological conditions, where it acts as a potent antimicrobial gas, among other functions. As macrophages and endothelial cells endogenously produce nitric oxide, incorporating nitric oxide donors into polymers and hydrogels introduces a biomimetic approach to mitigate clinical infections, including those caused by antibiotic-resistant micro-organisms. The incorporation of S-nitrosoglutathione into macro-scale spherical alginate beads is reported for the first time and shows exciting potential for biomedical applications. Herein, nitric oxide-releasing crosslinked alginate beads were fabricated and characterized for surface and cross-sectional morphology, water uptake, size distribution, and storage stability. In addition, the NO release was quantified by chemiluminescence and its biological effects against Gram-negative *Escherichia coli* and Gram-positive *Staphylococcus aureus* were investigated. The biocompatibility of the alginate beads was tested against 3T3 mouse fibroblast cells. Overall, nitric oxide-releasing alginate beads demonstrate biologically relevant activities without eliciting cytotoxicity, revealing their potential use as an antimicrobial material with multiple mechanisms of bacterial killing.

KEYWORDS: nitric oxide, S-nitrosoglutathione, antimicrobial, hydrogel, alginate

3.1 Introduction

Nitric oxide (NO) is a free radical gas that is endogenously produced in several areas of the body. It was first discovered in the endothelium as the endothelial-derived relaxation factor (EDRF) in 1980.¹ Several years later, scientists discovered that NO is released by activated macrophages as an antimicrobial and wound healing cytokine,² and is also capable of preventing blood platelet aggregation and activation.³ As an antimicrobial agent, its high reactivity leads to the formation of reactive oxygen (ROS) and nitrogen species (RNS) that induce oxidative and nitrosative stress on microbial membranes, proteins, and DNA. The multiple mechanisms of microbial killing exercised by NO and its ROS and RNS intermediates have ushered NO into the biomedical world as a potent antibacterial molecule to combat the rise in antibiotic-resistant organisms. Further, research in general is trending toward biomimetic approaches to combatting infections.⁴ S-nitrosothiols (RSNOs) are NO donor molecules that can be incorporated into various polymers and gels for localized delivery to the body for antimicrobial, wound healing, and blood compatibility applications. RSNOs demonstrate controlled release of NO upon exposure to heat, light, and metal ions.⁵ This encapsulation of RSNOs in a polymer or gel delivery platform is a necessary fabrication step, as free RSNOs, such as S-nitrosoglutathione (GSNO), have shown toxicity to human cells in concentrations as low as 200 $\mu\text{g mL}^{-1}$.⁶ GSNO is an endogenous RSNO commonly used in hydrogels as it is water soluble and can easily be blended into aqueous gel solutions.⁷ Therefore, the objective of this paper is to develop macro-scale GSNO-incorporated alginate beads with NO release for effective antimicrobial and pro-healing capabilities.

Alginate is a natural polysaccharide derived from brown seaweed and is widely used in the biomedical field due to its biocompatible and highly hydrophilic nature, leading to gel formation.⁸ In fact, swelling of alginate lends mechanical properties similar to the

extracellular matrix of tissues, highlighting its tissue interface potential. As a result, alginate gels are often used as wound dressings or drug delivery vehicles. On a structural level, alginate is a block copolymer composed of L-guluronate and D-mannuronate residues that vary slightly in number and arrangement depending on the source.⁹ These polymer chains can be easily crosslinked with the addition of divalent cations (such as Ca^{2+}) that bind to guluronate residues, increasing gel stiffness.¹⁰ The facile crosslinking process affords numerous conformations of alginate to be used in biomedical applications including bio ink, sheets, and microspheres, or beads, that are useful in tissue engineering, wound healing, and drug delivery platforms.^{9, 11}

The formation of spherical beads from an alginate solution affords the highly biocompatible polymer with new avenues of utilization. One of the most common uses of beads formed from alginate and other polysaccharides is for drug delivery.¹² Drugs such as anti-inflammatory agents,¹³ enzymes and probiotics for livestock digestion,¹⁴⁻¹⁶ and antibacterial agents¹⁷⁻²⁴ can easily be stirred into aqueous alginate solutions prior to ionic crosslinking to yield drug-encapsulated alginate beads. Successful fabrication of alginate beads has been accomplished using dropwise extrusion into a CaCl_2 crosslinking solution,¹³⁻³⁵ and electro spraying or electrospinning has also been employed to control the size of the spheres.^{28, 36} One study used oil-phase dispersion to create alginate beads crosslinked by CaCO_3 nanoparticles.³⁷ Alternative divalent crosslinking options such as Ba^{2+} or Al^{3+} have also been investigated, but it was found that crosslinking with Ca^{2+} provides beads with greater water uptake and more favorable biodegradation properties.³⁸ The fabrication technique utilized for this study involves the use of a superhydrophobic surface to form alginate beads and presents an inexpensive method without the use of harsh solvents or oils from emulsions, also eliminating the necessity of complex syringe pump systems.³⁹ Different methods can be used to create solidified beads from the

superhydrophobic surface, such as UV crosslinking or freezing of the beads before dropping into a CaCl_2 solution for crosslinking.

A review of recent literature in NO-releasing alginate and alginate bead research shows the potential for both concepts, but there are several limitations that must be addressed. In several studies, RSNOs were incorporated into alginate hydrogels (often in combination with synthetic hydrogel materials) and tested for antimicrobial and wound healing capabilities.⁴⁰⁻⁴³ Ahonen et al. covalently modified alginate oligosaccharides with different amine precursors to release NO, but the maximum half-life of NO release was only ~40 minutes.⁴⁴ Wu et al. utilized GSNO nanoparticles encapsulated into alginate and chitosan microbeads.⁴⁵ Micro-scale alginate and chitosan particles were fabricated using a double emulsion method, with GSNO-loaded nanoparticles crosslinking into alginate or chitosan droplets for oral delivery of GSNO. However, NO release did not last more than 24 h and storage was limited to 15 days at $-20\text{ }^\circ\text{C}$. Further, the low NO release would likely be ineffective in preventing or treating infection. In order for the technology to be commercially viable, the NO payload, storage stability, and cytocompatibility must be enhanced beyond that of previous work. The size of the beads may be investigated, as the high surface area to volume ratio does not afford long-term NO release.

Herein, we have developed NO-releasing alginate beads for antibacterial biomedical applications. The NO donor, GSNO, was incorporated in an alginate solution and spherical beads were formed via a superhydrophobic surface, followed by crosslinking by CaCl_2 . Three bead types were fabricated: pure alginate, 10 mg mL^{-1} GSNO in alginate (G10), and 20 mg mL^{-1} GSNO in alginate (G20). The three bead types were first characterized in terms of surface and cross-sectional morphology, size distribution, swelling capacity, and storage stability. Additionally, the GSNO diffusion and NO release from the G10 and G20 beads was analyzed over 24 h. Then, the antimicrobial potential of

the three bead types was tested against Gram-negative *Escherichia coli* and Gram-positive *Staphylococcus aureus*. Finally, biocompatibility of the beads was confirmed against 3T3 mouse fibroblast cells using a viability assay and scratch assay.

3.2 Materials and Methods

3.2.1 Materials

Sodium alginate, ethylenediaminetetraacetic acid (EDTA), calcium chloride (≤ 7 mm, $\geq 93.0\%$ purity), Hydrochloric acid (37%), sodium nitrite ($\geq 99.0\%$ purity), phosphate buffered saline (PBS), LB broth, LB agar, Tryptic Soy Broth, and Tryptic Soy Agar were purchased from Sigma Aldrich (St. Louis, MO USA). Reduced L-glutathione was purchased from Gold Biotechnology (Jersey City, NJ USA). Acetone ($\geq 99.5\%$ purity) was purchased from VWR (Radnor, PA, USA). Potassium bromide (KBr), FTIR grade was procured from Alfa Aesar. *Escherichia coli* (ATCC® 25922™) and *Staphylococcus aureus* (ATCC® 6538™) were purchased from American Type Culture Collection (ATCC, Manassas, VA, USA). 3T3 mouse fibroblast cells (ATCC® 1658™) were procured from ATCC. The cell counting kit (CCK-8) and Dulbecco's modified Eagle's medium (DMEM) was obtained from Sigma Aldrich (St. Louis, MO USA). Cell culture inserts were obtained from Ibidi (Fitchburg, WI, USA).

3.2.2 GSNO Synthesis and Characterization

GSNO was synthesized by first dissolving 2.7 g of glutathione in a 2 M HCl solution which was then chilled in an ice bath for 10 minutes. NaNO₂ was then added to the beaker and chilled again for 40 minutes. Chilled acetone was added while stirring for 10 minutes as the color changed from dark red to light pink. The precipitates were separated by vacuum filtration, rinsed, and dried in a desiccator in the dark overnight. Collected GSNO powder was stored at -20 °C until further use. ¹H NMR data of GSNO was characterized of its distinct functional groups (**Figure 3.S1**) to ensure batch-to-batch consistency using

a Varian/Agilent mercury spectrometer (300 MHz, D₂O, δ): 1.07-1.19 (**S**HCH₂CH-), 2.06 (CHC**H**₂CH₂C-), 2.32 (CHCH₂C**H**₂C-), 3.03 (ONSC**H**₂CH-), 3.28 (ONSC**H**₂CH-), 3.64 (-CO**C**HNH₂CH₂-), 3.86 (-NH**C**H₂COOH), 4.55 (CH₂C**H**NHCHO-), 13.18 (-CO**O**H). Fourier transform infrared spectroscopy (FTIR) was also completed using a Spectrum Two Spectrometer from PerkinElmer (Greenville, SC). Infrared spectra were recorded from 4000 to 650 cm⁻¹ with 64 scans using 4 cm⁻¹ resolution (**Figure 3.S2**). KBr loading method was used for the analysis. Approximately, 1 wt.% of the analyte was ground with anhydrous KBr. The ground mixture was subjected to 2-ton pressure for 5 min in a hydraulic press to create a translucent disk.

3.2.3 Hydrogel Bead Fabrication

The formation of alginate beads containing 0, 10, and 20 mg/mL of GSNO followed a straightforward and facile synthesis process. Briefly, the alginate precursor solution was made by adding sodium alginate to DI water and stirring at 90 °C until all particles were dissolved to create a 3 wt.% alginate solution. The solution was then removed from heat and allowed to stir until it cooled to room temperature. Once the solution cooled, GSNO was added at either 10 mg/mL (G10) or 20 mg/mL (G20) concentrations and stirred for at least 30 minutes. Droplets (20 μL) of pure alginate, G10, or G20 were pipetted onto a silicone rubber tube cut in half and coated with a superhydrophobic coating.⁴⁶ The superhydrophobic coating formed spheres of alginate from the 20 μL droplets. The beads on the tubing were then stored at -80 °C for ~30 minutes. During that time, a 5 wt.% aqueous calcium chloride (CaCl₂) solution was prepared. After freezing, hydrogel beads were removed from the superhydrophobic tubing with a spatula and placed in the 5 wt.% CaCl₂ solution for 5 minutes to allow for crosslinking of the alginate on the surface of the spheres. Pure alginate, G10, and G20 beads were crosslinked in separate CaCl₂ baths to prevent any solubilized GSNO in the crosslinking solution to interfere with later tests.

Following 5 minutes of crosslinking, beads were removed from the CaCl₂ bath, rinsed three times in DI water, and placed on a microfiber wipe to dry for ~5 minutes. Fabricated hydrogel beads were used immediately for characterizations, bacteria and cell studies, or stored in the appropriate location for stability studies.

3.2.4 Hydrogel Bead Characterization

3.2.4.1 Scanning Electron Microscopy (SEM) and Energy-Dispersive X-ray Spectroscopy (EDS) for Surface Analysis

In this study, pure alginate, G10, and G20 beads were imaged to determine differences in surface roughness and overall appearance. Hydrogel beads used for imaging were fabricated using the above technique, followed by 4 hours of lyophilization. Prior to imaging, lyophilized beads were sputter-coated with 10 nm of gold-palladium using a Leica sputter coater (Leica Microsystems) and mounted on SEM stubs with double-sided SEM stickers. Images were acquired through a scanning electron microscopy (SEM, FEI Teneo, FEI Co.) setup employed at an accelerating voltage of 5.00 kV. Magnifications ranging from 400x to 600x were used for image acquisition. The porosity of samples was calculated using cross-sectional SEM images. Using ImageJ analysis, the pixel area of pores was compared to that of the entire image, and a percent porosity was calculated. Analysis was carried out on $n = 4$ images of different areas of the cross-section for each sample type.

The SEM was also equipped with an energy-dispersive X-ray spectroscopy system (EDS, Oxford Instruments) used for elemental surface mapping and analysis. Oxygen and carbon were used to confirm the alginate surface and sulfur was utilized to map the distribution of GSNO in the hydrogel beads. An accelerating voltage of 20.00 kV was used for EDS measurements.

3.2.4.2 Size Distribution

Using a Mitutoyo IP65 digital micrometer, diameters for pure alginate, G10 and G20 beads were measured in mm. Measurements were taken directly after the rinsing and drying synthesis steps to avoid any potential water evaporation from the beads. No significant difference in the average diameter is expected between the sample types since all spheres were formed via 20 μ L droplets on a superhydrophobic surface.

3.2.4.3 Swelling Capacity

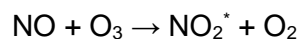
To investigate the hydrophilic nature of the beads, the swelling capacity of alginate, G10, and G20 beads was determined. Beads of each type were fabricated as mentioned above and dried in a desiccator in the dark for 1 hour. After drying, each bead was weighed and placed in a separate container of PBS. Half of the beads were kept at room temperature in the dark while the other half were kept in a 37 °C incubator shielded from light. The beads were removed from PBS and weighed after 1 hour of swelling, and **Equation 3.1** was used to determine swelling capacity of the hydrogel beads, where W_H represents the weight of the bead after hydration and W_D represents the weight of the bead while dehydrated.

$$\text{Swelling Capacity (\%)} = \frac{W^H - W^D}{W^D} \times 100 \quad \text{Equation 3.1}$$

3.2.4.4 GSNO Loading and Storage Stability

The loading of GSNO into the alginate beads was quantified and compared to the theoretical quantities calculated based on the concentration of GSNO in the precursor solutions. GSNO loading was determined by catalytically releasing all of the NO present in the beads and measuring NO release with Sievers Nitric Oxide Analyzers (NOAs) model 280i (Boulder, CO). NO was purged from the G10 and G20 beads using copper (II) chloride solution (CuCl_2) and ascorbic acid as catalyzers. One at a time, beads were placed

in an amber reaction chamber containing 2.8 mL phosphate buffered saline (PBS) with 200 μL of 0.1 M CuCl_2 and 100 μL of 0.1 M ascorbic acid. A nitrogen bubbler was placed in the solution containing the beads at a flow rate of 200 mL min^{-1} to carry any NO being emitted to the NOA reaction chamber. Inside the reaction chamber, an incoming flow of oxygen allowed for the following reactions to take place:



Equation 3.2

The excited photon released from the reaction is converted to a ppb or ppm reading and is recorded over time. The area under the NO release curve was calculated to determine the amount of GSNO initially present in each bead. NO release was standardized per mg of bead.

For storage stability studies, G10 and G20 beads were stored at $-80\text{ }^\circ\text{C}$, $-20\text{ }^\circ\text{C}$, and $4\text{ }^\circ\text{C}$ shielded from light. Beads were used immediately following fabrication, in their swollen state. The amount of GSNO remaining in the beads was measured at various timepoints over a 28-day period and again after a total of 6 months. During NO measurements, the amber reaction chamber was maintained at $37\text{ }^\circ\text{C}$ using a water bath. The percent of GSNO remaining was relative to the values found on day 0 post-fabrication.

3.2.4.5 GSNO Diffusion

The hydrophilic nature of alginate allows for water uptake and subsequent GSNO diffusion from the beads. This release was quantified via UV-Vis Spectroscopy due to the signature peak of GSNO at 340 nm (**Figure 3.S3**). Beads were placed in 1 mL PBS and stored at $37\text{ }^\circ\text{C}$ in the dark. At several time points, the PBS was removed, and the absorbance was taken. Following readings, fresh PBS was added to the beads, and they

were returned to storage conditions. Cumulative GSNO diffusion was calculated using a standard curve of varying GSNO concentrations (**Figure 3.S4**).

3.2.4.6 Nitric Oxide Release

The release of NO from the alginate beads was also quantified in real time using chemiluminescence detection methods over a 24 h period. Beads were weighed and placed in 3 mL of PBS in the sample chamber following the determination of a baseline reading. The sample chamber was protected from light and maintained at 37 °C using a water bath. NO released from the beads was purged from the sample chamber with 200 mL min⁻¹ N₂ gas. Inside the reaction chamber, NO reacts with ozone (O₃, converted from an O₂ inlet gas) to form NO₂* in an excited state. As NO₂* drops back down to ground state, a photon is released, measured by the instrument, and converted to a parts per billion (PPB) reading. Utilizing an NOA constant (mol PPB⁻¹ s⁻¹), this PPB reading is then converted to an NO release value (x10⁻¹¹ mol min⁻¹ mg⁻¹). Once a stabilized NO release was reached, the beads were removed from the sample chamber and stored at 37 °C and shielded from light between measurements. The release of NO was standardized per mg of beads.

3.2.5 Alginate Bead Biological Activity

3.2.5.1 Antimicrobial Activity – 24 h Bacterial Viability Assay

The antimicrobial activity of the NO releasing alginate beads was investigated against *Escherichia coli* (*E. coli*) and *Staphylococcus aureus* (*S. aureus*) using a 24 h viability assay. To begin, a single bacterial colony was inoculated into LB (*E. coli*) or TSB (*S. aureus*) media and incubated at 37 °C in a shaking incubator (150 rpm) until the log phase of bacterial growth was reached. The bacteria were collected by centrifugation, rinsed with PBS, and diluted to ~10⁸ CFU/mL in PBS. All three types of beads, prepared as mentioned above, were weighed, UV sterilized, and exposed to 1 mL of ~10⁸ CFU/mL

bacteria in PBS. Wells with only bacteria present were utilized as a control for comparison to wells treated with the three bead types. The well plate was sealed with parafilm and placed in a shaking incubator (150 rpm, 37 °C). After 24 h, solutions were diluted and plated on LB (*E. coli*) or TSA (*S. aureus*) agar plates. Viable CFUs were counted following 18-24 h of incubation of the agar plates. The reduction of viable bacteria was calculated using **Equation 3.3**.

$$\text{Reduction in Viable Bacteria (\%)} = \frac{\text{control CFU mL}^{-1} - \text{treatment CFU mL}^{-1}}{\text{control CFU mL}^{-1}} \times 100 \quad \text{Equation 3.3}$$

3.2.5.2 Cell Cytotoxicity

A cell viability assay was performed following ISO 10993 standards. NIH 3T3 mouse fibroblast cells were cultured in a T-75 flask containing DMEM media with 10% FBS and 5% penicillin-streptomycin (complete DMEM) at 37 °C with 5% CO₂. Once the cells reached 80% confluency, the cells were transferred to a 96-well plate at a seeding density of 1.5 × 10⁴ cells/ mL. Simultaneously, leachates of the alginate beads were prepared by soaking the samples in complete DMEM for 24 h. After 24 h, the cells in the 96-well plates were exposed to the leachates from the samples in complete DMEM and incubated in a CO₂ incubator at 37 °C with 5% CO₂. After 24 h exposure, the leachates were replaced with complete DMEM containing 10% CCK-8 solution and incubated for another 2 h to develop a yellow-orange colored end product, formazan, which is formed via the reduction of 2-(2-methoxy-4-nitrophenyl)-3-(4-nitrophenyl)-5-(2,4-disulfophenyl)-2H-tetrazolium monosodium salt (WST-8) by dehydrogenase activity of viable cells. The amount of formazan, detectable at 450 nm, is directly proportional to the number of viable cells. The results are reported as percent viability according to Equation 4.

$$\text{Cell viability (\%)} = \frac{\text{Absorbance of test samples}}{\text{Absorbance of control}} \times 100 \quad \text{Equation 3.4}$$

3.2.5.3 Scratch Assay

In vitro scratch assay was performed to assess the GSNO leaching effects on mammalian cells, as high levels of NO donors and NO have proven toxic in previous studies.⁶ Further, NO has shown to enhance cell migration in several wound healing studies.⁴⁷⁻⁵⁰ 3T3 mouse fibroblast cells were seeded into the cell culture inserts (Ibidi, Fitchburg, Wisconsin) at a 3×10^4 cells/ mL density. The inserts contain a divider at the center, which ensures a linear zone of no cells. After 24 h of incubation in a humidified atmosphere with 5% CO₂ at 37 °C, the divider was removed, and media was replaced with the leachates from the samples. Migration of cells was monitored using an EVOS-XL microscope at 0, 6, and 18 h timepoints. The experiment was performed in triplicates, and representative images were chosen. ImageJ was used to analyze the reduction in scratch gap area from hours 0 to 6.

3.2.5.4 Statistical Analysis

Reported data is the mean \pm standard deviation if not stated otherwise. All statistical analyses were carried out using Prism 9.1 (GraphPad Software, San Diego, CA USA). For characterization studies, statistical comparisons were determined using student's t-test. For biological studies, statistical comparisons were determined using ordinary one-way analysis of variance (ANOVA) for multiple comparisons between means of the sample groups. For antibacterial studies, analysis was performed on the logarithmic calculations. Values of $p < 0.05$ were deemed significant. Samples of $n = 3$ were used for each sample type in each experiment unless otherwise noted.

3.3 Results and Discussion

3.3.1 Alginate Bead Characterization

This study represents the first investigation of macro-scale nitric oxide releasing alginate beads. The fabrication process (**Figure 3.1**) yields alginate beads with tunable

GSNO content, encapsulated in the beads by the external crosslinking of the guluronate blocks of the polymer by the divalent cations (Ca^{2+}) on the surface, characterized as the egg-box model.^{9, 51} The spherical structure of the beads, as well as the gradient of a pink hue, characteristic of GSNO, can be seen in **Figure 3.2c**.

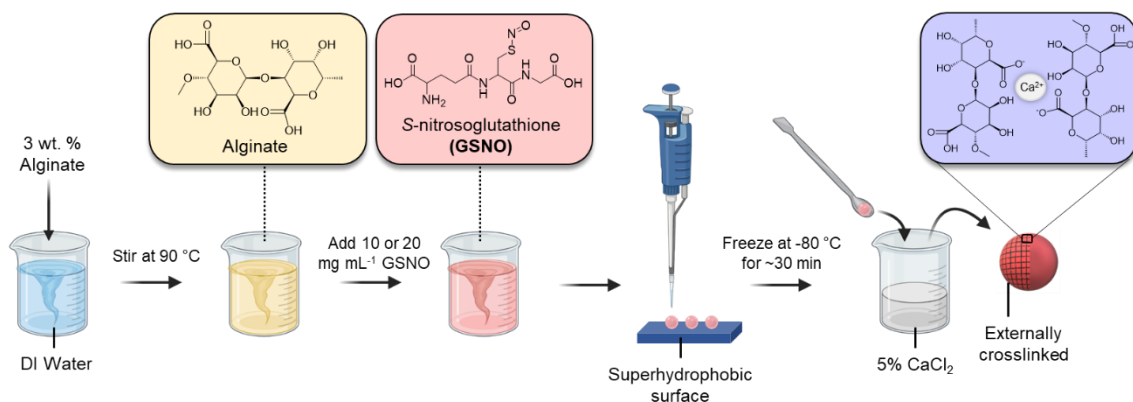


Figure 3.1 Alginate bead fabrication scheme. Alginate beads were formed by GSNO dissolution in an alginate solution, followed by bead formation via a superhydrophobic surface, freezing at $-80\text{ }^{\circ}\text{C}$, and external crosslinking in CaCl_2 solution.

3.3.1.1 Morphology via Scanning Electron Microscopy (SEM)

The surface and cross-sectional morphology of freeze-dried alginate, G10, and G20 beads were investigated using Scanning Electron Microscopy (SEM, **Figure 3.2a**). Surface crosslinking of the alginate beads and subsequent lyophilization leads to the shrunken outer shell of all three bead types. Interestingly, G10 and G20 reveal a slightly more textured surface, potentially due to the presence of the GSNO crystals within the polymer matrix. Cross-sectional cuts of the beads reveal the highly delicate porous nature of the natural polymer, crosslinked by the uptake of the CaCl_2 solution during submersion. Quantification of cross-sectional porosity revealed no statistically significant difference

between sample types with alginate beads displaying $46.9 \pm 6.2\%$, G10 showing $38.9 \pm 4.1\%$ and G20 revealing $42.9 \pm 2.3\%$ porosity (**Figure 3.2b**). Elemental mapping and sulfur detection within cross-sections of the alginate beads confirmed the presence of GSNO, with G20 beads revealing about twice the amount of sulfur compared to G10 beads, $3.7 \pm 0.1\%$ and $6.9 \pm 0.1\%$ respectively (**Figure 3.3a**). This displays the highly tunable nature of the beads, with adjustable GSNO content specific to the application.

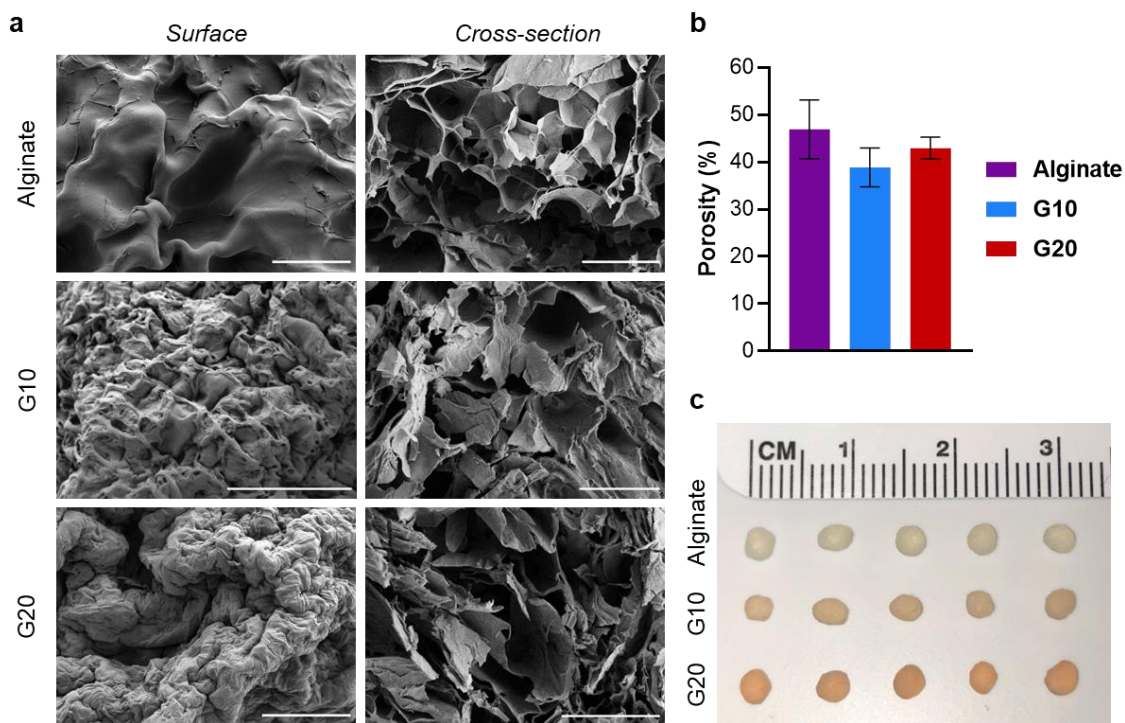


Figure 3.2 Morphological characterizations of alginate beads. (a) Alginate beads (with and without GSNO) were fabricated and imaged using SEM, showing similar surface morphologies and porous cross-sections. Scale bars for surface images represent 200 μm and scale bars for cross-sectional images represent 50 μm . (b) Percent porosity of each sample type was calculated using cross-sectional images, with no significant difference between samples ($n = 4$). (c) Alginate, G10, and G20 beads exhibited comparable size distribution with greater GSNO content visualized by an increase in pink hue.

3.3.1.2 Size Distribution

The size distribution of the alginate beads was calculated by measuring the average diameter of each bead type. The 20 μ L volume used to form beads was chosen to increase the NO longevity, as micro or nano beads have a higher surface area to volume ratio and would likely exhibit a large burst release of NO, depleting the GSNO reservoir.⁴⁵ As expected, no statistical difference between the bead types was found (pure alginate: 2.42 ± 0.19 mm, G10: 2.35 ± 0.19 mm, G20: 2.35 ± 0.14 mm, **Figure 3.3b**).

3.3.1.3 Swelling Capacity

Alginate's exceptional biocompatibility is largely attributed to the high water swelling capacity of the material, forming a swollen polymeric material with properties resembling those of extracellular matrices in tissues. This property endows immense potential for biomedical use of alginate but must be thoroughly investigated to properly characterize a material. Therefore, the swelling capacity of the fabricated alginate beads with and without GSNO was evaluated at room temperature and at physiological temperature (**Figure 3.3c**). At room temperature, each bead type showed remarkable swelling capacity (%) at 421.01 ± 69.0 , 410.28 ± 117.6 , and 481.63 ± 92.3 for alginate, G10, and G20, respectively. There was a slight rise in swelling for all bead types at 37 °C with alginate at $523.06 \pm 136.7\%$, G10 at $607.58 \pm 108.0\%$, and G20 at $550.83 \pm 75.0\%$. The increase in swelling at physiological temperature is due to the increase in flexibility between the polymer chains, creating greater space for water to absorb. It is also important to note that there was no significant difference in swelling capacity between any of the bead types, revealing that the inclusion of GSNO into the alginate structure does not affect the hydrophilicity of the material. This is most likely due to the fact that the GSNO within the alginate is water soluble, allowing for uninterrupted absorption of the fluid. High swelling capacity bestows the material with applicability in many biomedical applications

such as wound healing, as exudate absorption aids the wound healing process and in turn enhances NO release.

3.3.1.4 GSNO Loading and Storage Stability

The loading efficiency of GSNO into the alginate beads was determined by catalytically depleting the NO present in the beads. The value was then compared to the theoretical quantity of NO from the concentration of GSNO in the precursor solutions. For G10, 0.2 mg of GSNO was expected per bead due to the precursor concentration (10 mg/mL) and 20 μ L bead volume whereas 0.4 mg was the theoretical load of GSNO in G20 beads. Following catalytic NO release and depletion of the GSNO reservoir within the beads, the loading efficiency was found to be $28.31 \pm 2.1\%$ for G10 and $23.89 \pm 4.2\%$ for G20 (**Figure 3.S5**). This low loading level is likely due to GSNO lost during the Ca^{2+} crosslinking and DI water washing steps during synthesis. However, NO release in physiological conditions (discussed later) reveals sufficient NO impregnation into both bead types.

For storage stability studies, beads were stored at $-80\text{ }^{\circ}\text{C}$, $-20\text{ }^{\circ}\text{C}$, and $4\text{ }^{\circ}\text{C}$. The amount of GSNO present within the beads was measured intermittently for 28 days and then after 6 total months in storage (**Figure 3.3d**). At each time point, the GSNO content of the beads was compared to the initial GSNO loading study at day 0. The GSNO present within the beads was unstable at $4\text{ }^{\circ}\text{C}$, with merely $5.07 \pm 1.5\%$ of the initial loading for G10 and $2.13 \pm 0.5\%$ for G20 remaining after 5 days. GSNO within the beads was more stable at $-20\text{ }^{\circ}\text{C}$ as after 28 days in storage, $69.92 \pm 4.9\%$ for G10 and $77.55 \pm 5.9\%$ for G20 remained, a significant improvement over other NO-releasing alginate beads at the microscale.⁴⁵ However, the $-80\text{ }^{\circ}\text{C}$ storage condition yielded the most stable environment for GSNO in the beads, with $104.93 \pm 12.2\%$ for G10 and $116.57 \pm 8.2\%$ for G20 remaining after 28 days. A GSNO content greater than 100% is due to the variability among the

alginate beads and their comparison to the batch tested at day 0. Furthermore, after 6 months in storage at -80 °C, the GSNO remaining for G10 dipped to $72.90 \pm 8.9\%$ and G20 to $90.54 \pm 16.5\%$. The slight dip in GSNO content of the beads after 6 months of storage is likely due to the degradation of alginate over time leading to a less stable polymer matrix as well as the slow degradation of GSNO in the water-rich alginate beads. Although it is not uncommon for antimicrobial therapeutics to be stored at -80 °C prior to use, these storage conditions are not ideal. One potential way to improve storage stability and NO release over longer periods of time is to lyophilize the alginate beads immediately following fabrication. As GSNO releases NO through hydrolytic degradation, removal of the water from the polymer matrix may prolong NO release lifespan. Further, water uptake studies revealed the potential of the lyophilized bead to uptake large quantities of water upon immersion. This modification may allow for easier storage of the beads at room temperature or -20 °C to prevent heat-activated degradation and subsequent NO release, though more thorough studies must be conducted to confirm.

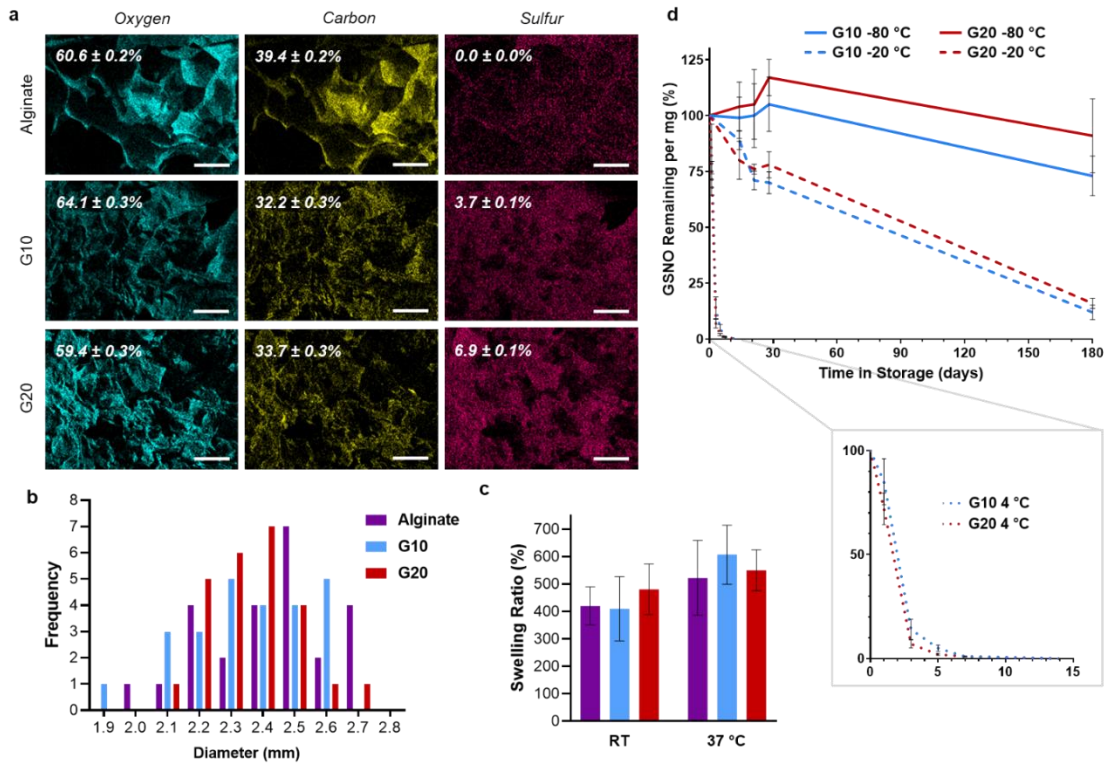


Figure 3.3 Physical characterizations of alginate beads. (a) Energy-Dispersive X-ray Spectroscopy (EDS) imaging of the cross-sections of alginate, G10, and G20 beads display equivalent oxygen and carbon concentrations attributed to the alginate base-polymer. An increase in the GSNO concentration was confirmed in G10 beads with 3.7% sulfur surface elemental analysis and 6.9% sulfur in G20 beads. (b) Size distribution revealed similar bead diameters among bead types ($n = 25$). (c) Swelling capacity of the beads at room temperature and physiological temperature revealed no significant change, though all bead types showed an increase in swelling at physiological temperature ($n = 4$). (d) Alginate, G10, and G20 beads were stored at 4 °C, -20 °C, and -80 °C for up to six months and displayed enhanced stability at lower temperatures, determined by GSNO content remaining ($n = 3$).

3.3.1.5 GSNO Diffusion

Owing to the high water-uptake of alginate and the water solubility of GSNO, the GSNO that diffused out of the alginate beads was investigated, as it provides an additional

mechanism of NO release from the material (**Figure 3.4a**). After soaking in PBS and measuring the absorbance of the solution, the GSNO release was determined over a 24-h period. For both G10 and G20, GSNO diffusion ceased at ~8 h, cumulatively releasing $24.21 \pm 0.36\%$ and $18.03 \pm 0.4\%$ of the total encapsulated GSNO, respectively (**Figure 3.4b**). After 24 h, the percentage of GSNO released from the beads did not increase substantially, with $24.61 \pm 0.12\%$ released for G10 and $18.22 \pm 0.03\%$ for G20. The fact that the majority of GSNO diffusion occurred in the first 8 h is not surprising due to the previously mentioned hydrophilic nature of alginate combined with the water solubility of GSNO. Further, as the alginate becomes more hydrated, the polymer chains become more separated, increasing water permeability and consequent diffusion. Any GSNO released after the 8 h time point was more deeply embedded in the beads and diffused out following further water absorption. The favorable levels of GSNO diffusion from the alginate beads will be investigated further for antibacterial efficacy and cytocompatibility.

3.3.1.6 Nitric Oxide Release

NO released from the alginate beads was measured over a 24-h period with the beads submerged in PBS with EDTA during the entire study. The quantitative NO release combines the release from GSNO diffused from the beads as well as that embedded in the polymer matrix. The instantaneous release profiles of G10 and G20 reveal a burst release of NO upon introduction to the sample chamber, with G10 reaching $\sim 0.5 \times 10^{-11}$ mol min⁻¹ mg⁻¹ and G20 reaching $\sim 2.5 \times 10^{-11}$ mol min⁻¹ mg⁻¹ within the first 5-8 min (**Figure 3.4c**). The burst of NO release is due to the GSNO molecules on the outer layers of the alginate beads, as well as any initial GSNO diffusion that leads to NO release in the 37 °C environment. After ~30 min, both bead types had a stabilized release of NO that remained relatively unchanged over the 24 h period. G10 released $0.075 \pm 0.04 \times 10^{-11}$ mol min⁻¹ mg⁻¹ at hour 0 (after stabilizing) and $0.053 \pm 0.02 \times 10^{-11}$ mol min⁻¹ mg⁻¹ at hour 24 (**Figure**

3.4d). G20 displayed a release roughly twice that of G10: $0.186 \pm 0.04 \times 10^{-11} \text{ mol min}^{-1} \text{ mg}^{-1}$ at hour 0 and $0.156 \pm 0.03 \times 10^{-11} \text{ mol min}^{-1} \text{ mg}^{-1}$ after 24 h. It is expected that G20 NO release is twice as high as G10 NO release as twice the GSNO was loaded into the precursor alginate solutions. Further, the GSNO embedded into the beads led to the longevity of NO release, while the GSNO diffusion enhanced initial NO release, a favorable release strategy to combat bacterial infections. Taking the two modes of NO release into account, this fabrication approach allows for tunable NO release characteristics depending on the amount of GSNO loaded into the precursor alginate solution.

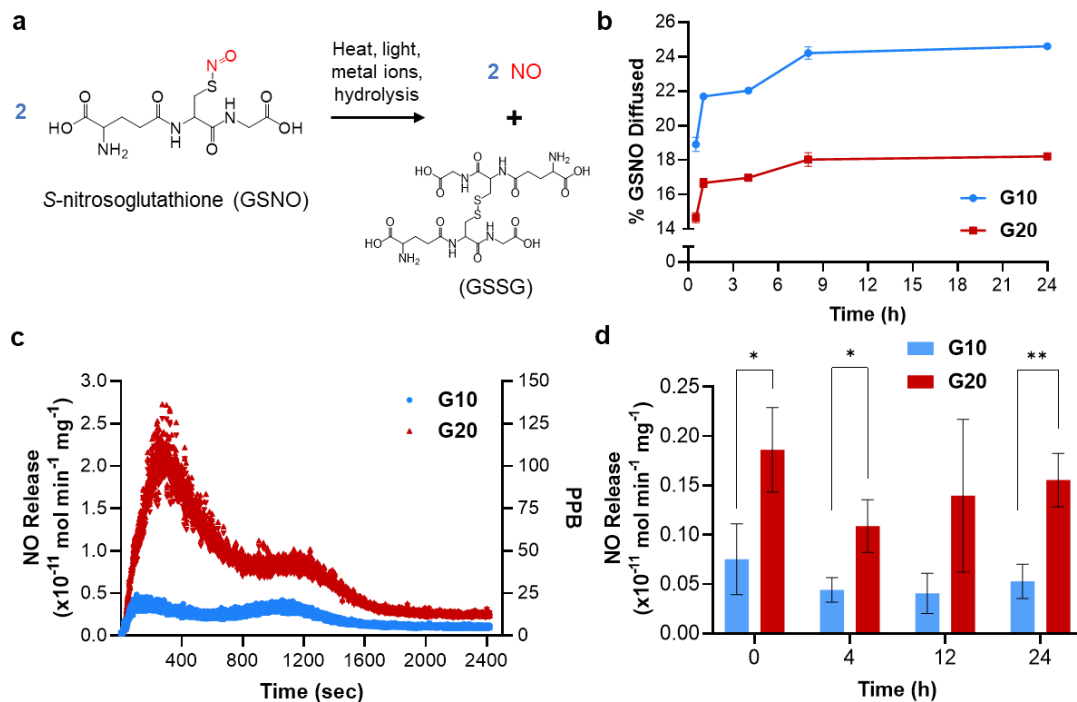


Figure 3.4 Nitric oxide release characteristics of alginate beads. (a) Degradation of GSNO via heat, light, metal ions, or hydrolysis leads to the release of 2 mol NO per 2 mol of GSNO followed by the formation of a disulfide bond between two glutathione molecules. (b) GSNO diffusion in PBS measured over 24 h for G10 and G20 beads ($n = 3$). (c) Instantaneous NO release profiles of representative samples of G10 and G20 beads measured at 0 h ($n = 1$). (d) Stabilized NO release from G10 and G20 beads measured over 24 h ($n = 3$). Statistical significance denoted by * ($p < 0.05$) and ** ($p < 0.01$).

3.3.2 Alginate Bead Biological Activity

3.3.2.1 Antimicrobial Activity

Antimicrobial activity of the alginate beads with and without GSNO was investigated against Gram-negative *E. coli* and Gram-positive *S. aureus*. Greater GSNO content was expected to be associated with higher bacterial reduction, as NO is a potent antimicrobial that has shown effectiveness against bacteria, fungi, and viruses.⁵² The NO released from GSNO reacts with environmental oxygen (O_2), generating reactive oxygen

(ROS) and nitrogen species (RNS) such as peroxynitrite (OONO⁻) which is exceptionally toxic due to high oxidation potential.^{52, 53} These free radical gases are then able to penetrate and disrupt the bacterial membrane and wreak havoc within the microorganism. Thiol nitrosation by NO can modify proteins, inhibiting their functions.⁵⁴ NO also actively attacks DNA through deamination and strand breaks, as well as DNA repair systems, causing irreparable damage.⁵⁵ NO and its ROS and RNS counterparts exhibit such specific and unique reactivity and antimicrobial strategies, bacterial lipids, proteins, and DNA are indefensible, enabling NO to obliterate microbes and thwart infections.⁵⁶

The antibacterial efficacy of GSNO containing alginate beads showed a promising trend over a 24 h period. For *E. coli* there was no significant bacterial reduction between the untreated bacterial solution and pure alginate beads, whereas G10 and G20 beads showed an $88.03 \pm 4.0\%$ and $98.99 \pm 0.6\%$ bacterial reduction compared to controls, respectively (**Figure 3.5a**). *S. aureus* treatment followed the same trend of enhanced bacterial killing with greater GSNO incorporation into the beads. Pure alginate beads showed negligible bacterial inhibition while G10 displayed $99.4 \pm 0.3\%$ greater killing and G20 revealed $99.92 \pm 0.02\%$ (**Figure 3.5b**). As previously mentioned, the improved killing of G20 beads compared to G10 is expected, as greater GSNO incorporation leads to higher NO release and therefore more oxidative and nitrosative stress exerted on the bacteria. The gaseous nature of NO allows rapid and effortless penetration of bacterial membranes to initiate killing from within as well as externally. These multiple mechanisms of killing leading to enhanced bacterial killing display the potential benefit of nitric oxide antimicrobial treatments compared to currently utilized antibiotics and should be further investigated for their clinical potential.

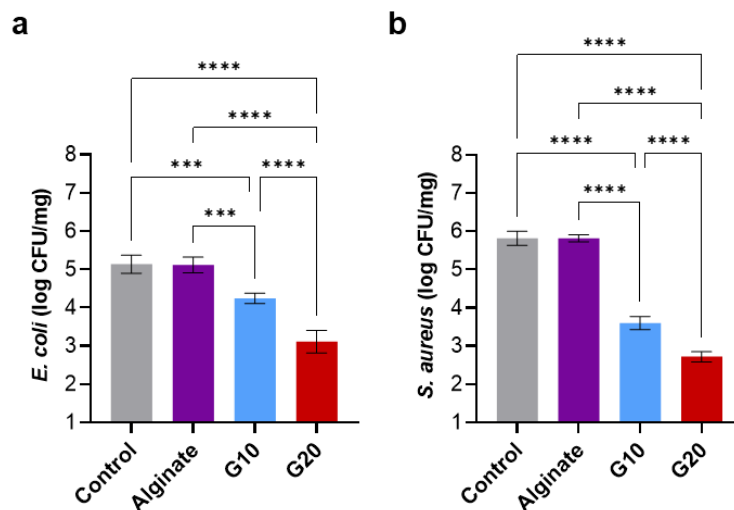


Figure 3.5 Antibacterial activity of alginate beads. The antibacterial activity of all bead types was tested against (a) *E. coli* ($n = 4$) and (b) *S. aureus* ($n = 4$) via colony counting. Statistical significance is represented as *** ($p < 0.005$) and **** ($p < 0.001$) when comparing the connected columns.

3.3.2.2 Cell Cytotoxicity

The antimicrobial activity of NO releasing alginate beads shows promise for biomedical applications, but the biocompatibility must first be examined. As alginate is a naturally derived polysaccharide it is not expected that there will be any toxicity against 3T3 mouse fibroblast cells. Mammalian cells are also much more highly resistant to NO than bacteria, as there are internal antioxidant mechanisms to prevent the conversion of NO into harmful peroxynitrite species. Similarly, GSNO is simply the nitrosated derivative of glutathione (GSH), the most abundant cellular thiol, therefore no harmful effects on mammalian cells of any GSH byproducts are expected from the beads as NO is exhausted. The viability of mouse fibroblast cells, as determined by a CCK-8 assay, was compared to untreated cells following treatment with leachates from alginate, G10, and G20 beads. No cytotoxicity was detected due to any of the treatments. Relative to

untreated cell viability, alginate beads showed $90.71 \pm 2.9\%$, G10 showed $101.04 \pm 9.6\%$, and G20 displayed $112.42 \pm 5.3\%$ viability (**Figure 3.6a**). Endogenously, NO promotes cell proliferation at low flux values such as those displayed by the alginate beads. The slow release of NO over the 24 h incubation time led to increased cell proliferation and therefore greater relative cell viability.

3.3.2.3 Scratch Assay

Endogenous NO has many physiological roles, such as acting as a cellular messenger to promote fibroblast proliferation and migration during wound healing and tissue reconstruction. This is demonstrated in the cell cytotoxicity data. Additionally, an *in vitro* cell migration scratch assay was utilized to determine if fibroblast migration was inhibited by the relatively high GSNO leaching from the beads. The scratch assay is a relatively inexpensive and simple assay designed to accurately mimic the migration of cells *in vivo* and can be used to directly compare cell migration rates among treatment groups.⁵⁷

At 0 h, a gap between the confluent monolayer of mouse fibroblast cells is visible and uniform among the various treatment groups (**Figure 3.6b**). After 6 h, NO release from G10 and G20 beads led to slightly enhanced cell migration, though not statistically significant. Blue arrows represent groups of cells in migration toward the opposite edge. Control beads showed $50.3 \pm 3.3\%$ reduction in wound gap area, followed by alginate with 47.6 ± 15.1 , G20 with $54.6 \pm 18.4\%$, and G10 with $56.0 \pm 11.2\%$ reduction in area (**Figure 3.6c**). After 18 h, the cell gap on all treatments closes completely. Alginate, G10, and G20 cells are fully confluent displaying a uniform monolayer, whereas control cells grew together with less homogeneity, shown by the red star in **Figure 3.6b**. Although the NO releasing beads only showed a moderate increase in the rate of cell migration, as displayed at hour 6, it is important to note that the high GSNO leaching values did not

have a detrimental impact on the cell proliferation or migration of mammalian fibroblast cells, revealing high biocompatibility for use in medical applications.

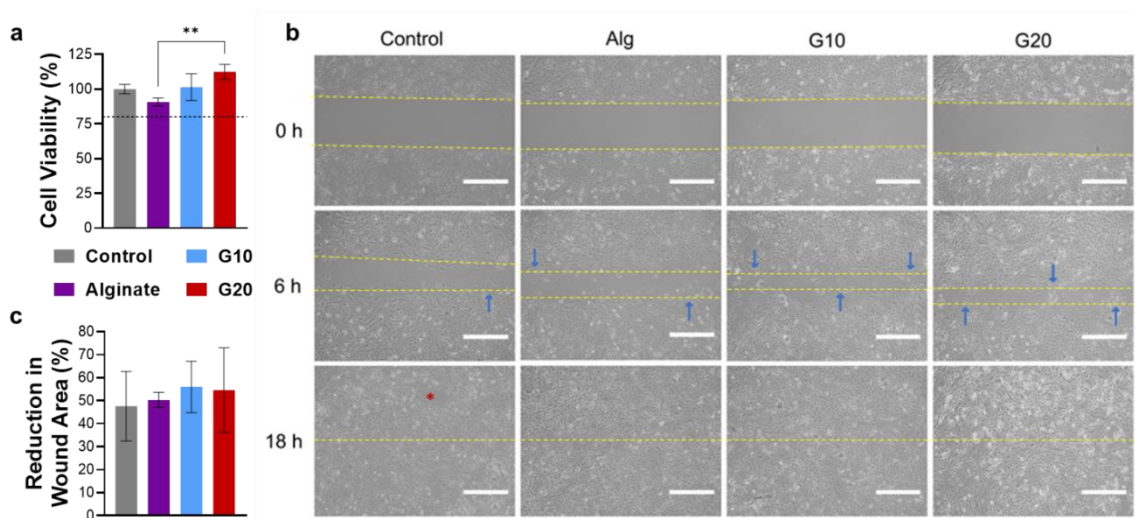


Figure 3.6 Biocompatibility assessment of alginate beads. (a) Relative cell viability was measured using a CCK-8 assay following incubation of 3T3 mouse fibroblast cells with leachates from Alginate, G10, and G20 beads. Statistical significance is represented by ** ($p < 0.01$). (b) An *in vitro* scratch assay was utilized to investigate the role of diffused GSNO and released NO in fibroblast cell migration across the scratch gap. Blue arrows represent areas of cell migration, and the red star signifies non-uniform cell distribution in the control treatment. These images are representative from $n = 3$ plates. (c) Reduction in wound gap area was quantified, revealing no significant difference in fibroblast migration at hour 6 between treatment groups ($n = 3$).

3.4 Conclusions

In summary, we fabricated the first macro-scale S-nitrosoglutathione-incorporated alginate beads through external ionic crosslinking with stable and tunable nitric oxide releasing capabilities. The beads demonstrated a spherical shape with a porous internal morphology. All three bead types (alginate, G10, and G20) shared a comparable size distribution averaging between 2.35 and 2.42 mm in diameter, which is comparable to

other hydrogel beads used for skin regeneration and bioactive treatments.^{58, 59} The beads also displayed high water uptake potential ranging from 410.3% to 481.6%, with an increase in swelling at physiological temperature. Chemiluminescent nitric oxide detection methods revealed stable nitric oxide release of ~ 0.4 ($\times 10^{-11}$ mol min⁻¹ mg⁻¹) for G10 beads and ~ 0.12 ($\times 10^{-11}$ mol min⁻¹ mg⁻¹) from G20 beads at 24 h, a significant increase in longevity of nitric oxide release compared to covalently modified alginates¹⁶ and micro-scale GSNO-alginate beads⁴⁵, and without the necessity of catalytic agents to induce release of NO from the beads.⁶⁰ The total percentage of nitric oxide donor diffused from the beads after 24 h was 24.6% for G10 and 18.2% for G20, and there was no cytotoxic response from 3T3 mouse fibroblast cells. In fact, these GSNO leachate levels led to a slight increase in cell viability for the G10 and G20 treated cells. These levels of S-nitrosoglutathione diffusion and consequent nitric oxide release led to a 1-log reduction against Gram-negative *E. coli* for G20 beads and a 2- and 3-log reduction in Gram-positive *S. aureus* for G10 and G20 beads, respectively, following 24 h treatment. Overall, the fabricated material has strong antimicrobial characteristics with enhanced mammalian cell viability and migration. The combination of the highly biocompatible properties of alginate with the antimicrobial properties of nitric oxide-releasing S-nitrosoglutathione gives a novel nitric oxide-releasing alginate material that shows potential for various biomedical applications. Future applications of the material may include *in vivo* wound healing studies for external infected wounds or drug delivery studies utilizing nitric oxide donors in combination with other treatments. Additionally, the GSNO content and size of the beads may also be modified to tune the nitric oxide release profile to fit specific applications.

Author Contributions

Lori M. Estes Bright: Conceptualization, Writing – Original Draft, Methodology, Investigation, Validation, Visualization. **Lauren Griffin:** Investigation, Writing – Review and Editing. **Arnab Mondal:** Investigation, Writing – Review and Editing. **Sean Hopkins:** Supervision, Writing – Review and Editing. **Ekrem Ozkan:** Supervision, Writing – Review and Editing. **Hitesh Handa:** Funding Acquisition, Supervision, Resources, Writing – Review and Editing.

3.5 References

1. Furchgott, R. F.; Zawadzki, J. V., The obligatory role of endothelial cells in the relaxation of arterial smooth muscle by acetylcholine. *Nature* 1980, 288 (5789), 373-6.
2. Anggard, E., Nitric oxide: mediator, murderer, and medicine. *The Lancet* 1994, 343 (8907), 1199-1206.
3. Hamilos, M.; Petousis, S.; Parthenakis, F., Interaction between platelets and endothelium: from pathophysiology to new therapeutic options. *Cardiovascular diagnosis and therapy* 2018, 8 (5), 568.
4. Saidin, S.; Jumat, M. A.; Amin, N. A. A. M.; Al-Hammadi, A. S. S., Organic and inorganic antibacterial approaches in combating bacterial infection for biomedical application. *Materials Science and Engineering: C* 2021, 118, 111382.
5. Williams, D. L. H., The Chemistry of S-Nitrosothiols. *Accounts of Chemical Research* 1999, 32 (10), 869-876.
6. Estes Bright, L. M.; Garren, M. R. S.; Ashcraft, M.; Kumar, A.; Husain, H.; Brisbois, E. J.; Handa, H., Dual Action Nitric Oxide and Fluoride Ion-Releasing Hydrogels for Combating Dental Caries. *ACS Applied Materials & Interfaces* 2022, 14 (19), 21916-21930.
7. Broniowska, K. A.; Diers, A. R.; Hogg, N., S-nitrosoglutathione. *Biochimica et Biophysica Acta (BBA)-General Subjects* 2013, 1830 (5), 3173-3181.
8. Kesharwani, P.; Bisht, A.; Alexander, A.; Dave, V.; Sharma, S., Biomedical applications of hydrogels in drug delivery system: An update. *Journal of Drug Delivery Science and Technology* 2021, 66, 102914.

9. Lee, K. Y.; Mooney, D. J., Alginate: properties and biomedical applications. *Progress in polymer science* 2012, 37 (1), 106-126.
10. Augustine, R.; Alhussain, H.; Zahid, A. A.; Raza Ur Rehman, S.; Ahmed, R.; Hasan, A., Crosslinking Strategies to Develop Hydrogels for Biomedical Applications. Springer Singapore: 2021; pp 21-57.
11. Sun, J.; Tan, H., Alginate-based biomaterials for regenerative medicine applications. *Materials* 2013, 6 (4), 1285-1309.
12. Cao, J.; Su, M.; Hasan, N.; Lee, J.; Kwak, D.; Kim, D. Y.; Kim, K.; Lee, E. H.; Jung, J. H.; Yoo, J.-W., Nitric Oxide-Releasing Thermoresponsive Pluronic F127/Alginate Hydrogel for Enhanced Antibacterial Activity and Accelerated Healing of Infected Wounds. *Pharmaceutics* 2020, 12 (10), 926.
13. Lee, J.; Hlaing, S. P.; Cao, J.; Hasan, N.; Ahn, H. J.; Song, K. W.; Yoo, J. W., In Situ Hydrogel-Forming/Nitric Oxide-Releasing Wound Dressing for Enhanced Antibacterial Activity and Healing in Mice with Infected Wounds. *Pharmaceutics* 2019, 11 (10).
14. Urzedo, A. L.; Gonçalves, M. C.; Nascimento, M. H.; Lombello, C. B.; Nakazato, G.; Seabra, A. B., Cytotoxicity and Antibacterial Activity of Alginate Hydrogel Containing Nitric Oxide Donor and Silver Nanoparticles for Topical Applications. *ACS Biomaterials Science & Engineering* 2020, 6 (4), 2117-2134.
15. Pant, J.; Pedaparthi, S.; Hopkins, S. P.; Goudie, M. J.; Douglass, M. E.; Handa, H., Antibacterial and Cellular Response Toward a Gasotransmitter-Based Hybrid Wound Dressing. *ACS Biomaterials Science & Engineering* 2019, 5 (8), 4002-4012.

16. Ahonen, M. J. R.; Dorrier, J. M.; Schoenfisch, M. H., Antibiofilm efficacy of nitric oxide-releasing alginates against cystic fibrosis bacterial pathogens. *ACS infectious diseases* 2019.
17. Castanheira, E. J.; Correia, T. R.; Rodrigues, J. M.; Mano, J. F., Novel biodegradable laminarin microparticles for biomedical applications. *Bulletin of the Chemical Society of Japan* 2020, 93 (6), 713-719.
18. Joshi, S.; Patel, P.; Lin, S.; Madan, P., Development of cross-linked alginate spheres by ionotropic gelation technique for controlled release of naproxen orally. *Asian Journal of Pharmaceutical Sciences* 2012, 7 (1).
19. Atia, A.; Gomaa, A.; Fernandez, B.; Subirade, M.; Fliss, I., Study and Understanding Behavior of Alginate-Inulin Synbiotics Beads for Protection and Delivery of Antimicrobial-Producing Probiotics in Colonic Simulated Conditions. *Probiotics and Antimicrobial Proteins* 2018, 10 (2), 157-167.
20. Mao, X.; Li, X.; Zhang, W.; Yuan, L.; Deng, L.; Ge, L.; Mu, C.; Li, D., Development of Microspheres Based on Thiol-Modified Sodium Alginate for Intestinal-Targeted Drug Delivery. *ACS Applied Bio Materials* 2019, 2 (12), 5810-5818.
21. Zhang, Y.; Wang, Q. C.; Yu, H.; Zhu, J.; De Lange, K.; Yin, Y.; Wang, Q.; Gong, J., Evaluation of alginate-whey protein microcapsules for intestinal delivery of lipophilic compounds in pigs. *Journal of the Science of Food and Agriculture* 2016, 96 (8), 2674-2681.
22. Kim, Y. S.; Kim, H. W.; Lee, S. H.; Shin, K. S.; Hur, H. W.; Rhee, Y. H., Preparation of alginate–quaternary ammonium complex beads and evaluation of their antimicrobial activity. *International journal of biological macromolecules* 2007, 41 (1), 36-41.

23. Osmokrovic, A.; Jancic, I.; Vunduk, J.; Petrovic, P.; Milenkovic, M.; Obradovic, B., Achieving high antimicrobial activity: Composite alginate hydrogel beads releasing activated charcoal with an immobilized active agent. *Carbohydrate Polymers* 2018, 196, 279-288.
24. Flórez-Castillo, J. M.; Roperó-Vega, J. L.; Perullini, M.; Jobbágy, M., Biopolymeric pellets of polyvinyl alcohol and alginate for the encapsulation of Ib-M6 peptide and its antimicrobial activity against *E. coli*. *Heliyon* 2019, 5 (6), e01872.
25. Benavides, S.; Cortés, P.; Parada, J.; Franco, W., Development of alginate microspheres containing thyme essential oil using ionic gelation. *Food Chemistry* 2016, 204, 77-83.
26. Otari, S. V.; Patil, R. M.; Waghmare, S. R.; Ghosh, S. J.; Pawar, S. H., A novel microbial synthesis of catalytically active Ag–alginate biohydrogel and its antimicrobial activity. *Dalton Transactions* 2013, 42 (27), 9966.
27. Rijo, P.; Matias, D.; Fernandes, A.; Simões, M.; Nicolai, M.; Reis, C., Antimicrobial Plant Extracts Encapsulated into Polymeric Beads for Potential Application on the Skin. *Polymers* 2014, 6 (2), 479-490.
28. Narayanan, K. B.; Han, S. S., Dual-crosslinked poly(vinyl alcohol)/sodium alginate/silver nanocomposite beads – A promising antimicrobial material. *Food Chemistry* 2017, 234, 103-110.
29. Park, H. J.; Min, J.; Ahn, J.-M.; Cho, S.-J.; Ahn, J.-Y.; Kim, Y.-H., Effect of pH on the formation of lysosome-alginate beads for antimicrobial activity. *Journal of microbiology and biotechnology* 2015, 25 (2), 234-237.

30. Elçin, Y. M., Encapsulation of urease enzyme in xanthan-alginate spheres. *Biomaterials* 1995, 16 (15), 1157-1161.
31. Fath-Bayati, L.; Ai, J., Assessment of mesenchymal stem cell effect on foreign body response induced by intraperitoneally implanted alginate spheres. *Journal of Biomedical Materials Research Part A* 2020, 108 (1), 94-102.
32. Ge, Y.; Cui, X.; Liao, C.; Li, Z., Facile fabrication of green geopolymer/alginate hybrid spheres for efficient removal of Cu(II) in water: Batch and column studies. *Chemical Engineering Journal* 2017, 311, 126-134.
33. Mali, N. M.; Kim, Y.-H.; Park, J. M.; Kim, D.; Heo, W.; Dao, B. L.; Lim, J. O.; Oh, J. W., Characterization of Human Dermal Papilla Cells in Alginate Spheres. *Applied Sciences* 2018, 8 (10), 1993.
34. Hu, Y.; Wei, X.; Hu, Y.; Wang, W.; Fan, J.; Liu, X.; Chai, W.; Zhou, Z.; Ren, Z., Facile preparation of sodium alginate-based gel spheres by droplet polymerization method for removal of levofloxacin from aqueous solution. *Chemical Engineering Journal* 2020, 392, 123718.
35. Kanafi, M. M.; Ramesh, A.; Gupta, P. K.; Bhonde, R. R., Dental pulp stem cells immobilized in alginate microspheres for applications in bone tissue engineering. *International Endodontic Journal* 2014, 47 (7), 687-697.
36. Rosowski, M.; Falb, M.; Tschirschmann, M.; Lauster, R., Initiation of Mesenchymal Condensation in Alginate Hollow Spheres? A Useful Model for Understanding Cartilage Repair? *Artificial Organs* 2006, 30 (10), 775-784.
37. Madry, H.; Cucchiari, M.; Stein, U.; Remberger, K.; Menger, M. D.; Kohn, D.; Trippel, S. B., Sustained transgene expression in cartilage defects in vivo after

transplantation of articular chondrocytes modified by lipid-mediated gene transfer in a gel suspension delivery system. *The Journal of Gene Medicine* 2003, 5 (6), 502-509.

38. Kumaravel, V.; Gopal, S. R., Immobilization of *Bacillus amyloliquefaciens* MBL27 cells for enhanced antimicrobial protein production using calcium alginate beads. *Biotechnology and Applied Biochemistry* 2010, 57 (3), 97-103.

39. Dall, G. F.; Tsang, S. T. J.; Gwynne, P. J.; Wilkinson, A. J.; Simpson, A. H. R. W.; Breusch, S. J. B.; Gallagher, M. P., The dissolvable bead: A novel in vitro biofilm model for evaluating antimicrobial resistance. *Journal of Microbiological Methods* 2017, 142, 46-51.

40. Walczak, J.; Marchewka, J.; Laska, J., Hydrogels based on ionically and covalently crosslinked alginates. *Engineering of Biomaterials* 2014, 17.

41. Vicini, S.; Castellano, M.; Mauri, M.; Marsano, E., Gelling process for sodium alginate: New technical approach by using calcium rich micro-spheres. *Carbohydrate polymers* 2015, 134, 767-774.

42. Paques, J. P.; Sagis, L. M. C.; Van Rijn, C. J. M.; Van Der Linden, E., Nanospheres of alginate prepared through w/o emulsification and internal gelation with nanoparticles of CaCO₃. *Food Hydrocolloids* 2014, 40, 182-188.

43. Bajpai, S.; Sharma, S., Investigation of swelling/degradation behaviour of alginate beads crosslinked with Ca²⁺ and Ba²⁺ ions. *Reactive and Functional Polymers* 2004, 59 (2), 129-140.

44. Costa, A. M.; Alatorre-Meda, M.; Alvarez-Lorenzo, C.; Mano, J. F., Superhydrophobic surfaces as a tool for the fabrication of hierarchical spherical polymeric carriers. *Small* 2015, 11 (30), 3648-3652.

45. Wu, W.; Gaucher, C.; Fries, I.; Hu, X.-M.; Maincent, P.; Sapin-Minet, A., Polymer nanocomposite particles of S-nitrosoglutathione: A suitable formulation for protection and sustained oral delivery. *International journal of pharmaceutics* 2015, 495 (1), 354-361.
46. Ozkan, E.; Mondal, A.; Douglass, M.; Hopkins, S. P.; Garren, M.; Devine, R.; Pandey, R.; Manuel, J.; Singha, P.; Warnock, J., Bioinspired ultra-low fouling coatings on medical devices to prevent device-associated infections and thrombosis. *Journal of Colloid and Interface Science* 2021.
47. Choi, M.; Hasan, N.; Cao, J.; Lee, J.; Hlaing, S. P.; Yoo, J.-W., Chitosan-based nitric oxide-releasing dressing for anti-biofilm and in vivo healing activities in MRSA biofilm-infected wounds. *International journal of biological macromolecules* 2020, 142, 680-692.
48. Champeau, M.; Pova, V.; Militao, L.; Cabrini, F. M.; Picheth, G. F.; Meneau, F.; Jara, C. P.; de Araujo, E. P.; de Oliveira, M. G., Supramolecular poly(acrylic acid)/F127 hydrogel with hydration-controlled nitric oxide release for enhancing wound healing. *Acta biomaterialia* 2018, 74, 312-325.
49. Kang, Y.; Kim, J.; Lee, Y. M.; Im, S.; Park, H.; Kim, W. J., Nitric oxide-releasing polymer incorporated ointment for cutaneous wound healing. *Journal of Controlled Release* 2015, 220, 624-630.
50. Schanuel, F. S.; Raggio Santos, K. S.; Monte-Alto-Costa, A.; de Oliveira, M. G., Combined nitric oxide-releasing poly(vinyl alcohol) film/F127 hydrogel for accelerating wound healing. *Colloids Surf B Biointerfaces* 2015, 130, 182-91.
51. Grant, G. T., Biological interactions between polysaccharides and divalent cations: the egg-box model. *Febs Lett.* 1973, 32, 195-198.

52. De Groote, M. A.; Fang, F. C., NO inhibitions: antimicrobial properties of nitric oxide. *Clinical Infectious Diseases* 1995, 21 (Supplement_2), S162-S165.
53. DeGroote, M. A.; Fang, F. C., Antimicrobial properties of nitric oxide. In *Nitric oxide and infection*, Springer: 2002; pp 231-261.
54. Stamler, J., S-nitrosothiols and the bioregulatory actions of nitrogen oxides through reactions with thiol groups. *The role of nitric oxide in physiology and pathophysiology* 1995, 19-36.
55. Juedes, M. J.; Wogan, G. N., Peroxynitrite-induced mutation spectra of pSP189 following replication in bacteria and in human cells. *Mutation Research/Fundamental and Molecular Mechanisms of Mutagenesis* 1996, 349 (1), 51-61.
56. Fang, F. C., Perspectives series: host/pathogen interactions. Mechanisms of nitric oxide-related antimicrobial activity. *The Journal of clinical investigation* 1997, 99 (12), 2818-2825.
57. Liang, C.-C.; Park, A. Y.; Guan, J.-L., In vitro scratch assay: a convenient and inexpensive method for analysis of cell migration in vitro. *Nature Protocols* 2007, 2 (2), 329-333.
58. Leite, Á. J.; Caridade, S. G.; Mano, J. F., Synthesis and characterization of bioactive biodegradable chitosan composite spheres with shape memory capability. *Journal of Non-Crystalline Solids* 2016, 432, 158-166.
59. Lima, A. C.; Mano, J. F.; Concheiro, A.; Alvarez-Lorenzo, C., Fast and mild strategy, using superhydrophobic surfaces, to produce collagen/platelet lysate gel beads for skin regeneration. *Stem Cell Reviews and Reports* 2015, 11 (1), 161-179.

60. Lautner, G.; Meyerhoff, M. E.; Schwendeman, S. P., Biodegradable poly(lactic-co-glycolic acid) microspheres loaded with S-nitroso-N-acetyl-D-penicillamine for controlled nitric oxide delivery. *J Control Release* 2016, 225, 133-9.

CHAPTER 4
DUAL ACTION NITRIC OXIDE AND FLUORIDE ION-RELEASING HYDROGELS FOR
COMBATting DENTAL CARIES³

³L. M. Estes Bright*, M. R. S. Garren*, M. Ashcraft, A. Kumar, H. Husain, E. J. Brisbois, and H. Handa. 2022. *ACS Applied Materials & Interfaces*. 14(19): 21916-21930.

Reprinted here with permission of the publisher. *Authors declare equal contribution.

ABSTRACT

Demineralization and breakdown of tooth enamel are characterized by a condition called dental caries, or tooth decay, which is caused by two main factors, 1) highly acidic food intake without proper oral hygiene, and 2) overactive oral bacteria generating acidic metabolic byproducts. Fluoride treatments have been shown to help rebuild the hydroxyapatite structures that make up 98% of enamel but do not tackle the bacterial overload that continues to threaten future demineralization. Herein, we have created a dual-function Pluronic F127-Alginate hydrogel with nitric oxide (NO)- and fluoride-releasing capabilities for the two-pronged treatment of dental caries. Analysis of the hydrogels demonstrated porous, shear-thinning behaviors with tunable mechanical properties. Varying the weight percent of the NO donor *S*-nitrosoglutathione (GSNO) within the hydrogel enabled physiologically actionable NO release over 4 h, with the fabricated gels demonstrating storage stability over 21 d. This NO-releasing capability resulted in a 97.59% reduction of viable *Streptococcus mutans* in the planktonic state over 4 h and reduced pre-formed biofilm mass by 52% after 24 h. Delivery of fluoride ions was confirmed by a fluoride-sensitive electrode, with release levels resulting in significant prevention of demineralization of hydroxyapatite discs after treatment with an acidic demineralization solution. Exposure to human gingival fibroblasts and human osteoblasts showed cytocompatibility of the hydrogel, demonstrating the potential for the successful treatment of dental caries in patients.

KEYWORDS: Nitric oxide, Dental carries, Demineralization, Antimicrobial, Hydrogel, *S*-nitrosoglutathione

4.1 Introduction

Dental caries, or tooth decay, are the leading cause of oral pain and tooth loss.¹ Deterioration is caused by several factors, the most prominent being decay-causing bacteria in the mouth producing strong acids that attack enamel and induce cavitation. Fortunately, several preventative measures for these infections exist including having good oral hygiene, limiting food high in sugars and starches, seeing a dentist for regular check-ups, and using fluoride – a mineral that can prevent, stop, and reverse tooth decay.² The successful prevention of cavities by fluoride in the oral environment is achieved through fluoride ions catalyzing the diffusion of calcium and phosphate from saliva into tooth enamel. The calcium and phosphate remineralize crystalline structures within cavities, forming surfaces of fluoridated hydroxyapatite (HA) and fluorapatite, which are more resistant to acidic erosion than primary HA, a mineral that comprises 95-98% of tooth enamel.^{1, 3} Due to the strengthening and rebuilding capabilities of fluoride, it is not only used in community water sources, but also as a component in some toothpastes. Further, most dental offices utilize fluoride treatments following bi-annual cleanings, usually in a foam or paste form. Fluoride serves as a useful treatment for minor cavities and tooth decay, but enamel reconstruction does not tackle the microbial source of dental caries.

The root of dental caries lies in the overactivity of bacteria on gums and teeth. *Streptococcus mutans* (*S. mutans*) and other dental pathogens colonize on the surface of teeth and form biofilms composed of protein, DNA, and polysaccharides.^{1, 4} These biofilms, known as dental plaque, act as a protective barrier against antimicrobial treatments and allow the bacteria to proliferate uncontrolled. The harmful aspect of these bacteria lies in their metabolism of fermentable carbohydrates which produces weak organic acids that decrease the localized pH of the oral environment.^{1, 5, 6} The acidity results in dissolution and decay of the tooth enamel. Untreated oral biofilms persisting on

the surface of teeth are the most common source of imbalance and can lead to large cavities necessitating dental treatment. Thus, many dentists focus on the prevention of oral biofilm formation to inhibit dental caries progression. Several therapeutics are utilized for plaque control including chlorhexidine, triclosan, and even amine fluoride.^{7, 8} However, these chemicals mainly prevent the adhesion of bacteria to the enamel surface and have a difficult time tackling mature plaque biofilms, oftentimes only killing bacteria on the surface of the plaque. Furthermore, the harsh chemical compounds easily disrupt the delicate biological environment of the mouth, killing beneficial oral microbes.⁸ It has been suggested that antiplaque agents would be more effective if they were able to enhance the local immune responses to bacterial biofilms, killing cavity-causing pathogens without detrimental effects on the oral environment.⁹

Rather than using synthetic constructs to prevent bacterial adhesion, our body attacks oral biofilms using an active and potent technique. Nitric oxide (NO) is an endogenously produced gaseous molecule with broad-spectrum antimicrobial and antiviral properties able to penetrate and disperse mature biofilms, killing microbes by inflicting oxidative and nitrosative stress on lipids, proteins, metabolic transporters, and DNA.¹⁰⁻¹³ Oral NO has even been shown to be upregulated during plaque deposition¹⁴ and in patients with periodontitis¹⁵, displaying our body's limited innate capacity to kill bacteria and break down biofilms before they can cause further complications. In an effort to mimic and enhance the physiological response to bacterial invasions, NO-releasing compounds have been developed with proven effectiveness against oral pathogens, including *S. mutans*¹⁶⁻¹⁹, and have even displayed increased efficacy at lower pH levels associated with dental caries.^{18, 19} However, unlike fluoride treatments, hydrogels have not been utilized in the delivery of NO for dental applications. If a hydrogel could stably release NO, it could implicate a dual treatment option for combined fluoride and NO delivery.

Several gels have been used for NO release as general antimicrobial platforms,²⁰ wound healing therapies,²¹ or analgesics²² based on Pluronic F127 formulations. Pluronic F127 is a synthetic thermosensitive triblock copolymer comprised of units of ethylene oxide and polypropylene oxide. Hydrogels formed from the polymer have complex network morphologies allowing for high permeability.²³ To add stability and decrease diffusion rates, Pluronic F127 can be combined with alginate, a natural polymer that is easily crosslinked by the addition of divalent cations such as Ca^{2+} .²⁴ Alginate is biocompatible, inexpensive, and widely used in the biomedical industry due to its resemblance to the extracellular matrix in human tissues, attributing to its successful delivery of small drugs and proteins.²⁵ The combination of Pluronic F127 and alginate creates a composite gel with increased erosion resistance while demonstrating a 'stronger,' more stable alginate gel interspersed within a 'softer' thermosensitive Pluronic F127 matrix.^{24,26} Through a dual crosslinking process, an interpenetrating network (IPN) of alginate is formed within the Pluronic F127 porous structure via CaCl_2 crosslinking, enabling gels with thermoresponsive properties and superior mechanical and rheological performance. Therefore, utilization of crosslinked alginate within the thermosensitive Pluronic F127 matrix allows for more stable NO and fluoride release without compromising biocompatibility.

Herein, we have developed NO- and fluoride ion-releasing hydrogels (**Figure 4.1**) to eradicate oral pathogens such as *S. mutans* and prevent demineralization of HA in tooth enamel. The fabricated gels were characterized for chemical and physical attributes, including quantification of NO and fluoride release. Combining antimicrobial properties from NO with the enamel strengthening potential of fluoride, the hydrogels were examined for antibacterial capacity against *S. mutans* and *Escherichia coli* (*E. coli*) and further evaluated for demineralization prevention using a hydroxyapatite enamel model. Finally,

gels were examined in 4 and 24-h studies of cellular cytocompatibility in mammalian cells. The proposed material provides an effective single treatment displaying antibacterial and remineralization potential. Since current treatment of dental caries involves a full cleaning in addition to fluoride treatments and harsh antibacterial chemicals, this solution presents a viable alternative with shorter treatment times and less disruption of the innately sensitive oral environment.

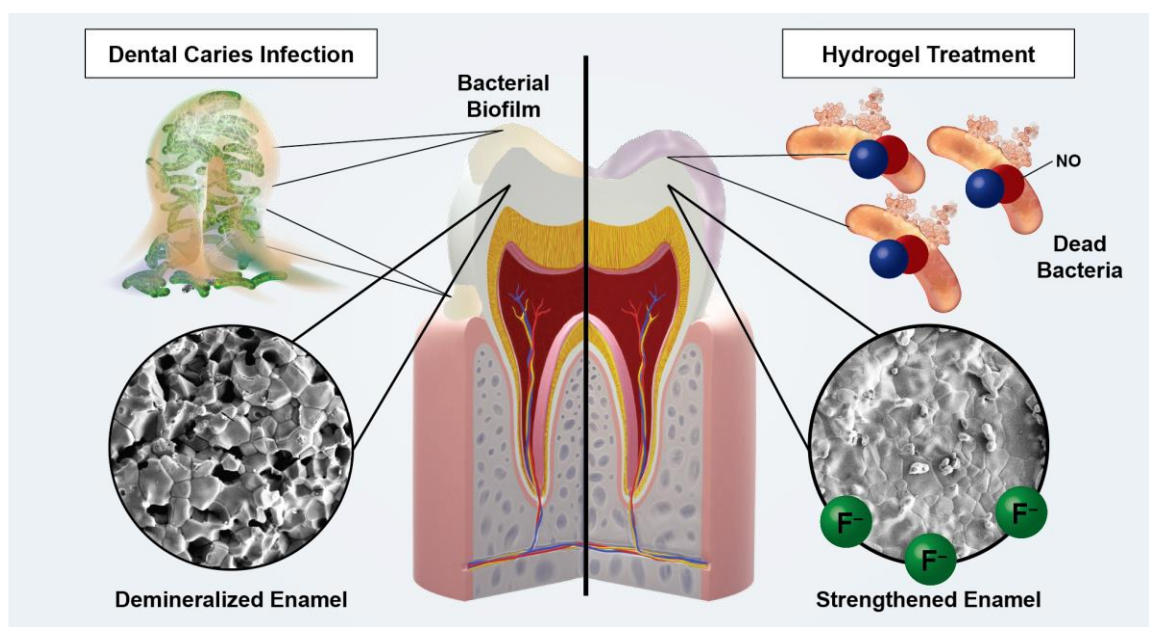


Figure 4.1 Effective treatment of dental caries with the NO and fluoride ion-releasing hydrogels

4.2 Materials and Methods

4.2.1 Materials

Acetone, calcium chloride dihydrate, ethylenediaminetetraacetic acid (EDTA), magnesium chloride, methanol, Pluronic® F-127, potassium phosphate dibasic, sodium

alginate, sodium ascorbate, sodium carboxymethylcellulose, sodium chloride, sodium nitrite, and Luria Bertani (LB) broth and agar were purchased from Sigma-Aldrich (St. Louis, MO USA). Reduced L-glutathione (GSH) and G-418 sulfate were purchased from Gold Biotechnology (Jersey City, NJ USA). Sodium fluoride was purchased from Himedia Laboratories (West Chester, PA USA). Citric acid was purchased from J.T. Baker (Phillipsburg, NJ USA). Hydrochloric acid (37%) and fetal bovine serum (FBS) were purchased from VWR (Radnor, PA USA). Hydroxyapatite disc coupons were obtained from BioSurface Technologies Corporation (Bozeman, MT USA). All buffers and other aqueous solutions were prepared using 18.2 M Ω ultra-pure water using an in-house distillation apparatus from Mettler Toledo (Columbus, OH USA). Phosphate-buffered saline (1x PBS) containing 2.7 mM KCl, 138 mM NaCl, 1.8 mM KH₂PO₄, and 10 mM Na₂HPO₄ at pH 7.4 was used in all *in vitro* experiments. Brain heart infusion agar and broth were purchased from McKesson Medical-Surgical (Irving, TX 75039). *Streptococcus mutans* (ATCC® 25175™) and *Escherichia coli* (*E. coli*, ATCC® 25922™) were purchased from American Type Culture Collection (ATCC, Manassas, VA, USA). Human derived osteoblast cell line hFOB 1.19 (ATCC® CRL-11372™), Primary Gingival Fibroblast, Normal, Human, Adult (HGF) (ATCC® PCS-201-018™), fibroblast basal medium, and corresponding fibroblast growth kit with low serum were also purchased from ATCC. Dulbecco's modified Eagle's medium with Nutrient Mixture F-12 (1:1 by volume) was purchased from Thermo Fisher Scientific (Waltham, MA USA). Trypsin-EDTA was obtained from Corning (Corning, NY USA). The Cell Counting Kit-8 (CCK-8) was procured from Enzo Life Sciences (Farmingdale, NY USA).

4.2.2 Synthesis of S-nitrosoglutathione (GSNO)

GSNO was readily synthesized by the acid-catalyzed nitrosation of GSH with sodium nitrite following previous literature.²⁷ Only GSNO batches of greater than 95%

purity were used for fabrication of hydrogels, as determined by measurement of NO moles released per mole of GSNO via chemiluminescent-based nitric oxide release analysis.

4.2.3 Artificial Saliva and Demineralization Solutions

Artificial saliva solution consisted of 1.2 g L⁻¹ KCl, 1 g L⁻¹ sodium carboxymethylcellulose, 0.8 g L⁻¹ NaCl, 0.3 g L⁻¹ K₂HPO₄, 0.1 g L⁻¹ CaCl₂•2H₂O, and 0.1 g L⁻¹ MgCl₂•6H₂O in deionized water.^{28, 29} Artificial saliva was thoroughly dissolved and sterilized by steam autoclaving for 45 min at 121°C before all experiments. Demineralization solution was comprised of 0.1 M citric acid adjusted to pH = 3.³⁰

4.2.4 Fabrication of Hydrogel Networks

Four kinds of alginate-Pluronic® F127 hydrogels were prepared: the first contained only alginate (2% w/v) and Pluronic® F127 (18% w/v) (PA), the second one added sodium fluoride (0.2% w/v, approximately 2,000 ppm) (PA-F), the third one added GSNO (PA-G_x), and the fourth added both sodium fluoride (0.2% w/v, approximately 2,000 ppm) and GSNO (PA-F-G_x) (**Table 4.S1**). GSNO-containing gels were prepared with a sol concentration of 10 (G₁₀), 20 (G₂₀), and 30 mg/mL (G₃₀) (**Figure 4.2**). The ratio of alginate to Pluronic® F127 was adopted from previous studies.^{24, 26} Precursor solutions were first prepared by dissolving sodium alginate in deionized water at 60 °C for 45 min. Afterward, the solution was cooled to room temperature and GSNO and NaF were added at the previously mentioned concentrations. Pluronic® F127 flakes were then added to the samples, which were stored at 4 °C for up to 24 h before use. Before casting, solutions were stirred at room temperature for 1 h to ensure complete dissolution of components, after which a proportionate volume of the precursor solution was aliquoted into a 60 x 15 mm petri dish. Dishes were covered and wrapped in parafilm to retain moisture and incubated at 37 °C for 30 min (thermal gelation of pristine Pluronic F127 starts at 20°C and concludes near 24 °C).³¹ Afterwards, a CaCl₂ crosslinking solution (1 g L⁻¹ in deionized

water) was quickly sprayed onto the gel in aliquots of exactly 100 μL each. The volume of crosslinking solution was approximately equal to the volume of the gel. The gel was left in contact with the crosslinking solution for 2 h at room temperature and protected from light. Afterward, the remaining solution was aspirated off the gel, which was then cut into individual gels (8 mm in diameter), briefly rinsed 3x with deionized water to remove excess components not swollen into the gel, and gently padded with a nonwoven wipe to remove excess surface moisture. All *in vitro* bacteria and cell culture experiments followed the same procedure for gel preparation, with the exceptions being that the precursor solution was UV sterilized for 30 min and the CaCl_2 crosslinking solution was sterile filtered (< 0.22 μm filter).

4.2.5 Attenuated Total Reflectance-Fourier Transform Infrared (ATR-FTIR)

Spectroscopy

ATR-FTIR spectroscopic measurements were performed using a Spectrum Two spectrometer from Perkin Elmer (Greenville, SC USA) to determine the chemical functionality of freeze-dried hydrogel samples and precursor materials. Infrared spectra were recorded from 4000 – 650 cm^{-1} with a total of 16 scans using a resolution of 4 cm^{-1} . A KBr loading method was used for each analysis. In a representative test, a 1 wt% mixture of analyte was dissolved in anhydrous potassium bromide, cast into a 7-mm die-cast, and processed for 5 min at 1.5 tons of applied force. Three independently prepared specimens were analyzed for each sample type. Final spectra were baseline corrected.

4.2.6 Scanning Electron Microscopy and Energy-Dispersive X-ray Spectroscopy

Microscopy techniques were used to examine the surface morphology and composition of each of the four gel types (PA, PA-F, PA-G₃₀, PA-F-G₃₀). After making 8 mm circular punches and rinsing, the samples were lyophilized for ~6 hours and stored at room temperature shielded from light. Samples were then coated with 10 nm gold-

palladium using a Leica sputter coater (Leica Microsystems). Scanning electron microscopy (SEM, FEI Teneo, FEI Co.) was utilized to acquire images of the cross-sectional morphology and porosity of the varying gels. An energy-dispersive x-ray spectroscopy system (EDS, Oxford Instruments) was used in conjunction with the SEM setup to perform elemental analysis of the four sample types. Fluorine measurements corresponded to the presence of sodium fluoride. An accelerating voltage of 5.00 kV was used for SEM and 20.00 kV for EDS.

4.2.7 Swelling Capacity

The swelling capacities of all four gel types were characterized to determine the change in water uptake characteristics with the addition of NaF and GSNO. Hydrogels were fabricated as previously described and 8 mm diameter punches were lyophilized for 6 h. Following lyophilization, gels were weighed (W_d) and then soaked in artificial saliva for 1 h or 4 h at 37 °C in the dark. At that time, gels were removed from the artificial saliva, placed on a nonwoven wipe for 5 seconds, flipped, and then weighed (W_s). The swelling capacity was calculated using **Equation 4.1**.

$$\text{Swelling Capacity (\%)} = \frac{W_s - W_d}{W_d} * 100 \quad \text{Equation 4.1}$$

4.2.8 Compression Testing

Uniaxial compression testing of the formulated hydrogels was performed with a Mark-10 Series 5 force gauge equipped with a motorized stand (Mark-10, Copiague, NY USA). For compressive testing, cylindrical samples of the crosslinked hydrogels (approximately 12 mm in diameter and 2 mm in height) were fabricated and tested. Samples were placed between two parallel plates and tested at 25% strain at a rate of 0.166 mm s⁻¹. A total of five independently prepared samples for each hydrogel formulation were tested.

4.2.9 Viscometry Testing

Controlled shear rate tests of the hydrogels were performed using a DV-II+ Pro Viscometer (Brookfield Engineering Laboratories, Middleboro, MA, USA) equipped with a cone-shaped spindle with a cone angle of 0.8° and radius of 2.4 cm. Speed ramping was performed following ISO 3219 standards following a geometric series for rotational shear rate from 0.1 to 100 s^{-1} with a multiplier of 2.5 and variable hold times to account for transient effects in the low shear regions of the studies. Approximately $500\ \mu\text{L}$ of each crosslinked gel was molded into a cylindrical sample and placed into the apparatus. Studies were performed with a temperature-controlled cup heated to $37\text{ }^\circ\text{C}$. A total of five independently prepared samples for each hydrogel formulation were tested. Shear-recovery studies were conducted similarly, with temperature control of the cup at $37\text{ }^\circ\text{C}$ with repeated ramping from low shear (10 s^{-1}) to high shear (100 s^{-1}) with hold times of 100 s. Temperature ramps at constant shear rates (i.e., 25, 50, 75, and 100 s^{-1}) were conducted for PA-F-G₃₀ gels with temperature control from 10 to $40\text{ }^\circ\text{C}$ in increments of $0.5\text{ }^\circ\text{C}$.

4.2.10 GSNO Loading

The relative number of moles of GSNO loaded per mass of hydrogel in PA-G_x and PA-F-G_x gels were determined via a modified NO loading quantification method using a Sievers chemiluminescence nitric oxide analyzer (NOA) 280i (Boulder, CO 80301).³² In the experimental setup, NO gas liberated from the solution phase inside an amber glass sample vial is swept by a nitrogen carrier stream into the reaction chamber of the NOA, wherein NO is reacted with ozone from a separate inlet stream and converted into NO₂ in an excited state. Relaxation of this excited state results in the emission of photons which are internally detected via a photomultiplier tube. This photon flux is then correlated against a calibration constant (nmol NO/PPB × min) established from a 45 ppm NO gas

standard to determine the instantaneous NO release with respect to the mass of gel tested (nmol NO/(mg gel × min)).

In a representative study, circular punchouts of the hydrogel films were weighed (~50 mg each) and placed in an amber glass sample vial supplemented with 3 mL of 1x PBS without EDTA. Alternating 200 µL injections of 100 mM solutions of copper (II) chloride and sodium ascorbate were added to the sample chamber to stimulate the degradation of the S-nitrosothiol bond in GSNO by Cu¹⁺ ions.³³ Injections were added until the NO payload was depleted from each sample. A plot of the NO release (nmol NO/min) against time (min) was then adjusted for a baseline reading without the sample, integrated over the duration of the experiment, and divided by the mass of the gel to obtain the loading ratio (nmol NO/mg gel).

4.2.11 NO Release Under Physiological Conditions

The instantaneous release profiles of NO from GSNO loaded hydrogels were determined across several sol concentrations of GSNO with and without NaF incorporation using chemiluminescence-based NO detection. In a representative study, a hydrogel film is weighed (~50 mg) and wrapped in a nonwoven wipe moistened with artificial saliva solution. The wrapped hydrogel is then suspended above 1x PBS without submerging in an amber glass sample vial placed in a water bath at 37 °C. No metal ion catalyst or reducing agent was added. The instantaneous NO release is measured over a 4 h study and corrected against a baseline reading of the instrument. Each gel-type was run in triplicate.

4.2.12 Storage Stability Analysis (28 d)

To assess the storage stability of the NO-releasing GSNO component of the dental gels, PA-G₃₀ and PA-F-G₃₀ gels were fabricated and stored at 4 °C for up to 28 d. Triplicates of gels were removed from storage conditions and tested in the NOA after 0,

1, 7, 14, 21, and 28 d of storage. Gels were discarded after measurement. The NOA setup was identical to that previously described in the prior NO release section. Therefore, this study assessed NO release in simulated physiological conditions at each time point to determine how much NO release capability was lost over time, or how long the gels could be stored at 4 °C and still maintain potency. NO release measurements were recorded as cumulative 1 h release sums (mmol NO/mg gel).

4.2.13 Fluoride Release

Fluoride ion release was quantified following International Organization for Standardization (ISO) 19448:2018 standards for the analysis of fluoride concentrations in aqueous solutions from dental products.^{34, 35} Cumulative fluoride ion release from the hydrogel samples was determined using a fluoride ion-selective TruLine electrode from Xylem Incorporated (Rye Brook, NY USA) against a standard calibration curve in artificial saliva developed against a total ionic strength adjustment buffer (TISAB) from YSI Incorporated (Yellow Springs, OH USA). In brief, hydrogel samples (50 mg each) were incubated in 3 mL of artificial saliva solution for corresponding time points of 10 and 60 min at room temperature. Afterward, the solution was aspirated off and stored at 4 °C until processing. The electric potential was then measured for each sample time point for PA-F and PA-F-G₃₀ gels (n = 5 per treatment time, per hydrogel type). A standard calibration curve was developed using sodium fluoride in TISAB by linearly fitting a plot of the average electric potentials to the log₁₀ of the known fluoride ion concentration in the analytes. From this, the number of moles of fluoride ions released per mass of hydrogel was calculated using **Equation 4.2**.

$$\frac{\text{Mole F}^-}{\text{Mass Gel}} = 10^{\frac{\text{Electric Potential}-\text{Intercept}}{\text{Slope}}} \times \frac{\text{Volume of Analyte}}{\text{Mass of Gel}} \quad \text{Equation 4.2}$$

4.2.14 Bacteria Culture

Viable bacterial colonies were prepared for antimicrobial tests using the following procedure. A single *S. mutans* colony was isolated, inoculated in BHI broth, and grown to mid-log phase at 37 °C and 150 rpm in a shaker incubator. The bacteria suspension was then rinsed with and resuspended in 1x PBS, and then diluted to $\sim 10^7$ CFU/mL. The diluted suspension of known bacteria counts was then used to study a 4 h bacterial exposure and 24 h treatment of a biofilm (grown for 36 h before treatment) with the antibacterial dental gel. The same procedures above were used to prepare the *E. coli* bacterial suspension except for the use of LB broth and agar rather than BHI.

4.2.15 Planktonic Bacterial Viability Study

A 4 h bacterial viability study was utilized to monitor the antibacterial efficacy of the gels against *S. mutans*, one of the most common pathogens known to cause dental caries, as well as *E. coli*, a common Gram-negative pathogen. Sterilized gels of each type ($n = 3$) were placed in a 24 well plate and incubated for 4 h at 37 °C and 150 rpm in a shaker incubator with 1 mL of the bacterial suspension in 1x PBS + 5% (v/v) media. Following incubation, 100 μ L from each well was removed and serial dilutions were performed. Diluted suspensions were plated on BHI agar and placed in an incubator for 48 h (24 h for *E. coli*). After 24 – 48 h of growth, bacterial colonies were counted to determine the number of viable bacteria per mg of hydrogel treatment. Viable CFUs for each sample were calculated using **Equation 4.3**, and the percentage of bacteria reduction from each treatment versus PA control was calculated using **Equation 4.4**.

$$\text{Viable CFUs per sample} = \frac{\text{number CFUs per sample} \times \text{dilution factor} \times \text{vol suspension treated}}{\text{vol suspension plated}} \quad \text{Equation 4.3}$$

$$\% \text{ Reduction in Bacterial Viability} = \frac{\text{control CFU mL}^{-1} - \text{treatment CFU mL}^{-1}}{\text{control CFU mL}^{-1}} \times 100\% \quad \text{Equation 4.4}$$

4.2.16 *S. mutans* Biofilm Dispersal

Crystal violet (CV) staining was utilized to quantify the ability of the NO-releasing PA-F-G₃₀ gels to disperse a biofilm grown on a HA disc. Before treatment, HA discs were sonicated in DI water for 30 min to remove any loose particles and then sterilized under UV light for 15 min on each side. Discs were then placed in a 24-well plate and a previously prepared inoculum of *S. mutans* in BHI media was added to the wells. The plate was sealed and placed in a shaking incubator at 37 °C for 36 h, with media changed every 8-12 h. Following 36 h of biofilm growth, HA discs were removed from the plate, lightly rinsed with 1 mL of 1x PBS, and placed in a new well plate. Sterile gels (PA or PA-F-G₃₀, n = 4) were then placed on top of the HA discs and 1 mL of 1x PBS was added to the wells. Control discs without gel treatment were also submerged in 1 mL 1x PBS to act as the untreated control. After 24 h of incubation at 37 °C and under shaking conditions the gels were rinsed off the HA discs and the discs were rinsed twice with 1x PBS. One sample from each treatment or control was prepared for SEM imaging, while the remaining three underwent the staining process. Treated and control HA discs were placed in a 48-well plate and 300 µL of 0.1% CV solution was added to each well. After incubation of the plate at room temperature for 15 min, each disc was rinsed 4 times with DI water and placed in a new well plate to dry overnight. The next day, 300 µL of 30% acetic acid was added to each well to dissolve the CV for 15 min. Following dissolution, 125 µL from each well was added to a 96-well plate and the absorbance at 540 nm was recorded and used for analysis, with 30% acetic acid used as a blank.

4.2.17 Demineralization of Hydroxyapatite Enamel Model

The potential of the gels to prevent the demineralization of HA discs was investigated. Before beginning the study, all HA discs were sonicated in DI water for 30 min and rinsed lightly to remove any loose HA particles. Discs were then placed in

individual wells of a 24 well plate, covered with an 8 mm in diameter gel disc of the corresponding treatment group (n = 3), and 1 mL artificial saliva solution was added to each well. Treatment groups included control (no gel), PA, PA-F, PA-G₃₀, and PA-F-G₃₀. Following HA disc treatment in a shaker incubator (37°C, 150 rpm) for 1 h, gels were removed, and discs were rinsed 3x with DI water. Treated HA discs were then exposed to 1 mL demineralization solution for 30 min in a shaker incubator (37°C, 150 rpm). Demineralization solution was aspirated off and discs were rinsed 3x with DI water and dried overnight in a desiccator. The demineralization of the treated discs, characterized as induced porosity, was compared to untreated HA discs that were not exposed to demineralization solution using ImageJ analysis. The pixel area of pores was compared to the pixel area of the entire HA disc within the image and a percent porosity was calculated. A single-blinded review of the images was carried out by three researchers, with final average percent porosity measurements reported from the independent analyses of images from each sample type.

4.2.18 Mammalian Cell Culture

The cell lines HGF and hFOB 1.19 were cultured for cytocompatibility assessments. HGF cells were cultured in a fibroblast basal medium supplemented with the manufacturer's recommended growth kit (2% fetal bovine serum, 50 µg/mL ascorbic acid, 5 µg/mL recombinant human insulin, 1 µg/mL hydrocortisone hemisuccinate, 5 ng/mL recombinant human fibroblast growth factor b, and 7.5 mM L-glutamine) and penicillin-streptomycin (10 units/mL and 10 µg/mL, respectively). hFOB 1.19 cells were maintained in a 1:1 mixture of Ham's F12 Medium and Dulbecco's Modified Eagle's Medium supplemented with L-glutamine (2.5 mM), fetal bovine serum (10%), and G418 antibiotic (0.3 mg/mL). Both cell types were incubated at 37 °C in a 5 % CO₂ humidified atmosphere. The media was replaced every 48 h and both cell lines were subcultured

once monolayers were 80% confluent. Cells were detached from the flask surface via enzymatic treatment with 0.05% trypsin and 5 mM EDTA for 5 min, with isolation of cell pellets via centrifugation at 200 RCF for 5 min.

4.2.19 Cellular Cytotoxicity of GSNO and Precursor Sol Materials

The cellular cytotoxicity of GSNO against HGF and hFOB 1.19 cells was tested over 24 h direct contact experiments. In brief, suspensions of the cultured cells (50,000 cells/mL) were seeded (100 μ L/well) onto 96-well TC-treated plates. The plates were pre-incubated for 24 h to permit the cells to reach > 80% confluency. Afterward, 10 μ L of a GSNO stock solution (GSNO in 1x PBS) or non-crosslinked hydrogel sol was added (n = 5) to corresponding wells and the plate was incubated for an additional 24 h. The media in each well was aspirated off and replaced with fresh media to avoid interference from residual GSH and related species. CCK-8 solution (10 μ L/well) was then added to each well and the plate was incubated for 2 h. A separate set of wells containing only media and the dye (n = 5) was also prepared to account for background readings. The absorbance of each well was measured at 450 nm and adjusted against the average absorbance reading of the wells with only media. **Equation 4.5** was used to calculate the percentage cell viability of a treatment dosage relative to the untreated control as follows:

$$\% \text{ Cell Viability} = \frac{\text{Adjusted Average ABS}_{450} \text{ of Treated Set}}{\text{Adjusted Average ABS}_{450} \text{ of Untreated Set}} \times 100\% \quad \text{Equation 4.5}$$

4.2.20 Cellular Proliferation in the Presence of Hydrogels

The proliferation of HGF and hFoB 1.19 cells against crosslinked gels was also tested via 24 h direct contact experiments to further evaluate the biocompatibility of the gel formulations. In short, suspensions of the cultured cells (50,000 cells/mL) were inoculated (400 μ L/well) into 24-well TC-treated plates. After 24 h of incubation, hydrogel film punches (50 mg each) were UV sterilized for 30 min and then inserted into

corresponding wells ($n = 5$ per type). After an additional 24 h of incubation, the hydrogel and media were aspirated off and replaced with 400 μL of fresh media. CCK-8 dye was added (40 $\mu\text{L}/\text{well}$) to determine the relative proliferation of cells in treated versus untreated samples, with measurements adjusted against blank wells and final cellular viability calculated using **Equation 4.5**.

4.2.21 Statistical Analysis

All data are reported as mean \pm standard deviation (SD) unless otherwise stated. All statistical analysis was performed using Prism 9.1 (GraphPad Software, San Diego, CA USA). Statistical comparisons among treatment groups were performed using ordinary one-way analysis of variance with corrections for multiple comparisons tests between means of sample groups via Tukey's method. Bacterial statistical analysis was performed on the log values of CFUs for each treatment. Values of $p < 0.05$ were deemed significant.

4.3 Results and Discussion

4.3.1 Fabrication of Hydrogel Networks

Thermoresponsive hydrogels featuring Pluronic F127 as the major network with an interpenetrating crosslinked alginate backbone have previously been shown as highly biocompatible and display promise for drug release applications.²⁴ Pluronic F127 is a synthetic poly(ethylene oxide) poly(propylene oxide)-poly(ethylene oxide) (PEO-PPO-PEO) tri-block copolymer that is nonionic with thermosensitive properties for micelle formation and stability in aqueous conditions. Combination systems of Pluronic F127 with non-crosslinked alginate have been shown to act as efficacious scaffolds for dental-derived cell encapsulation as well as the enhancement of cell adhesion and promotion of angiogenesis.³⁶ In this study, hydrogels of Pluronic F127 with crosslinked alginate (PA) were functionalized with different weight percentages of GSNO and NaF, resulting in the

PA-F-G_x hydrogels with unique antimicrobial and enamel strengthening properties (**Figure 4.2**).

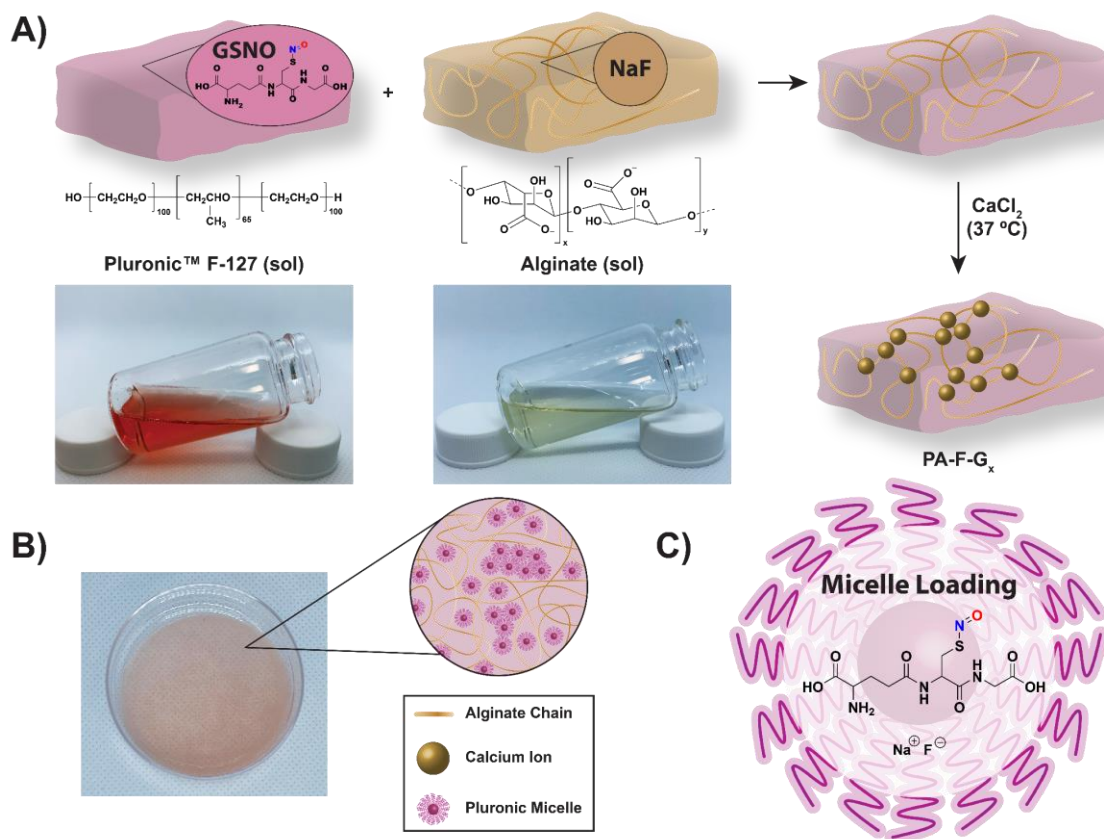


Figure 4.2 Overview of the NO-releasing hydrogel system. Fabrication (A) of Pluronic-alginate hydrogels begins with the preparation of a Pluronic sol blended with GSNO at different weight ratios. This sol is combined with an alginate sol (with NaF incorporated) slightly below room temperature. The mixture is cast into dishes, heated to 37 °C, and crosslinked via rapid application of calcium chloride solution. The as-prepared hydrogel (B) forms a gel nanostructure of organized domains of Pluronic micelles separated by a crosslinked network of alginate with variable distribution in domain size and number of micelles. The Pluronic micelles (C) are loaded with GSNO and the fluoride salt, enabling controlled release. The nonionic surfactant nature of Pluronic micelles facilitates adsorption onto enamel surfaces.

4.3.2 Materials Characterization

4.3.2.1 Attenuated Total Reflectance-Fourier Transform Infrared (ATR-FTIR)

Spectroscopy

The chemical compositions of synthesized GSNO and lyophilized hydrogels were determined using ATR-FTIR (**Figure 4.S1**). Nitrosation of glutathione was confirmed by the emergence of a $\nu(\text{N=O})$ at 1477 cm^{-1} , with GSNO purity further quantified by NO loading tests for a criterion of greater than 0.95 moles of NO per mol of GSNO tested. Hydrogel network formation with Pluronic F127 and crosslinked alginate were further evidenced by the presence of vibration bands in each gel formulation corresponding to the individual polymer components. Calcium ion crosslinking of alginate resulted in a modest shift in the $\nu(\text{-COO}^-)$ band from 1422 cm^{-1} in non-crosslinked alginate to lower wavenumbers at 1355 cm^{-1} , suggesting ionic interaction in agreement with previous reports.³⁷ Further characterization confirmed the composition of GSNO and Pluronic F127 in the freeze-dried gel matrices with respect to reference spectra. These results warranted further physical and mechanical testing to investigate the structure and functionality of the hydrogel materials.

4.3.2.2 Scanning Electron Microscopy

The cross-sectional morphology of the hydrogels was examined using SEM. Porosity and macroscopic network structure are critical components of hydrogel composition as they allow for high swelling potentials and gas exchange between tissues and surrounding environments. Imaging showed the highly porous nature of the hydrogels (**Figure 4.3A**) resulting from the temperature-dependent nanostructure and organization of the Pluronic-F127 micelles.²³ The ionic crosslinking of alginate with calcium chloride further affects porosity as the network of alginate chains is variably crosslinked throughout the polymeric structure, intertwined with Pluronic micelle domains. As all gel types

underwent the same fabrication and crosslinking process, no significant network changes were seen across gel formulations.

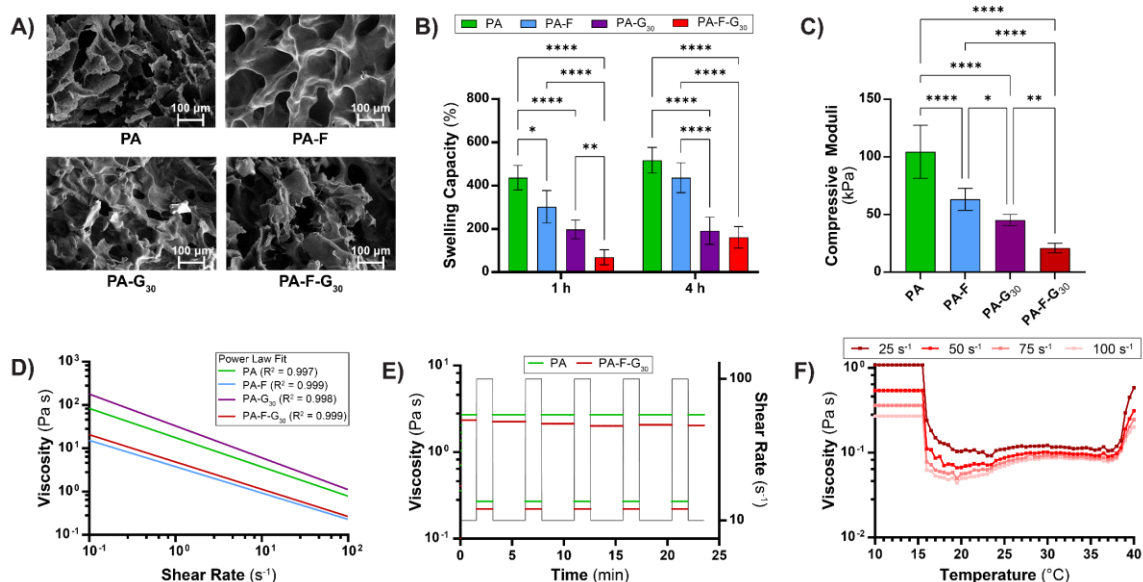


Figure 4.3 Physical and mechanical characterization of PA gels. (A) SEM imaging of freeze-dried gels shows the porous nanostructure of the material. (B) Swelling capacity studies demonstrate the decreased mechanical properties of the hydrogels with the incorporation of fluoride and GSNO. Data presented as mean \pm standard deviation ($n = 5$ per sample group). (C) Uniaxial compressive testing of the PA gels demonstrates the tunable mechanical properties based on GSNO and NaF loading. (D) Controlled shear rate testing of gels at 37 °C with power law curve fitting, demonstrating time-independent pseudoplastic and shear-thinning behavior. (E) Shear-recovery studies of gels show structure recovery after application of a high shear rate ramp (100 s^{-1}) from a low shear rate (10 s^{-1}). (F) Temperature ramps at constant shear rates (i.e., 25, 50, 75, and 100 s^{-1}) of PA-F-G₃₀ gels demonstrate increased micelle attraction forces and different rheological behaviors at physiological temperatures. Statistical significance shown as * ($p < 0.05$), ** ($p < 0.01$), *** ($p < 0.001$), and **** ($p < 0.0001$).

4.3.2.3 Swelling Capacity

Characterization of the water uptake capability can give further insight into the structure and physical properties of hydrogels. To simulate a physiological environment,

all four hydrogel types were incubated in artificial saliva for 1 and 4 h. The swelling capacity was calculated based on the mass of the gels after lyophilization. At both time points, there was a noticeable trend between swelling capacity and hydrogel makeup. As components were added to the hydrogel (NaF and GSNO), the swelling capacity decreased, with PA-F-G₃₀ hydrogels retaining the least amount of artificial saliva at 68.9% at 1 h and 161.0% at 4 h (**Figure 4.3B**). Control gels on the other hand swelled 436.7% and 517.2% at 1 h and 4 h, respectively. The hydrogels with only one component exhibited better swelling than PA-F-G₃₀, with PA-F retaining 301.8% and 436.2% at 1 and 4 h, while PA-G₃₀ swelled 197.6% at 1 h and 191.0% at 4 h. This relationship implicates that the addition of NaF and GSNO may lead to decreased mechanical strength. This is likely attributable to divalent cation interactions with fluoride, which affect Ca²⁺ availability for ionic interactions with alginate responsible for crosslinking and structural stability of the gels. Although the treatment gel (PA-F-G₃₀) shows the lowest mechanical strength and swelling capacity, soft tissue applications do not require extensive mechanical properties and these characteristics will not hinder the function of the designed hydrogel.

4.3.2.4 Compression Testing

Compression moduli of hydrogels is an important property relating the stiffness of the material with its resistance to deformation under compressive load. In many soft tissue applications (e.g. gum tissue), the compositional tunability of hydrogels is key to mimicking the complex viscoelastic properties of these tissues and mediating controlled drug diffusion at the hydrogel-tissue interface. Uniaxial compression testing was performed on the developed PA gels at 25% strain at a rate of 0.166 mm s⁻¹ (**Figure 4.3C**) to determine the mechanical properties in relation to gel composition based on stress-strain relationships (**Figure 4.S2**). Under loading conditions, the PA control gels exhibited compression moduli of 104.4 ± 23.3 kPa, with a statistically significant decrease ($p < 0.05$)

in moduli down to 20.99 ± 4.175 kPa in the composite PA-F-G₃₀. These results parallel our other swelling and viscometry findings, with NaF incorporation affecting the physical properties of the gels, possibly through interactions with divalent calcium ions used in the alginate crosslinking as well as interactions with GSNO that may affect micelle loading, packing, and stability. This high degree of compression moduli tunability based on GSNO and NaF incorporation parallels a need in soft tissue engineering applications for viscoelastic behavior that is tunable for different tissue microenvironments.³⁸

4.3.2.5 Viscometry Testing

Frequency sweep tests were conducted on the hydrogel formulations following ISO 3219 standards to correlate the apparent state-state viscosities under variable shear rate at 37 °C (**Figure 4.3D**). Fitting to a power series modeled after the Ostwald-de Waele model, flow behavior indices less than unity ($n < 1$) were observed, indicating shear thinning.³⁹ The calcium-crosslinked hydrogels exhibited time-independent pseudoplastic and shear-thinning behavior, indicated by the decrease in viscosity with increased shear rate and strong power law fits ($R^2 > 0.99$). Incorporation of GSNO generally increased the viscosity of gels, while NaF incorporation had the reverse effect. We reason these effects with GSNO to be the result of a cage effect with the micelles, whereby GSNO is susceptible to both encapsulation within the micelle cores and association with PEO blocks in the corona, increasing microviscosity.²³ Concurrently, non-encapsulated fluoride ions may interact with divalent ions (e.g., Ca²⁺), affecting crosslinking performance and the viscosity of gels.

Further analysis of the PA and PA-F-G₃₀ gels for shear recovery at 37 °C was performed to demonstrate structure recovery after the transition from low (10 s⁻¹) to high (100 s⁻¹) shear rates (**Figure 4.3E**). Following initial stabilization, the gels were shown to quickly recover in viscosity between ramps. Shear-thinning and fast structure recovery are

important factors in the development of therapeutic hydrogel formulations, especially for injectable applications. Prior investigation of Pluronic-alginate hydrogels crosslinked with calcium chloride has demonstrated their efficacy for artery endoluminal delivery of several drug classes.²⁴ However, it has been insofar unclear how these properties are affected by GSNO and NaF incorporation. The incorporation of GSNO and NaF in PA-F-G₃₀ gels led to an overall decrease in gel viscosity compared to PA controls, but retained shear recovery properties.

Further temperature ramping of the PA-F-G₃₀ gels demonstrated key thermal events occurring as the crosslinked gels were heated (**Figure 4.3F**). From 16 to 35 °C, gradual increases in viscosity may be attributed to interactions of micelles within the hydrogel, with increased attraction forces supporting aggregation. PA control gels exhibited similar trends in rheological behavior (**Figure 4.S3**), with increasing viscosity at near physiological temperatures. These observations were consistent with prior findings with other Pluronic hydrogel systems showing temperature-sensitive gelation.^{24, 40, 41} Above 35 °C, significant increases in viscosity were observed for the PA-F-G₃₀, suggesting further gelation from the Pluronic F127 component. While the addition of calcium chloride to the sol precursor incurs rapid gelation via the alginate minor network, this enhanced gelation at, or slightly above, the physiological temperature is critical to the long-term release of NO from the gel networks. With these tunable physical properties, further enhancement in NO and fluoride ion release was investigated.

4.3.2.6 Chemiluminescence-Based Measurements of NO Release from Hydrogels

NO-releasing hydrogels have previously been developed for dermal wound healing,^{22, 42, 43} promotion of angiogenesis,⁴⁴ and as stem cell carriers for treating myocardial infarction, hindlimb ischemia, and other illnesses.⁴⁵⁻⁴⁷ Prior work concerning Pluronic F127-alginate hydrogels with GSNO has demonstrated the robust efficacy of non-

crosslinked forms for dermal wound healing.⁴³ Similarly, previous work with NO-releasing hyperbranched polymers and silica nanoparticles has demonstrated the long-term efficacy of the material class towards resolving microbial adhesion and subsequent biofilm formation onto dental implants.^{48, 49} GSNO is frequently used in hydrogels and other hydrophilic environments due to its favorable stability in aqueous conditions and ready liberation of NO in the presence of heat, light, or metallic species (**Figure 4.4A**).^{50, 51} Herein, we report for the first time the application of a NO-releasing hydrogel material to address both bacterial proliferation on oral surfaces and demineralization of tooth enamel.

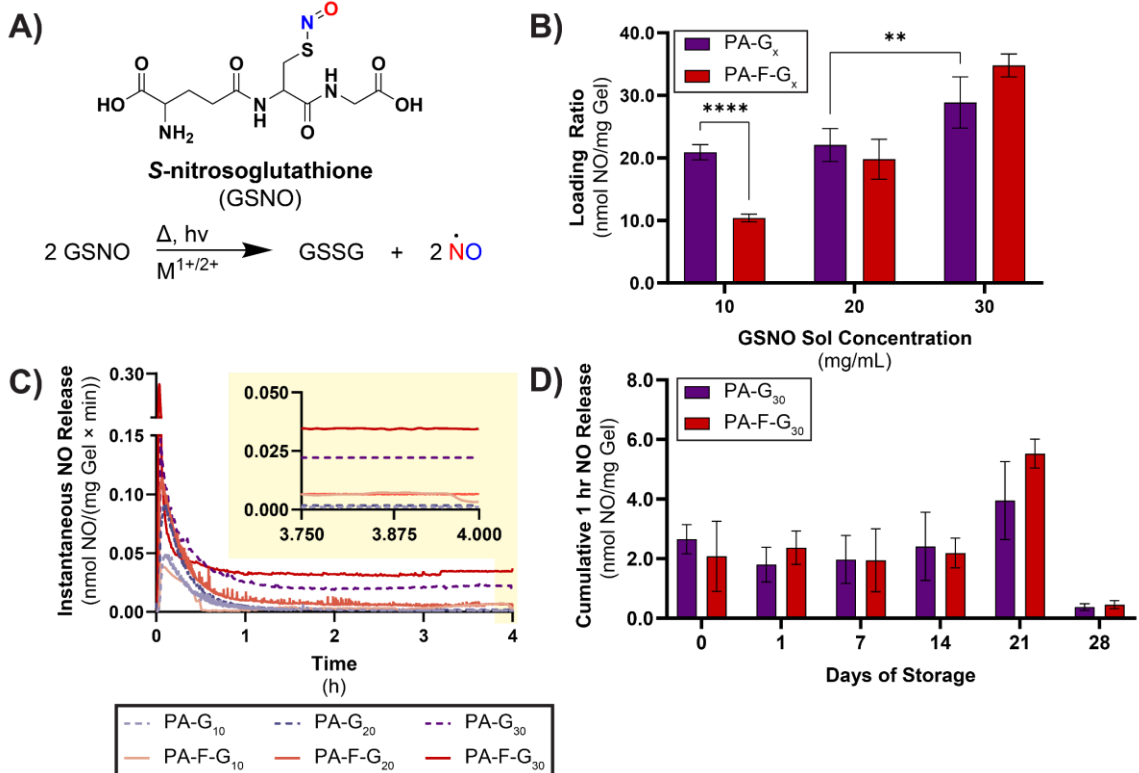


Figure 4.4 Overview of NO release from fabricated hydrogels. NO evolution is achieved (A) from the homolytic cleavage of the S-nitrosothiol bond in GSNO in the presence of heat, light, or metal ions under physiological conditions. Catalytically depleting all GSNO in the gels showed (B) the total molar loading of NO per mass of the gel for each formulation. The fabricated gels exhibited sustained, physiologically active release of NO during (C) the first four hours after fabrication and crosslinking. A further long-term study of the gels demonstrated (D) preserved NO release over fourteen days when fabricated, crosslinked, and immediately stored at 4 °C. Data are presented as mean ± SD (n = 5). Statistical significance shown as ** (p < 0.01) and **** (p < 0.0001).

4.3.2.6.1 GSNO Loading

After fabrication, a vigorous washing step with 1x PBS removes unbound GSNO from the gels, implicating that some amount of GSNO in the precursor sol may not be incorporated into the final gel. To assess the loading potential of GSNO into PA-G_x and PA-F-G_x gels, NO was liberated from GSNO incorporated within the crosslinked gels

through the presence of Cu^{1+} in a reductive environment. NO loading analysis using chemiluminescence-based NO detection showed that the initial GSNO concentration in the sol precursor significantly affected final loading in gels (**Figure 4.4B**). While higher concentrations of GSNO in PA-G₂₀ and PA-G₃₀ led to no statistically significant difference in loading when NaF was incorporated, the difference for PA-G₁₀ was more pronounced with an almost 50% decrease in GSNO loading of PA-F-G₁₀ gels compared to PA-G₁₀ ($p < 0.0001$). Considering the theoretical loading potential of GSNO into each gel based on the precursor sol concentration, this trend is mirrored with the PA-G₁₀ gel showing almost 85% loading efficiency, while all other GSNO-based gels had approximately 40-50% loading efficiency (**Table 4.S2**). These results viewed alongside trends in the mechanical performance of the gels (**Figure 4.3**) implicate GSNO and NaF-dependent structuring of the hydrogels, possibly by influencing Pluronic micellization behavior. Previous work with GSNO-containing, non-crosslinked F127-alginate gels demonstrated that GSNO accelerates micellization in the process of temperature-dependent gelation.⁴³ Therefore, we believe the differences in GSNO loading capacities for PA-G₁₀ and PA-F-G₁₀ to be the result of different solubilization capacities when the presence of fluoride ions can both affect the dominant microspecies of GSNO in the gel as well as alginate crosslinking via interaction with calcium ions.⁵²

Differences in GSNO loading potential across different sol concentrations of GSNO were also investigated up to 30 mg/mL of GSNO, after which incomplete solubility of GSNO prohibited further loading evaluation at higher concentrations (**Figure 4.4B**). While no significant difference in GSNO loading was obtained between PA-G₁₀ and PA-G₂₀, increased loading was observed between PA-G₂₀ and PA-G₃₀ ($p < 0.01$). Among fluoride-containing gels, differences were much more pronounced, with each incremental increase in GSNO sol concentration leading to at least a 75% increase in GSNO loading in the gel

($p < 0.0001$). In each instance, increased loading can be attributed to the higher GSNO sol concentration, with fluoride ions potentially affecting GSNO incorporation during the micellization process and having further ionic interaction with Ca^{2+} found in the crosslinked alginate network.

4.3.2.6.2 NO Release Under Physiological Conditions

Representative profiles of the NO release for each hydrogel formulation (compositions summarized in **Table 4.S1**) were determined over an initial four hours after fabrication under physiological conditions (**Figure 4.4C**). On average, PA-F-G₃₀ exhibited the highest release rates of NO over the study duration, with overall trends in NO release being strongly dependent on GSNO concentration in the sol precursor. The cumulative NO loadings of the representative spectra shown in **Figure 4.4C** are summarized in **Table 4.S3** for each hour of the study. By the fourth hour of the study, the fluoride-containing formulation at each given GSNO concentration had achieved higher cumulative NO release than its respective GSNO only counterpart. These results are consistent with mechanical findings, demonstrating that fluoride incorporation affects the elasticity and crosslinking of the gel, which may lead to greater GSNO availability at the physiological interface and therefore increased NO release. Initially enhanced NO release from the fluoride-containing gels is beneficial from a therapeutic perspective, especially for combatting opportunist pathogens at the center of dental caries infections.

4.3.2.6.3 Storage Stability Analysis (28 d)

The cumulative 1 h NO release from PA, PA-F, PA-G₃₀, and PA-F-G₃₀ after storage at 4°C was investigated to determine the storage stability of the gels in terms of maintaining the NO release and corresponding antimicrobial efficacy. The gels were tested after storage conditions of 0, 1, 7, 14, 21, and 28 d. All gels were made on day 0 and $n = 5$ for each sample type were removed, analyzed, and discarded on each measurement day.

Cumulative 1 h NO release from PA-G₃₀ was 2.65 nmol/mg on day 0 followed by 1.80, 1.97, and 2.41 nmol/mg on days 1, 7, and 14, respectively. Similarly, PA-F-G₃₀ released 2.08, 2.37, 1.95, and 2.19 nmol/mg on days 0, 1, 7, and 14 (**Figure 4.4D**). There was no significant difference between the cumulative 1 h NO release of PA-G₃₀ and PA-F-G₃₀ for the first 14 d, indicating the gels were able to maintain initial NO release and antimicrobial potential for at least 14 d when stored at 4 °C and in dark conditions. However, day 21 showed an increase in NO release from both sample types as PA-G₃₀ released 3.95 nmol/mg and PA-F-G₃₀ released 5.52 nmol/mg. The boost in NO release on day 21 is believed to be due to alginate degradation within the gels, leading to the less controlled GSNO decomposition and NO release, as GSNO is no longer bound by the polymeric matrix formed by the crosslinked Pluronic-alginate structure. The NO release on day 28 of storage at 4 °C confirms the degradation hypothesis, as much of the hydrogel structure has been lost by that time point and very little GSNO is remaining in the polymeric matrix, leading to a release of only 0.376 nmol/mg from PA-G₃₀ and 0.454 nmol/mg from PA-F-G₃₀. Although the gels were only tested for storage capacity at 4 °C, stability could be greatly enhanced by storing the gels at lower temperatures since GSNO is thermally degraded. Another option would be to freeze-dry the optimized gels to prevent alginate degradation and hydrolytic cleavage of the S-nitrosothiol bond in GSNO, maintaining the hydrogel structure and prolonging the NO release component. Finally, the addition of metal ion chelators into the hydrogel formulation may be considered for enhanced stabilization of GSNO, though this may affect calcium crosslinking and fluoride interactions. Further translation of the hydrogel system would necessitate additional studies to determine optimal conditions for prolonged shelf-stability in analogy to other NO donor-containing polymeric materials.

4.3.2.7 Fluoride Release

Fluoride ion release was assessed from representative PA-F and PA-F-G₃₀ gels to evaluate the capacity for leaching under physiological conditions to mediate processes of enamel demineralization prevention. EDS-SEM analysis of the various gel formulations demonstrated the surface distribution of fluorine across both PA-F and PA-F-G₃₀ gels, confirming its integration into the hydrogel matrix (**Figure 4.5A**). Full EDS spectra are provided in **Figure 4.S4**. Differences in fluorine surface distribution (**Figure 4.5B**) between PA-F (17.0%) and PA-F-G₃₀ (27.8%) are attributable to possible ionic interactions between GSNO and fluoride ions in PA-F-G₃₀ gels, enabling increased fluoride retention within the polymeric structure in analogy to other amine fluoride compounds used in dental products (**Figure 4.S5**). Furthermore, the surface crosslinking strategy utilized in this study may have led to a higher distribution of fluorine on the surface of the gels than what is maintained throughout the hydrogel network as calcium ions (present in the CaCl₂ crosslinking solution) are capable of deactivating fluoride ions through precipitation.⁷ However, the surface-localized fluorine induced by the chosen crosslinking method may enhance the demineralization prevention effects, as the fluoride is made more available to the exposed hydroxyapatite/enamel, leading to augmented fluorapatite formation and greater demineralization prevention.

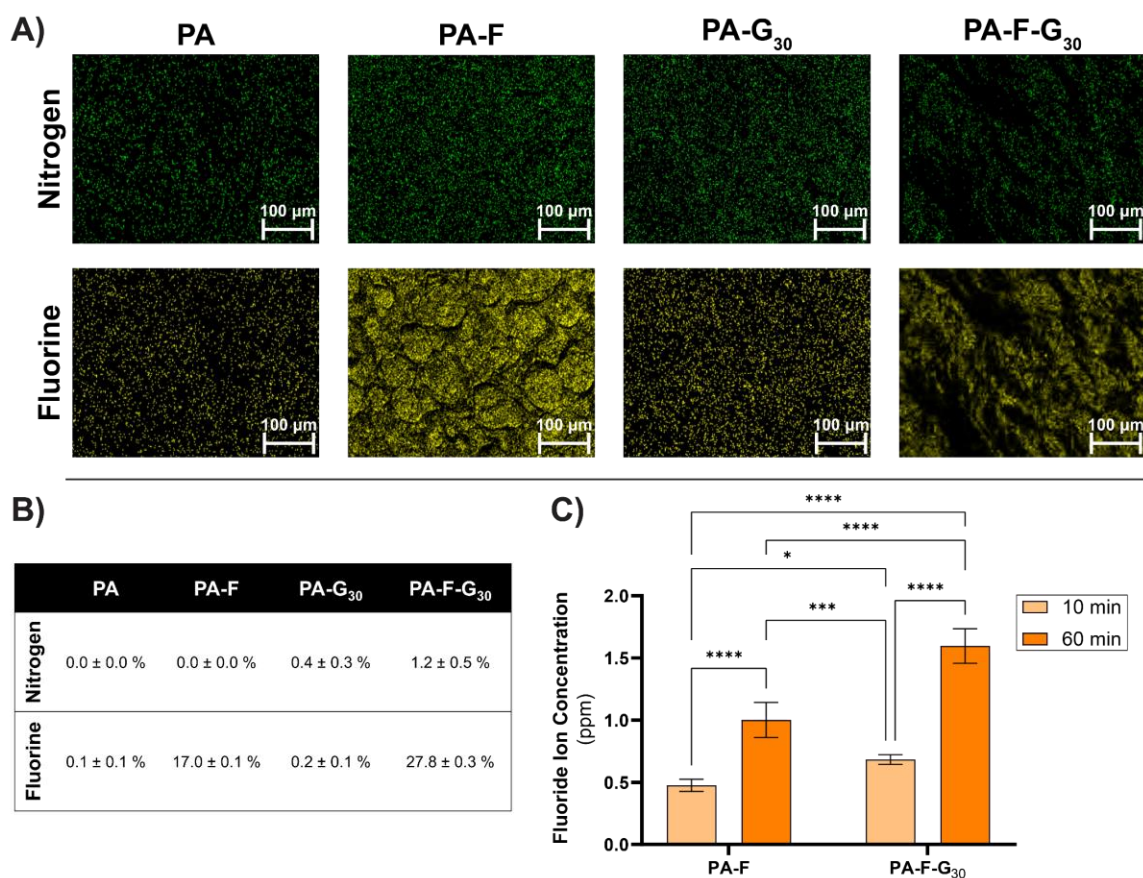


Figure 4.5 Analysis of fluoride in hydrogels. EDS-SEM surface analysis (A) and quantification (B) of freeze-dried hydrogels for nitrogen (corresponding to GSNO) and fluoride (corresponding to NaF). Total time-dependent fluoride release (C) was further measured for PA-F and PA-F-G₃₀ gels incubated in artificial saliva at 37 °C. Data represent mean ± SD ($n = 5$ per sample type). Statistical significance shown as *** ($p < 0.001$) and **** ($p < 0.0001$).

In addition to surface characterization, fluoride ion release from the gels was further quantified. Using a fluoride ion-selective electrode, leachates from gels were evaluated after 10- and 60-min incubation under physiological conditions (**Figure 4.5C**), with fluoride ion concentration calculated against a standard curve from sodium fluoride (**Figure 4.S6**). On a basis of 0.2% w/w fluoride loading (corresponding to ~2,000 ppm maximum loading), an average of 0.476 and 1.002 ppm fluoride ions was detected in

solution after 10 min of leaching, with each increasing by over 40% after 1 h. In both instances, PA-F-G₃₀ exhibited greater leaching of fluoride than PA-F alone ($p < 0.001$).

We justify these observations given the possibility for further ionic interactions with GSNO in PA-F-G₃₀ than PA-F alone, as well as the increased surface localization of fluorine in PA-F-G₃₀ (**Figure 4.5B**). GSNO contains one primary amine that is readily protonated in the microenvironment of artificial saliva (pH ~ 6.8), which may lead to further fluoride ion association (**Figure 4.S5**).⁵³ However, the exact association and any binding affinity of fluoride to GSNO is insofar unelucidated, and requires further mechanistic understanding alongside other commonly used amine fluoride compounds. A similar mechanism of controlled fluoride release is accomplished with other amine fluorides such as Olaflur and Dectaflur, which utilize a surfactant component to adsorb as monolayers onto enamel and elicit a controlled release of fluoride.⁷ Traditional therapeutic agents using NaF often show burst release of fluoride due to high solubility and interaction with other chloride salts in saliva, while stabilization of fluoride with aminated compounds has shown to develop controlled release in polymeric formulations.³⁵ In analogy, the coordination of fluoride with GSNO in association with Pluronic F127 may take advantage of the amphipathic character, prolonging surface contact for caries prevention.³⁵ By mirroring these characteristics with GSNO loaded micelles in the PA-F-G_x gels, the material class showed remarkable biological properties after further evaluation.

4.3.3 Antimicrobial Evaluation

4.3.3.1 Planktonic Bacterial Viability Study

The antimicrobial potential of the NO-releasing hydrogels was tested against *S. mutans*, a Gram-positive dental bacterium commonly found in the grooves and fissures of teeth, and *E. coli*, a common Gram-negative pathogen that is often used to test the antibacterial efficacy of dental materials.^{54, 55} The excess colonization of *S. mutans* in the

oral cavity can lead to an overproduction of acidic metabolic byproducts that are responsible for enamel decay and cavities. Therefore, a dental treatment that can effectively kill the microorganisms can help control the overproduction of harsh acids and deter tooth demineralization. At the same time, the fluoride released from PA-F-G₃₀ can help rebuild HA structures into more resilient enamel constructs that are less likely to decay if the bacterial infection were to return.

As the application of the hydrogel in translational settings would be short-term, 4-h studies of the hydrogels against *S. mutans* were conducted (**Figure 4.6A**). As expected, PA and PA-F gels were not able to effectively kill bacteria, while gels incorporated with GSNO demonstrated a significant antimicrobial outcome. The antimicrobial effects of NO released from GSNO are well characterized, showing broad-spectrum activity even against resistant strains such as methicillin-resistant *Staphylococcus aureus* and multidrug-resistant *Pseudomonas aeruginosa* due to the formation of reactive oxygen species (ROSs) such as peroxynitrite (ONOO⁻) and hydroxyl (•OH) radicals.^{10, 56} These species readily penetrate bacterial membranes and damage lipids, transport proteins, DNA and DNA repair systems, as well as inactivate heme proteins responsible for signal transduction, ultimately leading to bacterial death.¹⁰ Bacteria treated with PA-F showed no significant decrease in viable colony counts compared to bacteria treated with control PA gels, which was expected since alginate, Pluronic F127, and fluoride contain no active antimicrobial mechanism of action. On the other hand, the NO release from PA-G₃₀ resulted in a 60.9 ± 11.86 % bacterial reduction, and PA-F-G₃₀ showed a 97.59 ± 1.46 % reduction of viable bacteria compared to PA controls. The increase in killing is attributed to the greater GSNO loading ratio and subsequent increase in released NO from PA-F-G₃₀. Greater NO release leads to higher levels of ROSs in the bacterial environment, initiating membrane rupture, bacterial inactivation through protein and lipid disruption, and

consequent *S. mutans* death. Furthermore, recent studies have shown that NO is more effective at killing *S. mutans* in acidic conditions that would be present if an *in vivo* infectious oral cavity were being treated.¹⁹ Similar results were shown when the gels were exposed to an *E. coli* solution for 4 h. Compared to PA, PA-F gels did not display any bacterial reduction, while PA-G₃₀ and PA-F-G₃₀ demonstrated a $61.85 \pm 18.93 \%$ and $95.66 \pm 0.89 \%$ decrease in bacterial viability, respectively (**Figure 4.S7**).

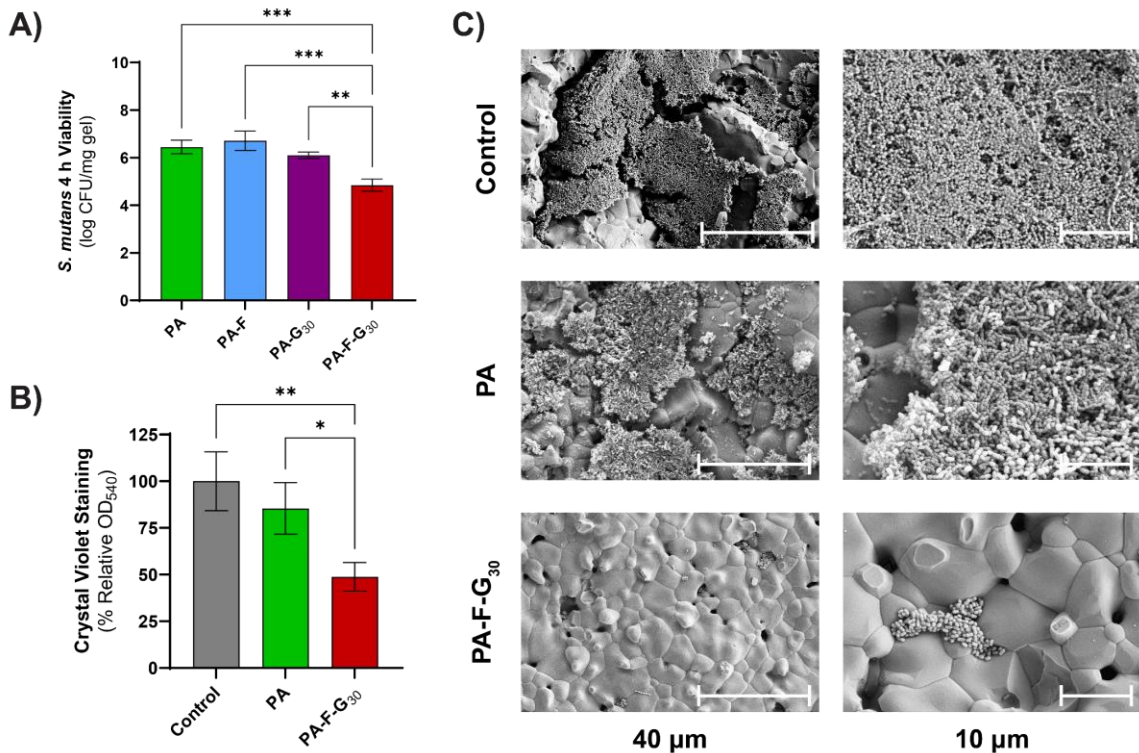


Figure 4.6 Analysis of antibacterial efficacy of gels against *S. mutans*. (A) The 4-h viability of *S. mutans* was determined following direct contact exposure to gel coupons. Biofilms of *S. mutans* were further grown on hydroxyapatite discs for 36 h and treated with gels for 24 h, after which (B) extracellular polymeric substance was quantified using crystal violet assay, and (C) bacteria adhesion was monitored via SEM. Scale bars correspond to 40 μm in the left column and 10 μm in the right column. Data are shown as the mean ± SD (n = 3 per sample type). Statistical significance shown as * (p < 0.05), ** (p < 0.01), and *** (p < 0.001).

4.3.3.2 *S. mutans* Biofilm Dispersal

In addition to inducing potent antimicrobial effects through the production of highly reactive ROSs, NO is also capable of dispersing biofilms through penetration of the extracellular polymeric substance (EPS) and disruption of quorum sensing, or bacterial communication and adaptation within a biofilm.⁵⁷

The ability of NO to penetrate biofilms is uniquely attributable to its gaseous nature, a feature that antibiotics do not possess and therefore makes them significantly less effective at infiltrating, dispersing, and killing bacteria within a biofilm. Crystal violet staining is a technique widely used in biomedical research to quantify biofilms as the dye binds to negatively charged molecules present in bacteria and their surrounding EPS matrix.⁵⁸ Herein, crystal violet staining was used to quantify *S. mutans* biofilms grown on HA discs. The use of HA as a model for *in vitro* tooth enamel studies is well recognized and accepted since HA is the mineral that makes up 95-98% of teeth.³ Following the growth of a *S. mutans* biofilm on HA discs for 36 h, the treatment with PA and PA-F-G₃₀ gels for 24 h demonstrated the ability of released NO to decrease biofilm structure by 52% compared to control, untreated biofilms (**Figure 4.6B**). PA gels reduced the biofilms slightly, but not by a significant amount. SEM imaging of the biofilms shown in **Figure 4.6C** demonstrated the dense, interconnected *S. mutans* biofilms formed on the HA surface of control discs and those treated with PA gels. HA-covered biofilms treated with PA-F-G₃₀ displayed a greater reduction in biomass, with *S. mutans* only surviving in deeper crevices of HA discs. However, compared to PA-treated discs, those treated with PA-F-G₃₀ had fewer pores, showing the necessity for the fluoride component in the gels to decrease possible sites for bacterial invasion, a concept more heavily explored in the demineralization study. Overall, the CV biofilm quantification and SEM imaging of biofilms demonstrated the ability of NO to penetrate and disperse pre-formed *S. mutans* biofilms,

validating the use of PA-F-G₃₀ gels to treat future cases of dental caries by breaking down mature biofilms and killing viable dental pathogens. Further, the 52% reduction of biofilm by PA-F-G₃₀ is likely to be enhanced in practical, *in vivo* use when used in conjunction with standard dental cleaning treatments, allowing for greater biofilm breakdown and deeper penetration of NO gas into the EPS.

4.3.4 Demineralization of Hydroxyapatite Enamel Model

The treatment of tooth enamel with fluoride to prevent demineralization and strengthen damaged enamel structures has been used for almost a century through supplementation of city water supplies and recommended toothpaste and mouthwash products. The enamel restoration occurs when calcium and phosphate ions in saliva are disseminated into tooth enamel by fluoride ions. The influx of calcium and phosphate leads to recrystallization within cavities or demineralized portions of enamel and the formation of fluoridated HA, which is more impervious to acidic erosion than HA.¹ To mimic the physiological conditions of enamel demineralization, HA discs in artificial saliva solutions were treated with PA, PA-F, PA-G₃₀, and PA-F-G₃₀ followed by a highly acidic (pH = 3) demineralization solution (**Figure 4.7A**). The ability of the fluoride released from the gels to prevent HA demineralization was investigated by quantifying the induced porosity of HA discs (n = 3 per sample type) after no gel treatment or treatment with each of the four gel types (**Figures 4.7B and C**). Porosity was correlated to demineralization, with higher porosity values corresponding to a greater extent of demineralization, which fluoride-releasing gels sought to prevent. SEM images and single-blinded porosity quantification demonstrated the effective prevention of demineralization. Untreated HA discs (i.e., no gel or demineralization solution) had an average porosity of 4.25% while discs treated with PA-F-G₃₀ followed by demineralization solution had a porosity of 4.76%, indicating almost no change in porosity (demineralization) compared to the negative control even after

treatment with a highly acidic demineralization solution. Treatment with PA-F before demineralization led to the next lowest porosity value at 7.54%, which correlated with fluoride ion release measurements, leading to greater demineralization protection with PA-F-G₃₀. Treatment with PA-F led to some protection, however, as HA not treated with hydrogel but incubated in demineralization solution resulted in 10.92% porosity, while HA treated with PA and acidic conditions showed 12.78% porosity. Incubation with PA-G₃₀ was also unsuccessful at preventing demineralization, with a porosity value of 10.10%. When comparing all treatment types to HA discs that did not undergo the demineralization process, the gels that prevented demineralization most successfully were PA-F-G₃₀ followed by PA-F, with surface structures most like native HA (**Figure 4.7C**). On the other hand, PA and PA-G₃₀ provided essentially no protection as seen by the numerous gaps and cavities found on the surface of the HA structure. The difference in demineralization protection potential is therefore due to the release of fluoride ions that allow for restructuring and strengthening of HA microstructures through the capture of calcium and phosphate found in the artificial saliva. Without the fluoride release, HA is prone to fracture and demineralization in an acidic environment caused by food and overactive oral bacteria.

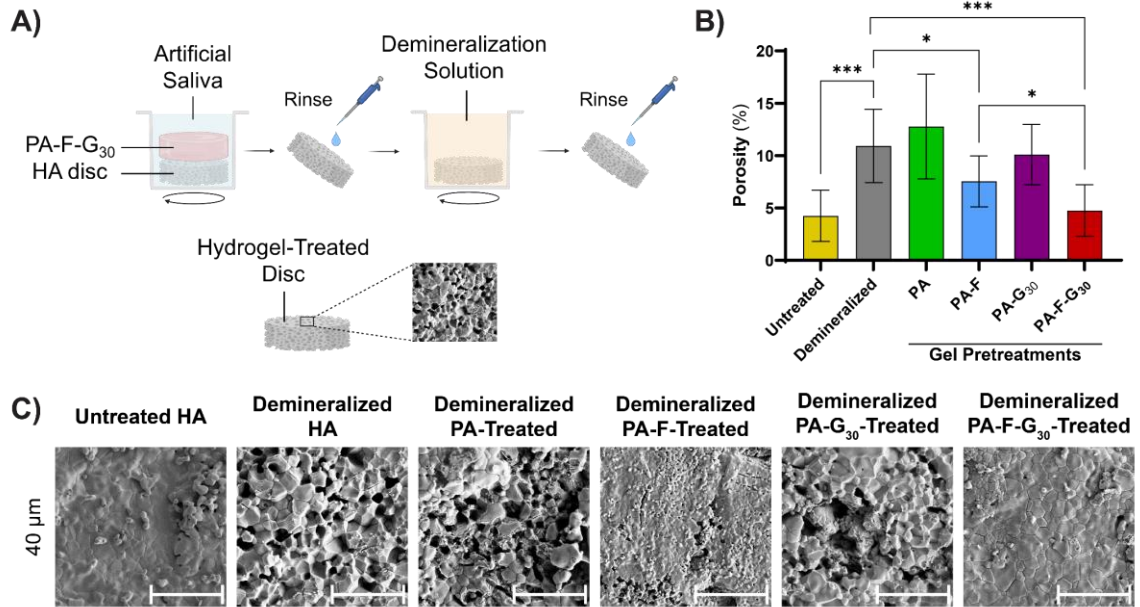


Figure 4.7 Demineralization prevention potential of PA gels in a hydroxyapatite disc model. Discs (A) were treated with gels for 1 h followed by rinsing and exposure to an acidic demineralization solution, rinsing, and lastly SEM imaging. Quantification (B) of the porous surface structures shown in (C) demonstrated decreased pore formation on discs treated with fluoride-containing gels, suggesting fluorapatite formation. These studies confirmed decreased percent porosity of the hydroxyapatite discs with prior treatment with fluoride-containing gels. Data presented as the mean \pm SD ($n = 3$ per treatment group). Statistical significance expressed as * ($p < 0.05$) and *** ($p < 0.001$).

4.3.5 Cytocompatibility Evaluation

4.3.5.1 Cellular Cytotoxicity of GSNO and Precursor Sol Materials

Drug-releasing hydrogels with degradable backbones such as alginate have attracted significant attention in recent years for tissue engineering and other therapeutic applications but can present issues if the drug release rate and degradation products induce a cytotoxic response. For this reason and to establish a baseline for further biological evaluation, the non-crosslinked hydrogel precursors, as well as GSNO, were evaluated for cytotoxic response in two representative human cell types: HGF and hFOB

1.19. In the oral cavity, fibroblasts are critical for developing the structural framework of connective tissue and propagating processes of inflammation and wound healing. Similarly, osteoblastic cells are essential to hard and soft tissue reconstruction following extreme cases of dental caries. During 4- and 24-h *in vitro* direct contact exposure studies, representative cytotoxic response curves were generated for both GSNO and the dissolved sol precursors (**Figure 4.S8**). GSNO elicited a controllable cytotoxic response at greater than 100 µg/mL treatments in HGFs, while the same was shown at nearly 400 µg/mL of GSNO in hFOB 1.19 cells. These results agree with the literature, as HGFs are known to produce pM levels of NO for cellular signaling while experiencing cytotoxic response at mM levels in response to dental caries that have progressed to periodontal disease.⁵⁹ Similarly, osteoblasts are known to respond to low levels of NO in the processes of bone remodeling⁶⁰ but can undergo apoptosis at higher levels.⁶¹ For these reasons, NO donors are frequently embedded into polymeric materials to control their diffusion and degradation rates.⁶²

Further evaluation for a cytotoxic response from the precursor hydrogels over 4 and 24 h in HGF and hFOB 1.19 showed minimal induction of a cytotoxic response (**Figure S8C-F**). In most cases, higher concentrations of the PA-G₃₀ and PA-F-G₃₀ hydrogel induced a mild cytotoxic response, in support of previous observations with increased GSNO concentrations. The presence of fluoride in PA-F and PA-F-G₃₀ even at higher doses did not significantly affect toxicity, supporting the use of NaF in the hydrogel composition without further concern for sodium fluoride-induced toxicity.⁶³

4.3.5.2 Cell Proliferation in Presence of Hydrogel

To further evaluate the cytocompatibility of the crosslinked AP gels, HGF and hFOB 1.19 were exposed to the various gel formulations over 4 and 24 h in direct contact studies. Alginate gels are quickly crosslinked using divalent cations such as Ca²⁺ through ionic

interaction stabilization between neighboring strand carboxylic acid groups forming chain-chain associations. This added structural rigidity helps in controlling the diffusion of drugs through alginate networks. Although alginate is biologically inert, its gradual degradation may present issues for cytotoxicity, especially through increased calcium ion availability.⁶⁴ Mirroring further antibacterial studies, cells were exposed to 8 mm circular hydrogel film punches for 4 and 24 h. Throughout these studies, no considerable cytotoxic response was observed with any of the crosslinked gel formulations (**Figure 6A and B**). Increased GSNO loading was observed to elicit a mild decrease in cell proliferation, with these effects attenuated by the presence of fluoride ions in the films. Further examination of cells treated with gels for 4 h via brightfield microscopy showed no substantial differences in cell morphology, with few dead cells present proportional to the relative cytotoxicity (**Figure 6C**). Taken all together, these results are justified by our prior mechanical testing and NO studies, which show that PA-F-G₃₀ are softer with greater NO release and loading compared to the other gels. By controlling the GSNO content of the gels, key mechanical and biological properties can be controlled for the desired effect, as previously shown with antimicrobial studies.

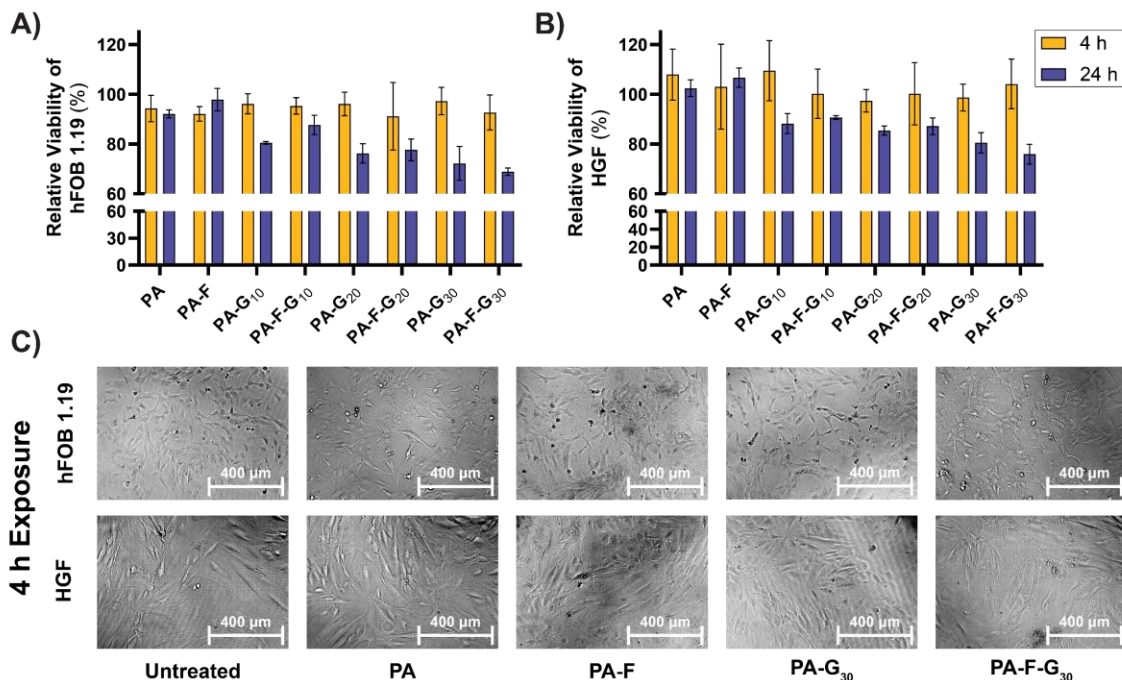


Figure 4.8 Cytocompatibility evaluation of fabricated gels in direct contact exposure against (A) hFoB 1.19 human osteoblasts and (B) human gingival fibroblasts (HGF) over 4 and 24 h. Corresponding images (C) of cell cultures after 4 h incubation under direct exposure with the hydrogels. Data presented as mean \pm SD ($n = 3$ per sample type).

4.4 Conclusions

In summary, we have investigated the feasibility and efficacy of a first-of-its-kind NO- and fluoride ion-releasing hydrogel with highly tunable biological properties suitable for combatting pathogens at the root of dental caries infections. This novel class of dental hydrogels exhibited porous nanostructures with tunable mechanical properties based on GSNO and NaF incorporation. This design enables tailoring of the material to application-specific circumstances for dental soft tissue, with shear-thinning behavior suitable for rapid self-healing. Measurements of NO release studied in the first four hours showed release in the nanomolar range, with gels retaining stability for over 14 d. Fluoride studies showed ppm fluoride ion release that was enhanced with the addition of GSNO to the gel. By

adopting crosslinked alginate as a stabilizing network with temperature-responsive F127 micelle structuring, GSNO and NaF are both incorporated into the hydrogel with controlled NO and fluoride ion release under physiological conditions.

Further biological testing of the fabricated gels first through *in vitro* cytotoxicity evaluation against human osteoblasts and gingival fibroblasts demonstrated robust cytocompatibility of the gels over 4 h and 24 h of exposure with adjustable cellular proliferation based on the extent of GSNO and NaF incorporation. Bacteria testing through a 4-h viability study against *S. mutans* showed potent antimicrobial properties in eliciting a nearly 98% reduction in viable bacteria with the combination GSNO and NaF gels. A further extended study of the gels in a biofilm growth model of *S. mutans* on hydroxyapatite surfaces showed over a 50% reduction in biofilm mass after treatment with the same combination gels. Finally, SEM analysis of hydroxyapatite discs in a simulated model of demineralization demonstrated that discs pretreated with the combination gels exhibited reduced porosity after acid treatment, signifying the successful prevention of demineralization of the enamel-like substrates. Taken altogether, this efficient strategy of NO and fluoride ion release holds great potential for the treatment of dental caries through the early disruption of biofilm formation. In terms of practical application, the gel could be utilized clinically as well as in an at-home environment, allowing for daily, weekly, or monthly treatment depending on the severity of caries infection. As a bioactive gel with such a facile yet efficacious fabrication strategy, this material class warrants the further investigation of other NO-releasing polymers for next-generation dental materials.

Author Contributions

Lori M. Estes Bright: Conceptualization, Methodology, Validation, Formal Analysis, Investigation, Writing – Original Draft, Visualization. **Mark R. S. Garren:**

Conceptualization, Methodology, Validation, Formal Analysis, Investigation, Writing – Original Draft, Visualization. **Morgan Ashcraft**: Formal Analysis, Investigation, Writing – Review and Editing, Visualization. **Anil Kumar**: Methodology, Investigation, Writing – Review and Editing. **Huzefa Husain**: Investigation, Writing – Review and Editing. **Elizabeth J. Brisbois**: Supervision, Funding Acquisition, Writing – Review and Editing. **Hitesh Handa**: Supervision, Funding Acquisition, Writing – Review and Editing.

4.5 References

1. Selwitz, R. H.; Ismail, A. I.; Pitts, N. B., Dental caries. *Lancet* 2007, 369 (9555), 51-9.
2. Jaffer, I. H.; Weitz, J. I., The blood compatibility challenge. Part 1: Blood-contacting medical devices: The scope of the problem. *Acta Biomater* 2019, 94, 2-10.
3. Enamel Structure and Composition.
4. Fejerskov, O.; Kidd, E., Dental caries: the disease and its clinical management. John Wiley & Sons: 2009.
5. Featherstone, J. D., Dental caries: a dynamic disease process. *Aust Dent J* 2008, 53 (3), 286-91.
6. Forssten, S. D.; Bjorklund, M.; Ouwehand, A. C., Streptococcus mutans, caries and simulation models. *Nutrients* 2010, 2 (3), 290-8.
7. Eppe, M.; Enax, J., Moderne Zahnpflege aus chemischer Sicht. *Chemie in unserer Zeit* 2018, 52 (4), 218-228.
8. Baehni, P. C.; Takeuchi, Y., Anti-plaque agents in the prevention of biofilm-associated oral diseases. *Oral Dis* 2003, 9 Suppl 1, 23-9.
9. Shapira, L.; Tepper, P.; Steinberg, D., The interactions of human neutrophils with the constituents of an experimental dental biofilm. *J Dent Res* 2000, 79 (10), 1802-7.
10. Fang, F. C., Perspectives series: host/pathogen interactions. Mechanisms of nitric oxide-related antimicrobial activity. *J Clin Invest* 1997, 99 (12), 2818-25.
11. Wink, D. A.; Kasprzak, K. S.; Maragos, C. M.; Elespuru, R. K.; Misra, M.; Dunams, T. M.; Cebula, T. A.; Koch, W. H.; Andrews, A. W.; Allen, J. S., DNA

deaminating ability and genotoxicity of nitric oxide and its progenitors. *Science* 1991, 254 (5034), 1001-3.

12. De Groote, M. A.; Fang, F. C., NO inhibitions: antimicrobial properties of nitric oxide. *Clinical Infectious Diseases* 1995, 21 (Supplement_2), S162-S165.

13. Garren, M. R.; Ashcraft, M.; Qian, Y.; Douglass, M.; Brisbois, E. J.; Handa, H., Nitric oxide and viral infection: Recent developments in antiviral therapies and platforms. *Applied Materials Today* 2021, 22, 100887.

14. Carossa, S.; Pera, P.; Doglio, P.; Lombardo, S.; Colagrande, P.; Brussino, L.; Rolla, G.; Bucca, C., Oral nitric oxide during plaque deposition. *Eur J Clin Invest* 2001, 31 (10), 876-9.

15. Pan, Z.; Guzeldemir, E.; Toygar, H. U.; Bal, N.; Bulut, S., Nitric oxide synthase in gingival tissues of patients with chronic periodontitis and with and without diabetes. *J Periodontol* 2010, 81 (1), 109-20.

16. Carpenter, A. W.; Reighard, K. P.; Saavedra, J. E.; Schoenfisch, M. H., O 2-Protected diazeniumdiolate-modified silica nanoparticles for extended nitric oxide release from dental composites. *Biomaterials science* 2013, 1 (5), 456-459.

17. Backlund, C. J.; Sergesketter, A. R.; Offenbacher, S.; Schoenfisch, M. H., Antibacterial efficacy of exogenous nitric oxide on periodontal pathogens. *J Dent Res* 2014, 93 (11), 1089-94.

18. Backlund, C. J.; Worley, B. V.; Schoenfisch, M. H., Anti-biofilm action of nitric oxide-releasing alkyl-modified poly(amidoamine) dendrimers against *Streptococcus mutans*. *Acta Biomater* 2016, 29, 198-205.

19. Backlund, C. J.; Worley, B. V.; Sergesketter, A. R.; Schoenfisch, M. H., Kinetic-dependent Killing of Oral Pathogens with Nitric Oxide. *J Dent Res* 2015, 94 (8), 1092-8.
20. Pelegriño, M. T.; De Araujo Lima, B.; Do Nascimento, M. H. M.; Lombello, C. B.; Brocchi, M.; Seabra, A. B., Biocompatible and Antibacterial Nitric Oxide-Releasing Pluronic F-127/Chitosan Hydrogel for Topical Applications. *Polymers (Basel)* 2018, 10 (4).
21. Champeau, M.; Povoá, V.; Militão, L.; Cabrini, F. M.; Picheth, G. F.; Meneau, F.; Jara, C. P.; de Araujo, E. P.; de Oliveira, M. G., Supramolecular poly(acrylic acid)/F127 hydrogel with hydration-controlled nitric oxide release for enhancing wound healing. *Acta biomaterialia* 2018, 74, 312-325.
22. Vercelino, R.; Cunha, T. M.; Ferreira, E. S.; Cunha, F. Q.; Ferreira, S. H.; de Oliveira, M. G., Skin vasodilation and analgesic effect of a topical nitric oxide-releasing hydrogel. *J Mater Sci Mater Med* 2013, 24 (9), 2157-69.
23. Shishido, S. M.; Seabra, A. B.; Loh, W.; Ganzarolli de Oliveira, M., Thermal and photochemical nitric oxide release from S-nitrosothiols incorporated in Pluronic F127 gel: potential uses for local and controlled nitric oxide release. *Biomaterials* 2003, 24 (20), 3543-53.
24. Abrami, M.; D'Agostino, I.; Milcovich, G.; Fiorentino, S.; Farra, R.; Asaro, F.; Lapasin, R.; Grassi, G.; Grassi, M., Physical characterization of alginate-Pluronic F127 gel for endoluminal NABDs delivery. *Soft Matter* 2014, 10 (5), 729-37.
25. Lee, K. Y.; Mooney, D. J., Alginate: properties and biomedical applications. *Prog Polym Sci* 2012, 37 (1), 106-126.

26. Grassi, G.; Crevatin, A.; Farra, R.; Guarnieri, G.; Pascotto, A.; Rehimers, B.; Lapasin, R.; Grassi, M., Rheological properties of aqueous Pluronic-alginate systems containing liposomes. *J Colloid Interface Sci* 2006, 301 (1), 282-90.
27. Mondal, A.; Douglass, M.; Hopkins, S. P.; Singha, P.; Tran, M.; Handa, H.; Brisbois, E. J., Multifunctional S-Nitroso-N-acetylpenicillamine-Incorporated Medical-Grade Polymer with Selenium Interface for Biomedical Applications. *ACS Appl Mater Interfaces* 2019, 11 (38), 34652-34662.
28. Fan, Y.; Wen, Z. T.; Liao, S.; Lallier, T.; Hagan, J. L.; Twomley, J. T.; Zhang, J. F.; Sun, Z.; Xu, X., Novel amelogenin-releasing hydrogel for remineralization of enamel artificial caries. *J Bioact Compat Polym* 2012, 27 (6), 585-603.
29. Oshiro, M.; Yamaguchi, K.; Takamizawa, T.; Inage, H.; Watanabe, T.; Irokawa, A.; Ando, S.; Miyazaki, M., Effect of CPP-ACP paste on tooth mineralization: an FE-SEM study. *J Oral Sci* 2007, 49 (2), 115-20.
30. Valentijn-Benz, M.; van 't Hof, W.; Bikker, F. J.; Nazmi, K.; Brand, H. S.; Sotres, J.; Lindh, L.; Arnebrant, T.; Veerman, E. C., Sphingoid bases inhibit acid-induced demineralization of hydroxyapatite. *Caries Res* 2015, 49 (1), 9-17.
31. Grassi, G.; Farra, R.; Noro, E.; Voinovich, D.; Lapasin, R.; Dapas, B.; Alpar, O.; Zennaro, C.; Carraro, M.; Giansante, C., Characterization of nucleic acid molecule/liposome complexes and rheological effects on pluronic/alginate matrices. *Journal of drug delivery science and technology* 2007, 17 (5), 325-331.
32. Hopkins, S. P.; Pant, J.; Goudie, M. J.; Nguyen, D. T.; Handa, H., Electrospun Bioabsorbable Fibers Containing S-Nitrosoglutathione for Tissue Engineering Applications. *ACS Applied Bio Materials* 2020, 3 (11), 7677-7686.

33. Pant, J.; Pedaparathi, S.; Hopkins, S. P.; Goudie, M. J.; Douglass, M. E.; Handa, H., Antibacterial and Cellular Response Toward a Gasotransmitter-Based Hybrid Wound Dressing. *ACS Biomater Sci Eng* 2019, 5 (8), 4002-4012.
34. ISO 19448:2018(en) Dentistry — Analysis of fluoride concentration in aqueous solutions by use of fluoride ion-selective electrode. International Organization for Standardization: 2018.
35. Marko, T.; Ivana, S.; Kristina, P., Comparison of Fluoride Ion Release from Fluoride Gel in Various Solvents. *Acta Stomatol Croat* 2020, 54 (2), 147-154.
36. Diniz, I. M.; Chen, C.; Xu, X.; Ansari, S.; Zadeh, H. H.; Marques, M. M.; Shi, S.; Moshaverinia, A., Pluronic F-127 hydrogel as a promising scaffold for encapsulation of dental-derived mesenchymal stem cells. *J Mater Sci Mater Med* 2015, 26 (3), 153.
37. Saari, A.; Kasparikova, V.; Sedlacek, T.; Saha, P., On the development and characterisation of crosslinked sodium alginate/gelatine hydrogels. *J Mech Behav Biomed Mater* 2013, 18, 152-66.
38. Xia, T.; Liu, W.; Yang, L., A review of gradient stiffness hydrogels used in tissue engineering and regenerative medicine. *J Biomed Mater Res A* 2017, 105 (6), 1799-1812.
39. Ghica, M.; Hîrjău, M.; Lupuleasa, D.; Dinu-Pîrvu, C.-E., Flow and Thixotropic Parameters for Rheological Characterization of Hydrogels. *Molecules* 2016, 21 (6), 786.
40. Shriky, B.; Kelly, A.; Isreb, M.; Babenko, M.; Mahmoudi, N.; Rogers, S.; Shebanova, O.; Snow, T.; Gough, T., Pluronic F127 thermosensitive injectable smart hydrogels for controlled drug delivery system development. *J Colloid Interf Sci* 2020, 565, 119-130.

41. Müller, M.; Becher, J.; Schnabelrauch, M.; Zenobi-Wong, M., Nanostructured Pluronic hydrogels as bioinks for 3D bioprinting. *Biofabrication* 2015, 7 (3), 035006.
42. Masters, K. S.; Leibovich, S. J.; Belem, P.; West, J. L.; Poole-Warren, L. A., Effects of nitric oxide releasing poly(vinyl alcohol) hydrogel dressings on dermal wound healing in diabetic mice. *Wound Repair Regen* 2002, 10 (5), 286-94.
43. Cao, J.; Su, M.; Hasan, N.; Lee, J.; Kwak, D.; Kim, D. Y.; Kim, K.; Lee, E. H.; Jung, J. H.; Yoo, J. W., Nitric Oxide-Releasing Thermoresponsive Pluronic F127/Alginate Hydrogel for Enhanced Antibacterial Activity and Accelerated Healing of Infected Wounds. *Pharmaceutics* 2020, 12 (10), 926.
44. Zahid, A. A.; Ahmed, R.; Raza Ur Rehman, S.; Augustine, R.; Tariq, M.; Hasan, A., Nitric oxide releasing chitosan-poly (vinyl alcohol) hydrogel promotes angiogenesis in chick embryo model. *Int J Biol Macromol* 2019, 136, 901-910.
45. Yao, X.; Liu, Y.; Gao, J.; Yang, L.; Mao, D.; Stefanitsch, C.; Li, Y.; Zhang, J.; Ou, L.; Kong, D.; Zhao, Q.; Li, Z., Nitric oxide releasing hydrogel enhances the therapeutic efficacy of mesenchymal stem cells for myocardial infarction. *Biomaterials* 2015, 60, 130-40.
46. Zhang, K.; Chen, X.; Li, H.; Feng, G.; Nie, Y.; Wei, Y.; Li, N.; Han, Z.; Han, Z. C.; Kong, D.; Guo, Z.; Zhao, Q.; Li, Z., A nitric oxide-releasing hydrogel for enhancing the therapeutic effects of mesenchymal stem cell therapy for hindlimb ischemia. *Acta Biomater* 2020, 113, 289-304.
47. Carpenter, A. W.; Schoenfisch, M. H., Nitric oxide release: part II. Therapeutic applications. *Chem Soc Rev* 2012, 41 (10), 3742-52.

48. Carpenter, A. W.; Reighard, K. P.; Saavedra, J. E.; Schoenfisch, M. H., O(2)-Protected Diazeniumdiolate-Modified Silica Nanoparticles for Extended Nitric Oxide Release from Dental Composites. *Biomater Sci* 2013, 1 (5), 456-459.
49. Reighard, K. P.; Schoenfisch, M. H., Antibacterial Action of Nitric Oxide-Releasing Chitosan Oligosaccharides against *Pseudomonas aeruginosa* under Aerobic and Anaerobic Conditions. *Antimicrob Agents Chemother* 2015, 59 (10), 6506-13.
50. Garren, M.; Maffe, P.; Melvin, A.; Griffin, L.; Wilson, S.; Douglass, M.; Reynolds, M.; Handa, H., Surface-Catalyzed Nitric Oxide Release via a Metal Organic Framework Enhances Antibacterial Surface Effects. *ACS Appl Mater Interfaces* 2021, 13 (48), 56931-56943.
51. Amadeu, T. P.; Seabra, A. B.; de Oliveira, M. G.; Costa, A. M., S-nitrosoglutathione-containing hydrogel accelerates rat cutaneous wound repair. *J Eur Acad Dermatol Venereol* 2007, 21 (5), 629-37.
52. Shin, D. Y.; Cheon, K. H.; Song, E. H.; Seong, Y. J.; Park, J. U.; Kim, H. E.; Jeong, S. H., Fluorine-ion-releasing injectable alginate nanocomposite hydrogel for enhanced bioactivity and antibacterial property. *Int J Biol Macromol* 2019, 123, 866-877.
53. Park, J.-W.; Means, G. E., An unusually stable S-nitrosothiol from glutathione. *Archives of Pharmacal Research* 1989, 12 (4), 257-258.
54. Li, H.; Gao, C.; Tang, L.; Wang, C.; Chen, Q.; Zheng, Q.; Yang, S.; Sheng, S.; Zan, X., Lysozyme (Lys), Tannic Acid (TA), and Graphene Oxide (GO) Thin Coating for Antibacterial and Enhanced Osteogenesis. *ACS Applied Bio Materials* 2020, 3 (1), 673-684.

55. Wang, X.; Fan, H.; Zhang, F.; Zhao, S.; Liu, Y.; Xu, Y.; Wu, R.; Li, D.; Yang, Y.; Liao, L.; Zhu, H.; Wang, X., Antibacterial Properties of Bilayer Biomimetic Nano-ZnO for Dental Implants. *ACS Biomaterials Science & Engineering* 2020, 6 (4), 1880-1886.
56. Ashcraft, M.; Douglass, M.; Garren, M.; Mondal, A.; Bright, L. E.; Wu, Y.; Handa, H., Nitric Oxide-Releasing Lock Solution for the Prevention of Catheter-Related Infection and Thrombosis. *ACS Appl Bio Mater* 2022.
57. Barraud, N.; Storey, M. V.; Moore, Z. P.; Webb, J. S.; Rice, S. A.; Kjelleberg, S., Nitric oxide-mediated dispersal in single- and multi-species biofilms of clinically and industrially relevant microorganisms. *Microb Biotechnol* 2009, 2 (3), 370-8.
58. Ommen, P.; Zobek, N.; Meyer, R. L., Quantification of biofilm biomass by staining: Non-toxic safranin can replace the popular crystal violet. *J Microbiol Methods* 2017, 141, 87-89.
59. Daghigh, F.; Borghaei, R. C.; Thornton, R. D.; Bee, J. H., Human gingival fibroblasts produce nitric oxide in response to proinflammatory cytokines. *J Periodontol* 2002, 73 (4), 392-400.
60. Chae, H. J.; Park, R. K.; Chung, H. T.; Kang, J. S.; Kim, M. S.; Choi, D. Y.; Bang, B. G.; Kim, H. R., Nitric oxide is a regulator of bone remodelling. *J Pharm Pharmacol* 1997, 49 (9), 897-902.
61. Kuzushima, M.; Mogi, M.; Togari, A., Cytokine-induced nitric-oxide-dependent apoptosis in mouse osteoblastic cells: involvement of p38MAP kinase. *Arch Oral Biol* 2006, 51 (11), 1048-53.

62. Rong, F.; Tang, Y.; Wang, T.; Feng, T.; Song, J.; Li, P.; Huang, W., Nitric Oxide-Releasing Polymeric Materials for Antimicrobial Applications: A Review. *Antioxidants (Basel)* 2019, 8 (11), 556.
63. Agalakova, N. I.; Gusev, G. P., Molecular Mechanisms of Cytotoxicity and Apoptosis Induced by Inorganic Fluoride. *ISRN Cell Biology* 2012, 2012, 1-16.
64. Cao, N.; Chen, X. B.; Schreyer, D. J., Influence of calcium ions on cell survival and proliferation in the context of an alginate hydrogel. *ISRN Chemical Engineering* 2012, 2012.

CHAPTER 5

CONCLUSIONS AND FUTURE DIRECTIONS

5.1. Conclusions

Throughout the previous three projects, my goal was to answer this **Essential Research Question**: How can GSNO be utilized in alginate-based hydrogels for clinical infection treatment?

Before diving into the use of GSNO in alginate-based hydrogels, the relevance of the use of GSNO in such systems must be restated. As shown in **Chapter 2** and several studies discussed in the introduction and literature review, the water-soluble nature of GSNO allows for facile physical incorporation into aqueous systems of one or multiple types of hydrogels. Further, this study highlights the clinical relevance of NO therapy for infections, or for the prevention of infections. Based on all the experiments performed with both lab and clinical bacterial strains, the results give us no reason to believe that a hydrogel formulated with NO release and tested in a laboratory setting against commercially sourced bacterial strains would then fail against infections found clinically. Granted, since the studies performed in the lab were all *in vitro*, there is no claim that these results would be exactly translatable to an *in vivo* setting. However, the antibacterial activity of GSNO-based (and other NO-releasing) materials does not wane when competing with bacterial strains with multiple drug-resistance genes, such as those found in this study.

The water-soluble nature of GSNO and its antibacterial capabilities against clinically sourced and antibiotic-resistant bacteria were displayed in Chapter 2. Next, the

incorporation of GSNO into an alginate hydrogel was investigated and characterized physically and biologically in **Chapter 3**. Following morphological characterizations, it was seen that GSNO impregnation into the spherically crosslinked alginate beads did not alter the internal porous structure, nor the size distribution of the beads. NO release studies revealed that the desired NO release for the application of a hydrogel can be fine-tuned depending on the concentration of the incorporated GSNO. Further, the inclusion of GSNO into the alginate beads imbued the material with potent antibacterial capabilities against Gram-negative *E. coli* and Gram-positive *S. aureus*. Most importantly for practical applications, GSNO leachates from the beads did not interfere with the proliferation or migration of fibroblast cells. In summary, the addition of GSNO to the alginate beads introduced relevant properties for clinical infection treatment, while highlighting the versatility of alginate materials through a unique ion crosslinking strategy.

Further functionalization of an alginate-based hydrogel system was explored in **Chapter 4**. In this project, the hydrogel was designed for a specific application, treatment of dental caries, which would require NO release and the release of fluoride ions into aqueous solution. GSNO was employed as the NO donor molecule, while NaF was used to supply the fluoride ions. In an attempt to improve the mechanical properties of the gel, alginate was combined with a synthetic hydrogel, Pluronic-F127, which gels to form micelles within the polymer at physiological temperatures. Ionic crosslinking of alginate was used in tandem, so that the inner structure of the gel was an interpenetrating network of Pluronic micelles interspersed between crosslinked alginate polymer chains. Rheological studies revealed that inclusion of GSNO and NaF greatly decreased the mechanical properties of the gel, as the molecules likely interfered with the crosslinking of the gels. However, fully formed gels showed storage stability of 21 days at 4 °C with consistent NO release upon immersion in physiological conditions. The NO release

achieved was tunable depending on the GSNO concentration and showed capabilities of killing *S. mutans*, a common dental pathogen present in dental caries. NO release from the fabricated gels was able to significantly break down and disperse a pre-formed biofilm on a hydroxyapatite enamel model. Lastly, F⁻ release from the material successfully prevented artificial demineralization on a hydroxyapatite enamel model, whereas control gels without NaF showed enhanced porosity due to degradation from the highly acidic demineralization solution. Overall, the gel showed promise for the treatment of dental caries, as it tackled both the bacterial and enamel concerns associated with the disorder. This project, with a dental-specific application, revealed the programmable nature of GSNO-infused alginate-based hydrogel systems.

In conclusion, GSNO can be utilized in alginate-based hydrogel systems as an antimicrobial treatment against a broad-spectrum of bacteria with a range of antibiotic resistant mechanisms. Precise crosslinking strategies can be used to re-shape the hydrogel depending on the application. Furthermore, GSNO incorporation depending on concentration affords tunable NO release with no cytotoxicity observed from the GSNO leachates. In combination, the previous studies showcase the potential for alginate hydrogel systems with GSNO as the NO donor in clinical infection treatment, with potential for further modifications depending on specific applications.

5.2. Future Directions

5.2.1 Antibacterial efficacy of NO against drug-resistant bacteria

The findings of Chapter 2 regarding the broad-spectrum antibacterial capacity of NO released from GSNO despite bacteria exhibiting drug-resistance mechanisms present hope for NO as a clinical infection treatment. However, *E. coli* specifically was the one pathogen that displayed variation in membrane permeability by NO in a 4 h propidium iodide study. To investigate this phenomenon further, the study will be repeated with lab

and clinical *E. coli* strains, but PI will be added at more frequent time points (1 h, 4 h, 8 h, 12 h, 16 h, 20 h, and 24 h). The goal of the study will be to discover if there is a time threshold where NO is more capable of membrane permeation for the clinical isolate, or if NO appears to kill this bacteria strain by affecting metabolism and other factors.

Another aspect of clinical infection treatment that has only been investigated once is the ability of bacteria to develop resistance to NO.¹ For this study, clinical isolates with numerous known drug-resistance mechanisms will be tested for a minimum inhibitory concentration (MIC) of GSNO treatment that initiates bacterial killing. Then, bacterial solutions will be repeatedly exposed to GSNO at and below MIC levels to determine if the bacteria can develop resistance to NO antibacterial treatment. Resistance development will be determined by changes in the MIC concentrations of the bacterial solutions following numerous rounds of exposure. To date, no developed resistance to NO has been documented, which shows promise for infection treatment.

5.2.2 Optimization and further testing of NO and F⁻ releasing dental hydrogel

The simplistic design of GSNO-incorporated hydrogels holds promise in clinical treatment, especially for external infection control such as in wound healing or dental pathogen therapy. In the case of the dental hydrogel designed to treat dental caries, the material successfully killed dental bacteria and dispersed a preformed biofilm, in addition to demineralization prevention of an enamel model. However, one shortcoming of the design lies in the stability of the hydrogel after it has formed. As GSNO is broken down by hydrolysis, even storage below physiological temperatures cannot completely prevent the degradation of the NO donor overtime leading to a loss of NO release capabilities. Therefore, studies will be employed to examine the rehydration and NO release properties of the final hydrogel formulation following lyophilization and subsequent storage. First, the hydrogel will be fabricated using the optimized procedures described in the methodology

section of Chapter 4. Then, the hydrogel will undergo lyophilization until the complete removal of water from the substrate (6 – 8 h). Storage stability studies will then be implemented, where freeze-dried samples will be stored at room temperature (25 °C) and 4 °C shielded from light. At weekly and monthly time points, samples will be removed from storage conditions and NO release analysis will be performed to quantify the stability of the NO donor within the modified gel. Ideally, removal of the aqueous component of the gel will prolong the lifetime of the NO donor and allow for longer storage times with equivalent antibacterial potential.

5.2.3 Covalent attachment of NO-donor to hydrogel polymer backbone

GSNO dissolution into hydrogel systems provides adequate NO release for antimicrobial therapies. However, there are some applications that require NO release without the potential for NO donor leaching into tissues. For this reason, future studies will investigate the potential of covalently linking an NO donor to the polymer backbone of a hydrogel system. Poly(vinyl alcohol) (PVA) is a highly biocompatible and hydrophilic polymer used readily in biomedical engineering, often in tissue engineering and wound healing.² It was chosen as the hydrogel backbone as it can easily be chemically modified or crosslinked using UV light.³ Our lab has previously utilized a technology that allows NO donor conjugation to free amine groups of a polymer, equipping the polymer with several months of NO release.^{4, 5} PVA does not contain any free amines, but it can be modified with lysine for amine end group functionalization.⁶ This will then allow attachment of NAP-thiolactone (NAPTH) that can be nitrosated with sodium nitrite to form an NO-releasing hydrogel. Although hydrolysis within the hydrogel will initiate NO release, the covalent attachment of the donor to the gel will prevent leaching out in aqueous environments. Optimization of NAPTH attachment and thiol nitrosation will allow for tunable NO release dependent on amine attachment and nitrosation efficiency.

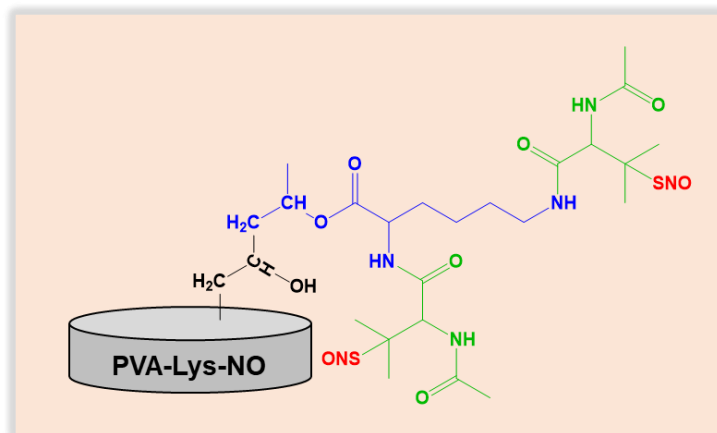


Figure 5.1 Covalent attachment of NO donor to a PVA hydrogel. Lysine (blue) conjugated to PVA will be modified with NAPTH (green) at both amine sites. Thiol bonds will then be nitrosated (red) to endow NO release to the PVA hydrogel.

5.3. References

1. Privett, B. J.; Broadnax, A. D.; Bauman, S. J.; Riccio, D. A.; Schoenfisch, M. H., Examination of bacterial resistance to exogenous nitric oxide. *Nitric Oxide* **2012**, *26* (3), 169-173.
2. Schmedlen, R. H.; Masters, K. S.; West, J. L., Photocrosslinkable polyvinyl alcohol hydrogels that can be modified with cell adhesion peptides for use in tissue engineering. *Biomaterials* **2002**, *23* (22), 4325-4332.
3. Miranda, T. M. R.; Gonçalves, A. R.; Amorim, M. T. P., Ultraviolet-induced crosslinking of poly (vinyl alcohol) evaluated by principal component analysis of FTIR spectra. *Polymer international* **2001**, *50* (10), 1068-1072.
4. Hopkins, S.; Frost, M., Synthesis and Characterization of Controlled Nitric Oxide Release from S-Nitroso-N-Acetyl-D-Penicillamine Covalently Linked to Polyvinyl Chloride (SNAP-PVC). *Bioengineering* **2018**, *5* (3), 72.
5. Hopkins, S. P.; Pant, J.; Goudie, M. J.; Schmiedt, C.; Handa, H., Achieving long-term biocompatible silicone via covalently immobilized S-nitroso-N-acetylpenicillamine (SNAP) that exhibits 4 months of sustained nitric oxide release. *ACS applied materials & interfaces* **2018**, *10* (32), 27316-27325.
6. Mahanta, N.; Valiyaveetil, S., Surface modified electrospun poly (vinyl alcohol) membranes for extracting nanoparticles from water. *Nanoscale* **2011**, *3* (11), 4625-4631.

APPENDICES

APPENDIX A

Supporting Information for Chapter 2

Table 2.S1 NO release from GSNO.....	151
Table 2.S2 Lab <i>E. coli</i> growth curves fit to Gompertz model.....	152
Table 2.S3 Clinical <i>E. coli</i> growth curves fit to Gompertz model	152
Table 2.S4 Lab <i>P. aeruginosa</i> growth curves fit to Gompertz model.....	153
Table 2.S5 Clinical <i>P. aeruginosa</i> growth curves fit to Gompertz model	153
Table 2.S6 Lab MRSA growth curves fit to Gompertz model	154
Table 2.S7 Clinical MRSA growth curves fit to Gompertz model.....	154
Table 2.S8 Lab <i>S. epidermidis</i> growth curves fit to Gompertz model	155
Table 2.S9 Clinical <i>S. epidermidis</i> growth curves fit to Gompertz model.....	155
Figure 2.S1 UV-Vis spectroscopy of S-nitrosoglutathione (GSNO)	156
Figure 2.S2 FTIR spectra of GSNO	157
Figure 2.S3 Bacterial enumeration	158
Figure 2.S4 Gompertz model growth parameters	159

Table 2.S1 NO release levels from GSNO in MHB

[GSNO] (mM)	Average NO release 0 h (x 10⁻¹⁰ mol mL⁻¹ min⁻¹)	Average NO release 6 h (x 10⁻¹⁰ mol mL⁻¹ min⁻¹)	Average NO release 24 h (x 10⁻¹⁰ mol mL⁻¹ min⁻¹)
1	3.50 ± 0.22	3.98 ± 0.53	2.85 ± 0.10
5	9.95 ± 0.61	5.01 ± 1.48	2.65 ± 0.07
7.5	22.22 ± 2.63	13.63 ± 1.04	14.74 ± 2.87
10	30.37 ± 1.97	18.79 ± 1.77	37.79 ± 1.43
12.5	25.12 ± 1.8	40.35 ± 1.24	46.79 ± 5.14
15	37.47 ± 0.91	76.30 ± 9.31	69.46 ± 7.12

Table 2.S2 Lab *E. coli* growth curves of control and GSNO-treated bacteria, fitted to the Gompertz model of growth

	<i>E. coli lab</i>	1 mM	5 mM	7.5 mM	10 mM	12.5 mM	15 mM
Y_M	1.094	1.029	1.102	1.020	1.065	1.144	---
Y_0	0.044	0.027	0.017	0.021	0.018	0.022	---
K	0.297	0.296	0.280	0.276	0.242	0.174	---
$1/K$	3.361	3.371	3.572	3.620	4.120	5.740	---

Table 2.S3 Clinical *E. coli* growth curves of control and GSNO-treated bacteria, fitted to the Gompertz model of growth

	<i>E. coli clinical</i>	1 mM	5 mM	7.5 mM	10 mM	12.5 mM	15 mM
Y_M	1.788	1.793	1.693	1.686	1.653	1.145	0.133
Y_0	0.035	0.030	0.021	0.026	0.020	0.024	0.024
K	0.234	0.227	0.212	0.183	0.122	0.049	0.080
$1/K$	4.263	4.394	4.707	5.460	8.186	20.34	12.48

Table 2.S4 Lab *P. aeruginosa* growth curves of control and GSNO-treated bacteria, fitted to the Gompertz model of growth

	<i>P. aeruginosa</i> <i>lab</i>	1 mM	5 mM	7.5 mM	10 mM	12.5 mM	15 mM
Y_M	1.401	1.309	1.421	1.315	1.315	0.522	---
Y_0	0.017	0.018	0.018	0.018	0.018	0.006	---
K	0.191	0.183	0.175	0.162	0.162	0.054	---
$1/K$	5.246	5.458	5.740	6.235	6.235	18.82	---

Table 2.S5 Clinical *P. aeruginosa* growth curves of control and GSNO-treated bacteria, fitted to the Gompertz model of growth

	<i>P. aeruginosa</i> <i>clinical</i>	1 mM	5 mM	7.5 mM	10 mM	12.5 mM	15 mM
Y_M	1.446	1.441	1.415	1.419	1.220	---	---
Y_0	0.026	0.026	0.025	0.023	0.021	---	---
K	0.182	0.186	0.168	0.145	0.059	---	---
$1/K$	5.486	5.412	5.956	6.867	16.74	---	---

Table 2.S6 Lab MRSA growth curves of control and GSNO-treated bacteria fitted to the Gompertz model of growth

	MRSA lab	1 mM	5 mM	7.5 mM	10 mM	12.5 mM	15 mM
Y_M	1.767	1.773	1.636	1.543	1.482	1.401	0.4627
Y_0	0.045	0.046	0.039	0.035	0.035	0.031	0.028
K	0.261	0.252	0.268	0.195	0.116	0.066	0.092
$1/K$	3.830	3.966	3.738	5.114	8.581	15.02	11.23

Table 2.S7 Clinical MRSA growth curves of control and GSNO-treated bacteria fitted to the Gompertz model of growth

	MRSA clinical	1 mM	5 mM	7.5 mM	10 mM	12.5 mM	15 mM
Y_M	1.766	1.779	1.685	1.637	1.601	1.394	0.7167
Y_0	0.046	0.039	0.033	0.029	0.025	0.022	0.018
K	0.270	0.264	0.252	0.212	0.136	0.064	0.043
$1/K$	3.697	3.789	3.969	4.724	7.300	15.61	23.03

Table 2.S8 Lab *S. epidermidis* growth curves of control and GSNO-treated bacteria, fitted to the Gompertz model of growth

	<i>S. epidermidis</i> lab	1 mM	5 mM	7.5 mM	10 mM	12.5 mM	15 mM
Y_M	1.560	1.500	1.150	1.347	0.657	0.380	---
Y_0	0.031	0.034	0.032	0.030	0.028	0.026	---
K	0.265	0.258	0.225	0.185	0.138	0.102	---
$1/K$	3.789	3.878	4.438	5.423	7.501	9.831	---

Table 2.S9 Clinical *S. epidermidis* growth curves of control and GSNO-treated bacteria, fitted to the Gompertz model of growth

	<i>S. epidermidis</i> clinical	1 mM	5 mM	7.5 mM	10 mM	12.5 mM	15 mM
Y_M	1.143	1.170	0.981	1.034	0.592	0.116	---
Y_0	0.033	0.031	0.028	0.029	0.028	0.025	---
K	0.192	0.174	0.192	0.176	0.071	0.096	---
$1/K$	5.209	5.979	5.263	5.712	14.033	10.473	---

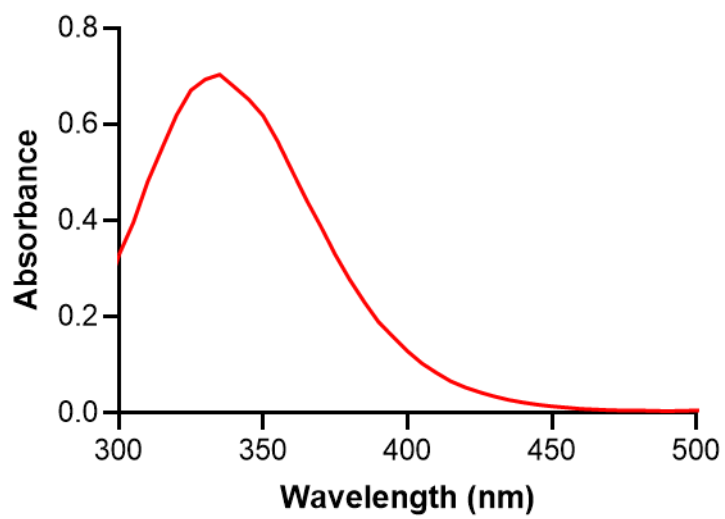


Figure 2.S1. UV-Vis spectroscopy of S-nitrosoglutathione (GSNO)

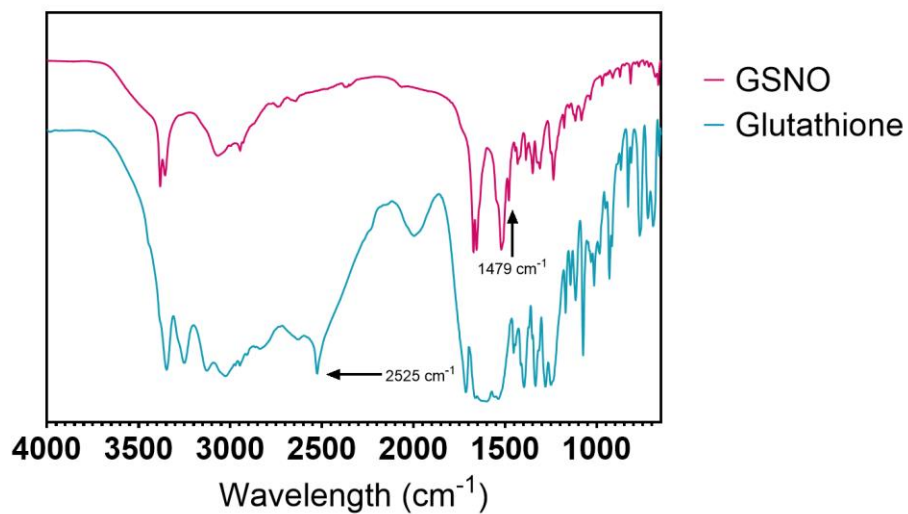


Figure 2.S2 FTIR of GSNO and Glutathione. Note the disappearance of the thiol peak at 2525 cm^{-1} in the nitrosated compound as well as the appearance of the NO peak at 1479 cm^{-1} .

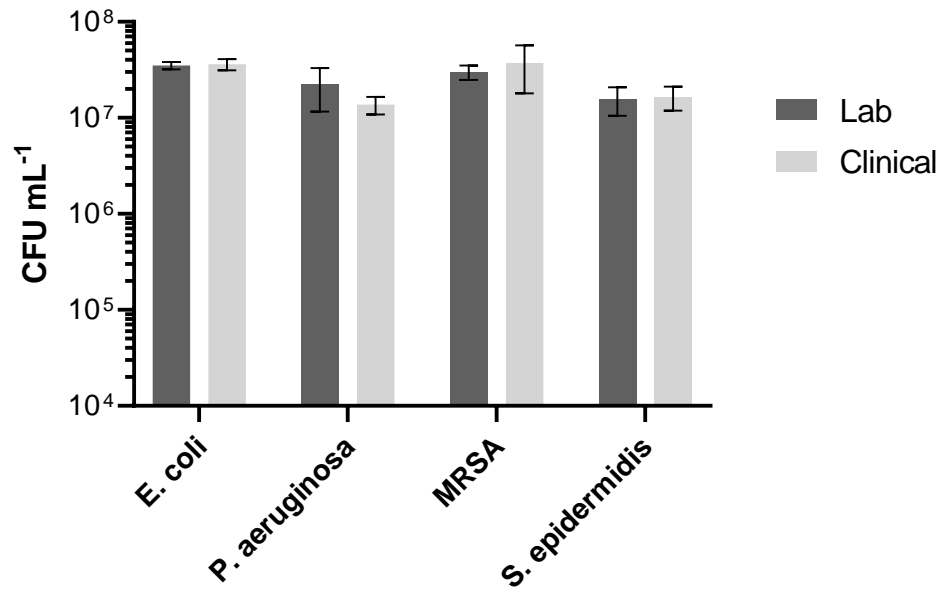


Figure 2.S3 Bacterial enumeration of 0.05 OD₆₀₀ for all 8 strains used in the bacterial studies

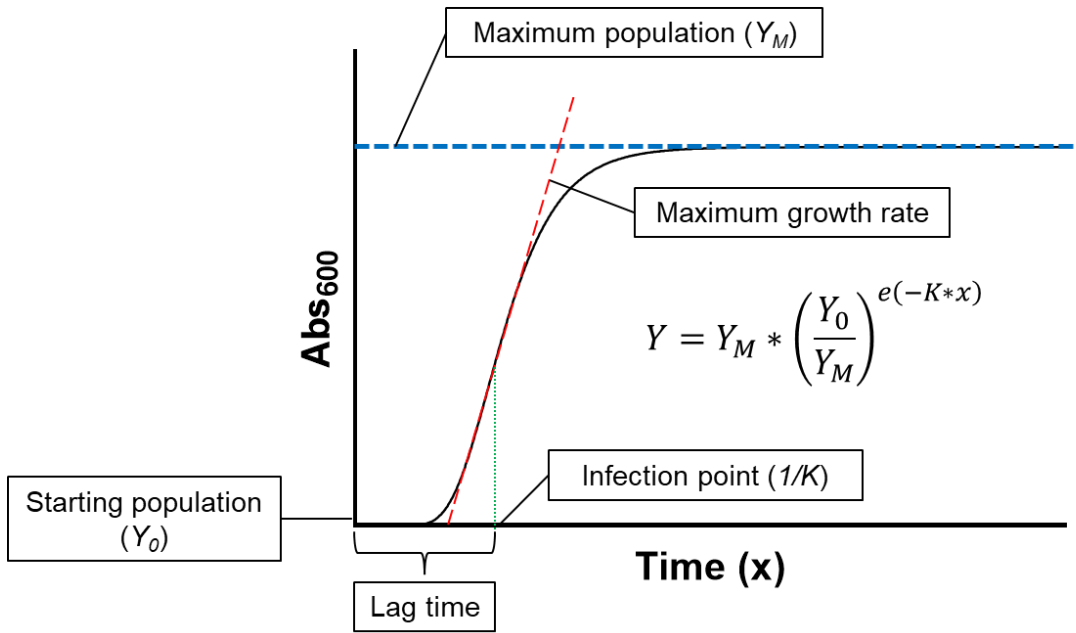


Figure 2.S4 Gompertz model growth parameters

APPENDIX B

Supporting Information for Chapter 3

Table 3.S1 Bacterial reductions of alginate beads	162
Figure 3.S1 NMR of S-nitrosoglutathione (GSNO).....	163
Figure 3.S2 FTIR spectra of GSNO	164
Figure 3.S3 UV spectra of GSNO	165
Figure 3.S4 Standard curve of GSNO	166
Figure 3.S5 GSNO loading of alginate beads	167

Table 3.S1 Bacterial reductions of alginate beads

	Treatment	Avg CFU/mg	SD CFU/mg	Reduction Efficiency	<i>p</i> Value (compared to control)	<i>p</i> Value (compared to alginate)
<i>E. coli</i>	Control	1.52E+05	7.8E+04	---	---	---
	Alginate	1.42E+05	6.9E+04	27.22%	<i>p</i> = 0.9085	---
	G10	1.82E+04	6.1E+03	88.03%	<i>p</i> < 0.005	<i>p</i> < 0.005
	G20	1.53E+03	9.3E+02	98.99%	<i>p</i> < 0.001	<i>p</i> < 0.001 (<i>p</i> < 0.001 compared to G10)
<i>S. aureus</i>	Control	7.12E+05	3.0E+05	---	---	---
	Alginate	6.71E+05	1.3E+05	5.68%	<i>p</i> = 0.9971	---
	G10	4.27E+03	1.9E+03	99.40%	<i>p</i> < 0.001	<i>p</i> < 0.001
	G20	5.44E+02	1.7E+02	99.92%	<i>p</i> < 0.001	<i>p</i> < 0.001 (<i>p</i> < 0.001 compared to G10)

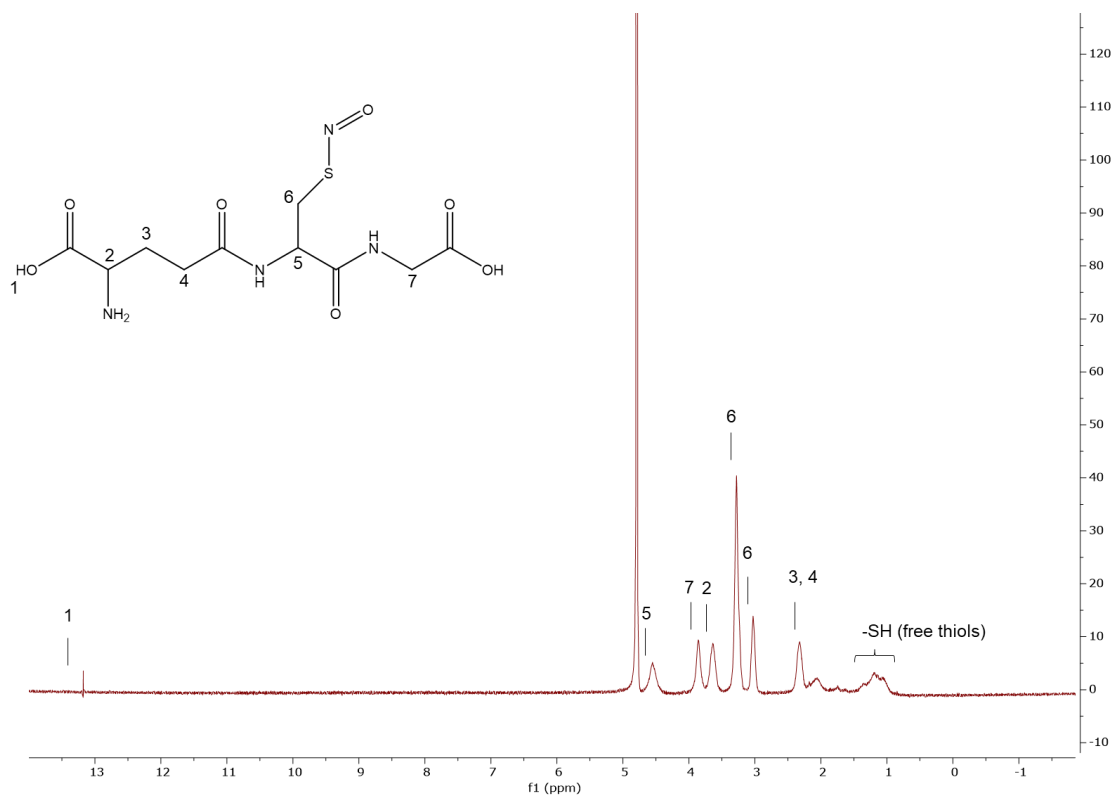


Figure 3.S1 NMR of *S*-nitrosoglutathione (GSNO)

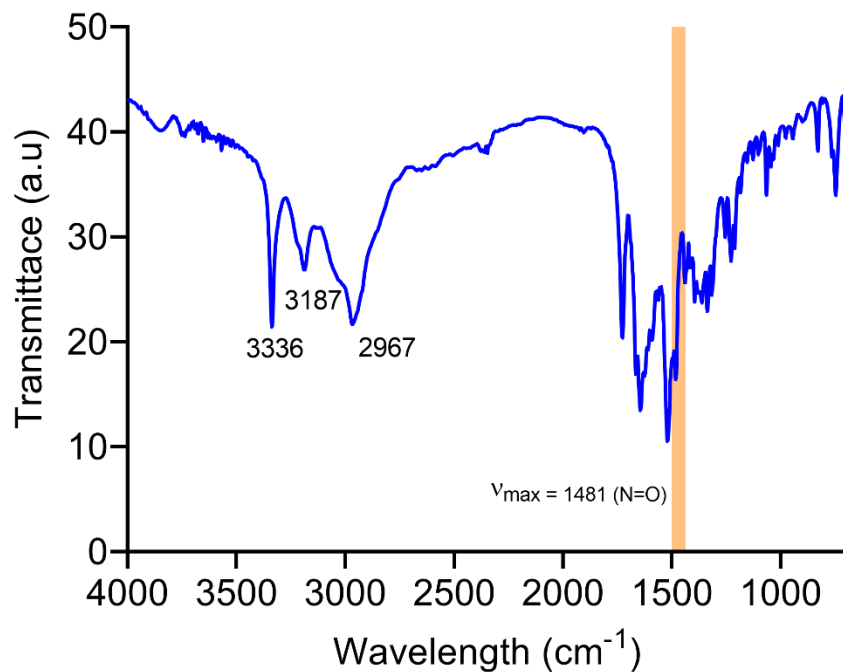


Figure 3.S2 FTIR spectra of GSNO. Major IR Peaks: (ν_{\max} , cm^{-1}) 3336 (s), 3187 (m), 2967 (s), 1726 (s), 1664 (s), 1643 (s), 1519 (s), 1481 (s), 1438 (m), 1394 (m).

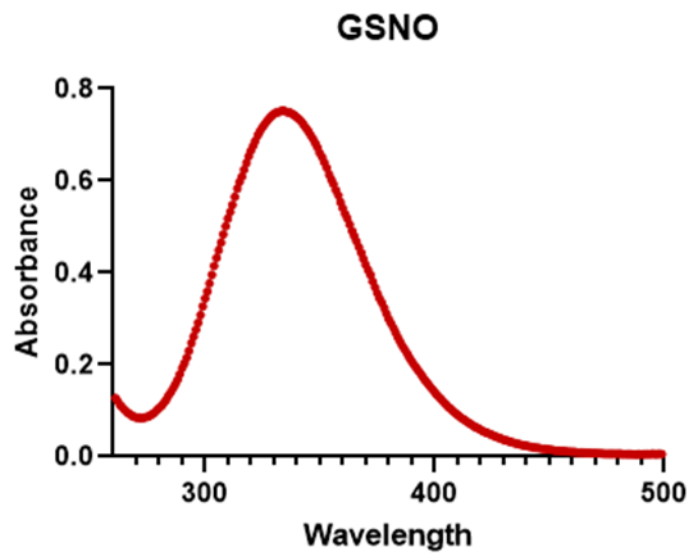


Figure 3.S4 UV spectra of GSNO

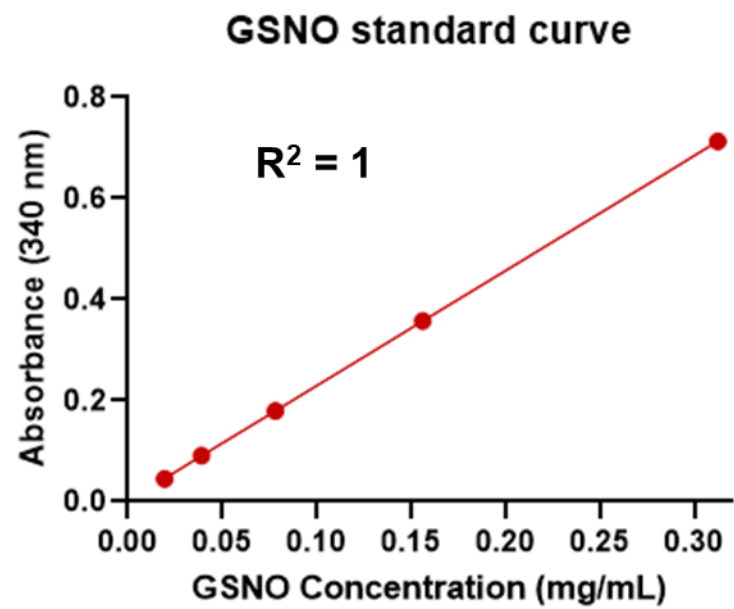


Figure 3.S4 Standard curve of GSNO

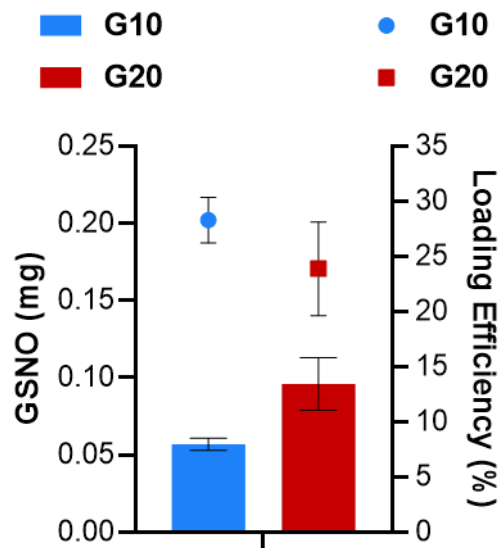


Figure 3.S5 GSNO loading of alginate beads

APPENDIX C

Supporting Information for Chapter 4

Table 4.S1: Sol precursor composition (by mass fraction, x)	170
Table 4.S2 Gel loading efficiency	171
Table 4.S3 Cumulative 4 h NO release (mean, nmol NO/mg gel).....	172
Figure 4.S1 ATR-FTIR spectroscopy of GSNO and freeze-dried gels.....	173
Figure 4.S2 Stress-strain curves of gels	174
Figure 4. S3 Temperature ramps at constant shear rates	175
Figure 4.S4 Full EDS-SEM surface analyses.....	176
Figure 4.S5 Amine fluoride compounds are used as anti-cavity agents for controlled release of F ⁻ to facilitate fluorapatite conversion on dental enamel	177
Figure 4.S6 Standard curve for electrochemical quantification of fluoride ions in artificial saliva solution.....	178
Figure 4.S7 Evaluation of the antibacterial capacity of all four gel types against Gram- negative E. coli in a 4 h study	179
Figure 4.S8 Evaluation of GSNO and precursor sol materials in in vitro models of human cell cytocompatibility.....	180

Table 4.S1 Sol precursor composition (by mass fraction, x)

Formulation	X_{F127}	X_{Alginate}	X_{GSNO}	X_{NaF}	X_{Water}
PA	0.150	0.0167	0.00000	0.00000	0.833
PA-F	0.150	0.0166	0.00000	0.00166	0.832
PA-G ₁₀	0.149	0.0165	0.00826	0.00000	0.826
PA-F-G ₁₀	0.149	0.0165	0.00825	0.00165	0.825
PA-G ₂₀	0.148	0.0164	0.0164	0.00000	0.820
PA-F-G ₂₀	0.147	0.0164	0.0164	0.00164	0.818
PA-G ₃₀	0.146	0.0163	0.0244	0.00000	0.813
PA-F-G ₃₀	0.146	0.0162	0.0244	0.00162	0.812

Table 4.S2 Gel loading efficiency

Formulation	Theoretical GSNO Loading (nmol GSNO/mg Gel)	Experimental NO Loading (nmol NO/mg Gel)	Loading Efficiency (%)
PA-G₁₀	24.6	20.9 ± 1.2	84.9 ± 4.9
PA-F-G₁₀	24.5	10.4 ± 0.6	42.4 ± 2.6
PA-G₂₀	48.7	22.1 ± 2.6	45.3 ± 5.4
PA-F-G₂₀	48.7	19.8 ± 3.2	40.6 ± 6.6
PA-G₃₀	72.5	28.9 ± 4.1	39.8 ± 5.6
PA-F-G₃₀	72.4	34.8 ± 1.8	48.0 ± 2.5

Table 4.S3 Cumulative 4 h NO release (mean, nmol NO/mg gel)

Formulation	Hour 1	Hour 2	Hour 3	Hour 4
PA-G₁₀	1.02 ± 0.11	1.17 ± 0.24	1.25 ± 0.10	1.32 ± 0.05
PA-F-G₁₀	0.75 ± 0.09	0.92 ± 0.18	1.08 ± 0.06	1.40 ± 0.11
PA-G₂₀	1.71 ± 0.05	1.87 ± 0.12	1.96 ± 0.16	2.06 ± 0.20
PA-F-G₂₀	2.14 ± 0.81	2.61 ± 0.74	2.98 ± 0.48	3.32 ± 0.82
PA-G₃₀	2.65 ± 0.49	4.28 ± 1.22	5.48 ± 0.55	6.79 ± 2.09
PA-F-G₃₀	2.08 ± 1.17	4.91 ± 1.41	6.79 ± 1.97	8.83 ± 2.15

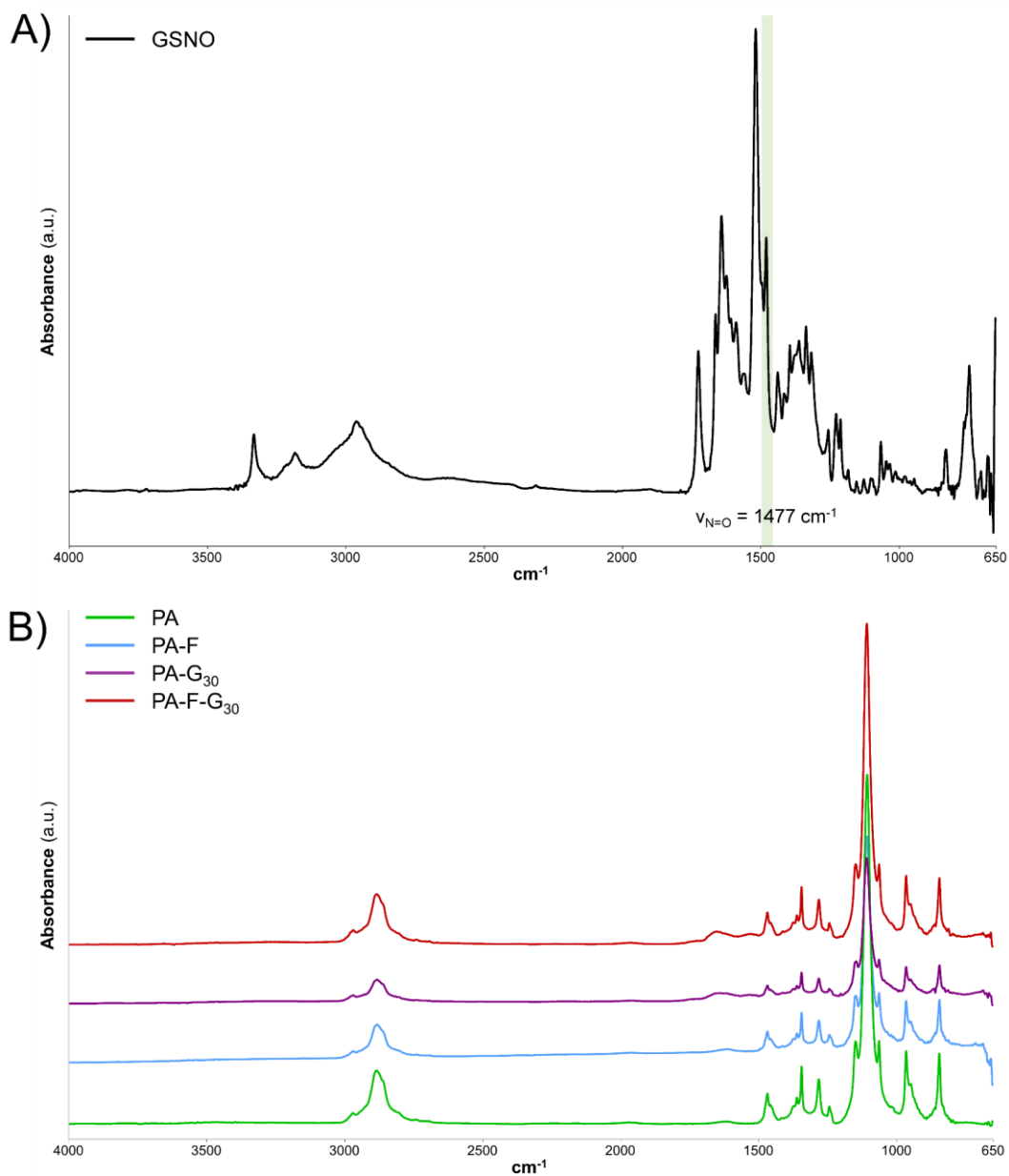


Figure 4.S1 ATR-FTIR spectroscopy of GSNO and freeze-dried gels. (A) Synthesized GSNO shows a characteristic NO bond vibration band at 1477 cm^{-1} . (B) Fabricated gels show nearly identical polymeric composition and bond vibrational stretching, with some phase shifting of the $\nu(-\text{COO}^-)$ band to lower wavenumbers at 1355 cm^{-1} in crosslinked alginate.

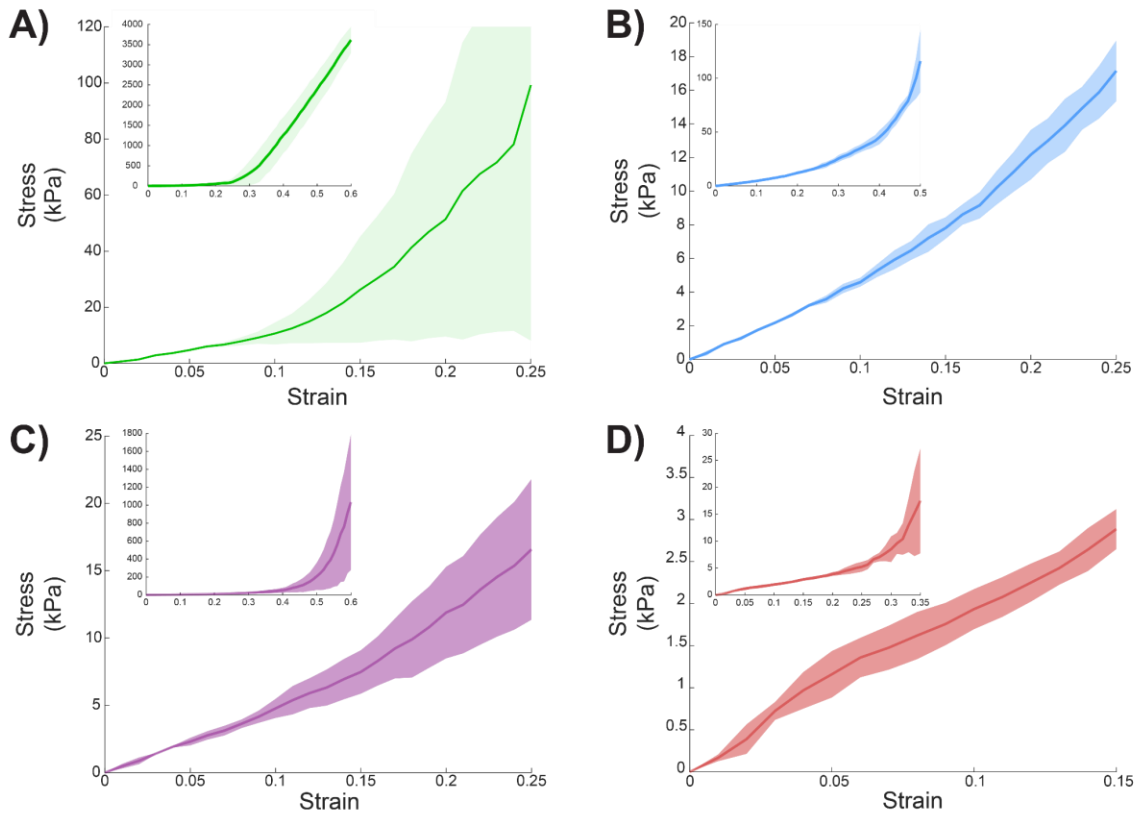


Figure 4.S2 Stress-strain curves of gels generated from uniaxial compressive testing of (A) PA, (B) PA-F, (C) PA-G₃₀, and (D) PA-F-G₃₀ gels.

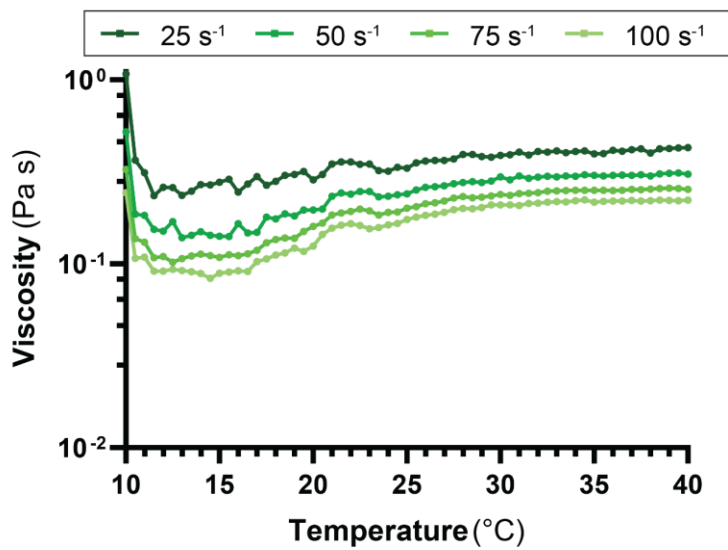


Figure 4.S3 Temperature ramps at constant shear rates (i.e., 25, 50, 75, and 100 s^{-1}) of PA gels demonstrate changes in rheological behavior above 24 $^{\circ}\text{C}$.

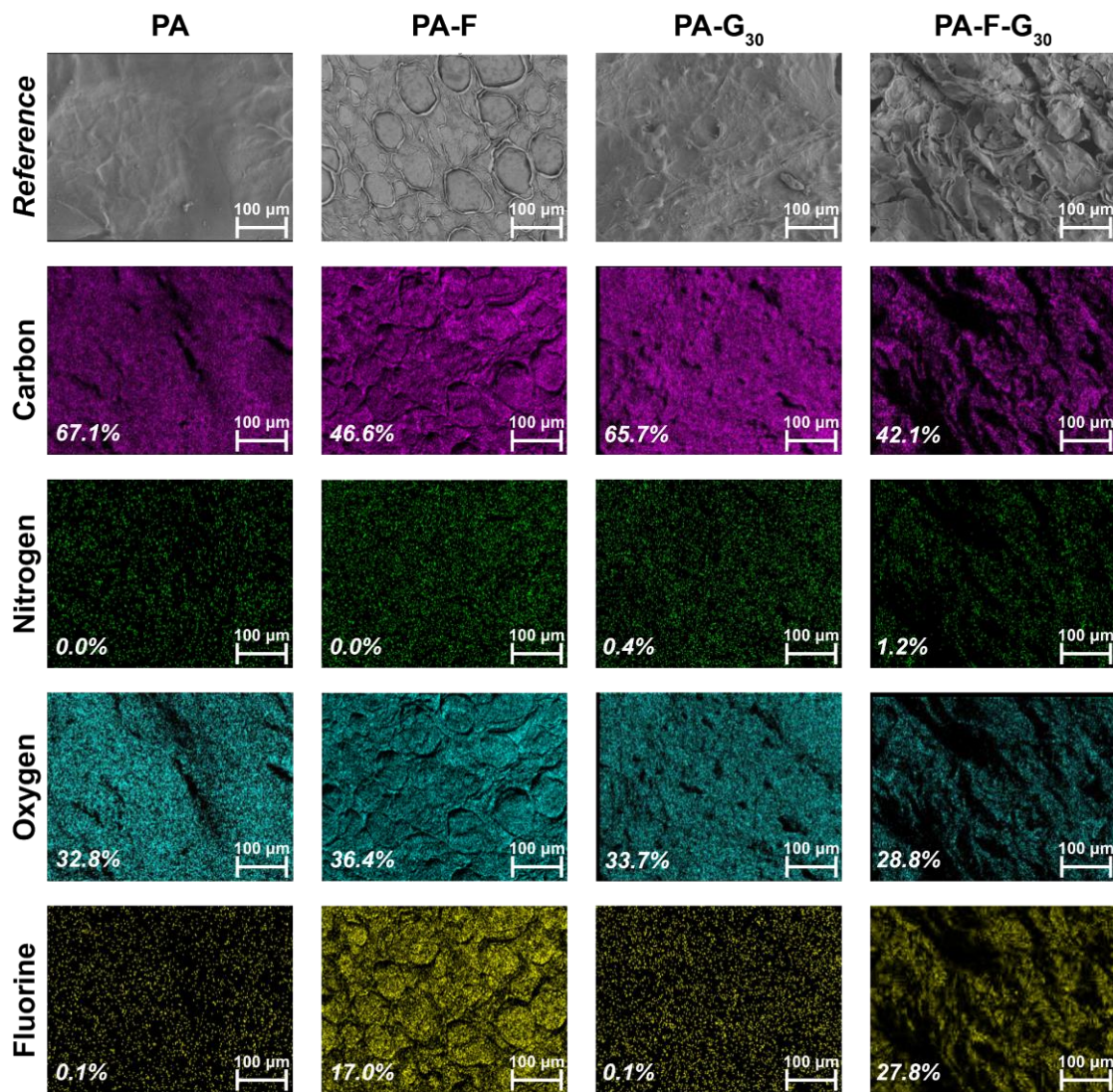


Figure 4.S4 Full EDS-SEM surface analyses of freeze-dried hydrogels from several of the formulations.

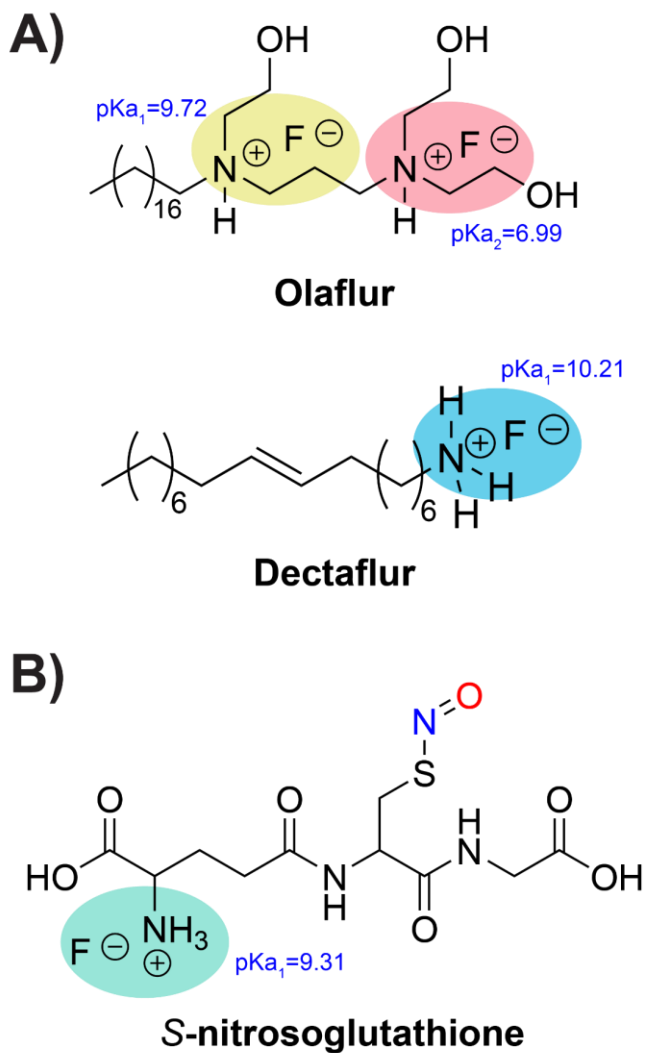


Figure 4.S5 Amine fluoride compounds are used as anti-cavity agents for controlled release of F^- to facilitate fluorapatite conversion on dental enamel. (A) Olaflur and dectaflur are two amine fluorides frequently used in commercial products, compared to (B) S-nitrosoglutathione (GSNO) which consists of a primary amine group also suitable for binding to fluoride ions for controlled delivery of anti-cavity (F^-) and antimicrobial (NO) agents. Theoretical pK_a 's calculated using Marvin (ChemAxon) based on atomic partial charge distribution following Brønsted's rule.

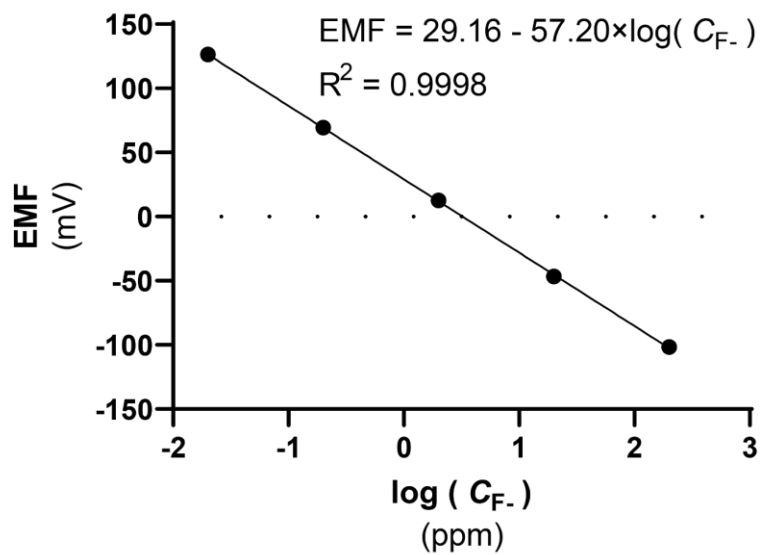


Figure 4.S6 Standard curve for electrochemical quantification of fluoride ions in artificial saliva solution

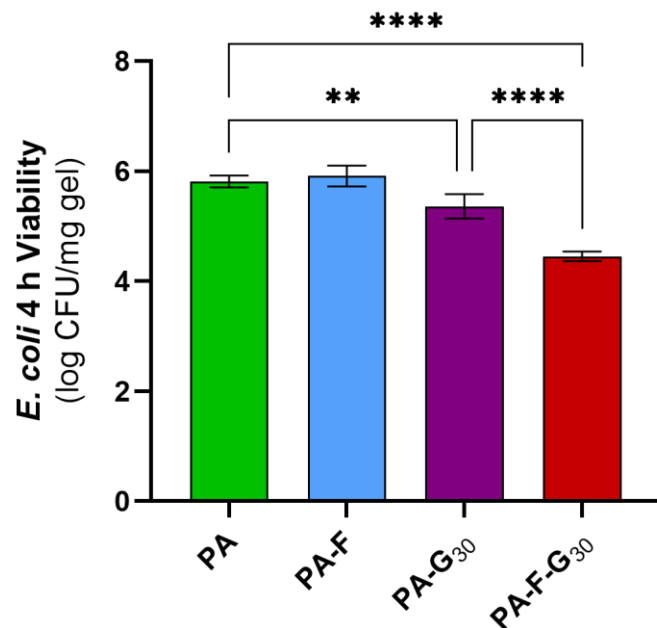


Figure 4.S7 Evaluation of the antibacterial capacity of all four gel types against Gram-negative *E. coli* in a 4 h study. PA-G₃₀ showed a 61.95 ± 18.9 % reduction of viable *E. coli* and PA-F-G₃₀ showed a 95.66 ± 0.897 % reduction compared to the PA control gel. Statistical significance shown as ** ($p < 0.01$) and **** ($p < 0.0001$).

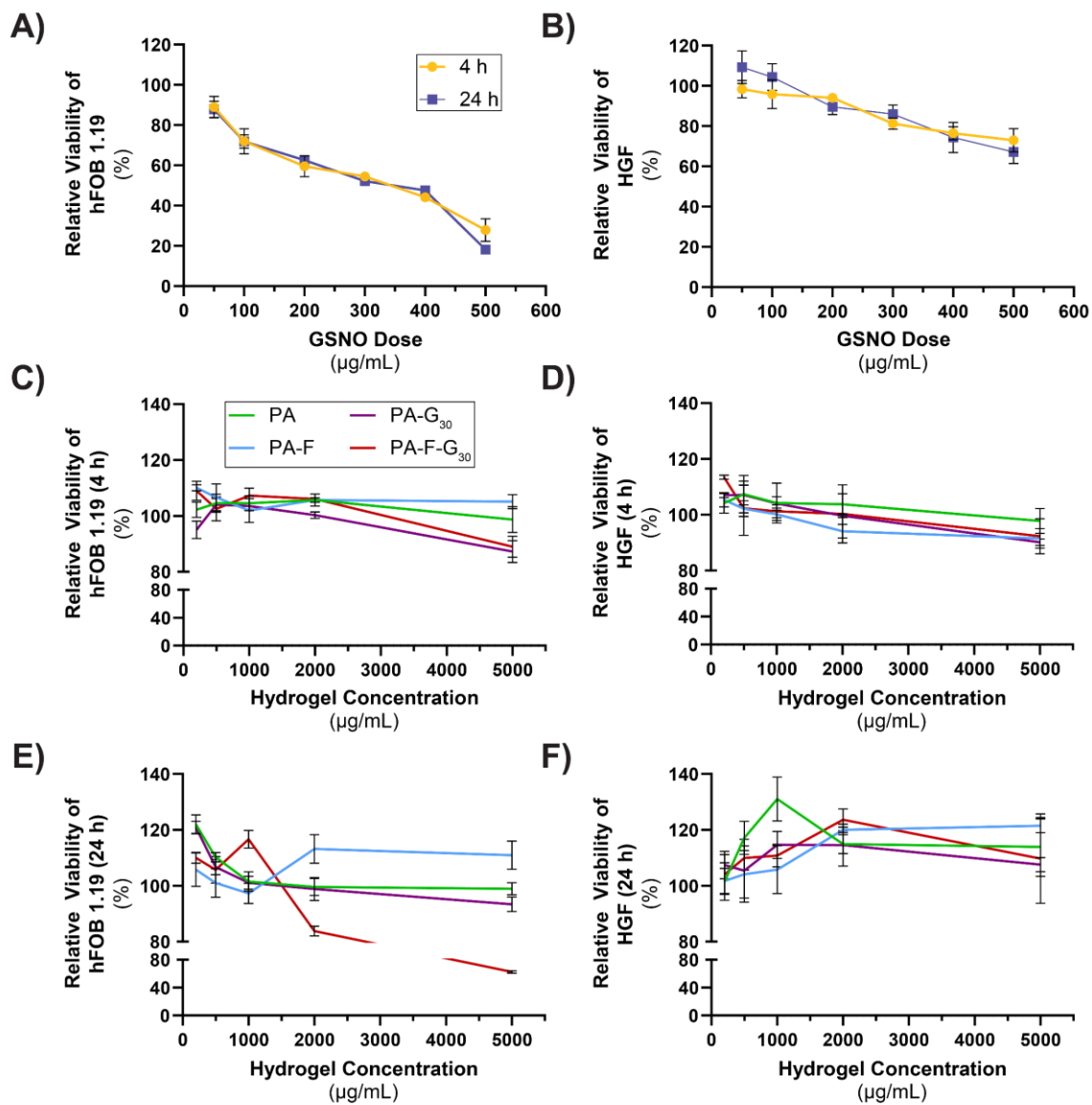


Figure 4.S8 Evaluation of GSNO and precursor sol materials in in vitro models of human cell cytocompatibility. Relative viability of (A) hFOB 1.19 human osteoblasts and (B) human gingival fibroblasts (HGF) challenged against synthesized GSNO. Relative cell viability after 4 h of exposure to sol materials in (C) hFOB 1.19 and (D) HGF. Further evaluation of cellular viability after 24 h exposure to sol materials in (E) hFOB 1.19 and (F) HGF.